

**Characterization of the new htau-KI mouse model for
Alzheimer's disease with a focus on the role of immune
cells during progressing cerebral amyloidosis**

Thesis

to attain

the title of Doctor of natural sciences (Dr. rer. nat.)

of the

Faculty of Natural Sciences I – Biological Science –

of the Martin-Luther-University
Halle-Wittenberg,

submitted

by Susan Barendrecht

born on August 5th, 1992 in The Hague

Thesis successfully defended on 11th of November 2021, in Halle.

Gutachter:

Prof. Guido Posern

Prof. Christian Eckmann

Prof. Oliver Wirths

Table of contents

Table of figures	II
Table of tables	IV
Abbreviation list	V
1. Introduction.....	1
1.1 Background of Alzheimer's disease	1
1.2 Neuropathological hallmarks	3
1.3 Immune cells in AD.....	7
1.4 Mouse models for AD	10
2. Goals of the thesis	12
3. Materials & methods	13
4. Results	29
5. Discussion	64
6. Summary	78
7. References	79
8. Supplementary data	91
9. Curriculum vitae	94
10. Statutory Declaration	96
11. Acknowledgements.....	97

Table of figures

Figure 1. Development of Alzheimer's disease.....	2
Figure 2. Neuropathology of Alzheimer's disease.....	3
Figure 3. Cleavage of amyloid β from the amyloid precursor protein (APP).	4
Figure 4. Different splicing isoforms of tau.....	6
Figure 5. Microgliosis in the brain of an AD mouse model.	6
Figure 6. <i>In vivo</i> ramified morphology of microglial cell.....	7
Figure 7. Activation of microglial cell and phagocytosis in response to tissue injury. ..	8
Figure 8. Plaques in the brain of a 5xFAD mouse.....	10
Figure 9. Targeting vector used to generate the htau-KI mouse line.	13
Figure 10. Y maze set up.	15
Figure 11. Confirmation of gene- and protein expression of human tau.	29
Figure 12. 3R- and 4R tau expression in htau-KI mice.	30
Figure 13. Quantification of 3R- and 4R tau mRNA expression in htau-KI mice.....	31
Figure 14. Expression of different tau isoforms in dephosphorylated brain extracts analysed by Western blot.	32
Figure 15. Dystrophic neurites in 5xFAD and 5xFADxhtau-KI mice.....	33
Figure 16. MC1 staining in hypothalamus at 7 months of age.....	34
Figure 17. MC1 ⁺ dystrophic neurites specifically in hypothalamus of 13-month-old htau-KI and 5xFADxhtau-KI mice.....	35
Figure 18. MC1 staining in brain stem of 7-month-old mice.	36
Figure 19. MC1 ⁺ dystrophic neurites specifically in brain stem of 13-month-old htau-KI and 5xFADxhtau-KI mice.....	37
Figure 20. MC1 staining in cortex of mice at 7 months of age.....	38
Figure 21. MC1 ⁺ staining specifically in cortex of 13-month-old htau-KI and 5xFADxhtau-KI mice.	39
Figure 22. Plaque quantification in 7- and 13-month-old 5xFAD and 5xFADxhtau-KI mice.....	41
Figure 23. Microgliosis and astrocytosis in 13-month-old 5xFADxhtau-KI mice, but not in htau-KI mice.	42
Figure 24. Differentially expressed genes in htau-KI mice compared to WT in the Nanostring mouse AD panel.	43
Figure 25. Differentially expressed genes in 5xFADxhtau-KI mice compared to 5xFAD and WT mice in the NanoString mouse AD panel.....	44
Figure 26. Correlation of NanoString gene expression data of mice with data on <i>post-mortem</i> human brain regions reveals a protective effect of htau in 5xFADxhtau-KI mice.....	45
Figure 27. Gene set enrichment analysis of 5xFADxhtau-KI mice compared to 5xFAD at 7 months of age.	46
Figure 28. Gene set enrichment analysis of 5xFADxhtau-KI mice compared to 5xFAD at 13 months of age.	47

Figure 29. CCL2 ELISA of culture supernatant of control and A β -stimulated primary microglia.	48
Figure 30. Gene-dose dependent RFP/CCR2 expression in spleen tissue of WT, CCR2 ^{+RFP} and CCR2 ^{RFP/RFP} mice and lack of expression in microglia.....	49
Figure 31. Lack of RFP production in WT, 5xFAD and 5xFADxCCR2 ^{+RFP} mouse brain.	49
Figure 32. Occurrence of MHCII ⁺ cells in the CNS in response to AD-like pathology and co-staining with Iba1.	50
Figure 33. Neuropathology in 5xFAD and 5xFADxCCR2 ^{+RFP} mice.....	51
Figure 34. Gene expression of immune-related factors in prefrontal cortex of mouse brains.	53
Figure 35. Behavioural data at 6 months of age.....	55
Figure 36. Morris water maze learning curves.....	56
Figure 37. Behavioural data at 12 months of age.....	58
Figure 38. Basal synaptic transmission, paired-pulse response, and LTP in the CA1 region of the hippocampus at 8 months of age.....	59
Figure 39. Action potential-independent activity in hippocampal neurons at 8 months of age.....	61
Figure 40. Western blot of human APP expression in different breeding pairs.....	62
Figure 41. GFP expression in CX3CR1 ^{GFP/GFP} mouse brain.	63
Supplementary Figure 1. Differentially expressed genes in male vs. female and old vs. young mice in the NanoString mouse AD panel.....	93

Table of tables

Table I - Primers	27
Table II - Antibodies	28
Supplementary Table I - Differentially expressed genes in 5xFADxhtau-KI mice compared to WT mice in the NanoString mouse AD panel.....	91
Supplementary Table II - Differentially expressed genes in 5xFAD mice compared to WT mice in the NanoString mouse AD panel.....	92

Abbreviation list

A β	Amyloid beta
AD	Alzheimer's Disease
ApoE	Apolipoprotein E
APP	Amyloid Precursor Protein
BBB	Blood brain barrier
BMDM	Bone marrow-derived macrophages
CCL2	See MCP-1
CCR2	C-C chemokine receptor 2
CNS	Central nervous system
CSF	Cerebrospinal fluid
CX3CL1	Fractalkine
CX3CR1	Fractalkine receptor
DAM	Disease-associated microglia
DNA	Deoxyribonucleic acid
ECM	Extracellular matrix
ELISA	Enzyme-linked immunosorbent assay
FACS	Fluorescence-activated cell sorting
FBS	Fetal bovine serum
fEPSP	Field extracellular postsynaptic potential
GFAP	Glial fibrillary acidic protein
GFP	Green fluorescent protein
hAPP-KI	Human amyloid precursor protein knock-in
HFIP	Hexafluoroisopropanol
HLA	Human leukocyte antigen
hPCNs	Human primary cortical neurons
htau-KI	Human tau knock-in
Iba1	Ionized calcium binding adaptor molecule 1
IL	Interleukin
LPS	Lipopolysaccharides
MAPT	Microtubule associated protein tau
MCI	Mild cognitive impairment
MCP-1	Monocyte chemoattractant protein (CCL2)
mEPSP	Mini extracellular postsynaptic potential
MEA	Multi electrode assay
MHCII	Major histocompatibility complex II
mIPSP	Mini inhibitory postsynaptic potential

mPN	Mouse primary neurons
(m)RNA	(messenger) Ribonucleic acid
NFT	Neurofibrillary tangle
NMDA	N-methyl-d-aspartate
NSAIDs	Non-steroidal anti-inflammatory drugs
PHF	Paired helical filament
PLO	Poly-L-ornithine
PSEN	Presenilin
(q)RT-PCR	(quantitative) reverse transcriptase polymerase chain reaction
RFP	Red fluorescent protein
SF	Straight filament
TREM2	Triggering receptor expressed on myeloid cells 2
3R tau	3 repeat tau
4R tau	4 repeat tau

1. Introduction

1.1 Background of Alzheimer's disease

Alzheimer's disease (AD) is a neurodegenerative disorder, first presented by the German physician Alois Alzheimer in 1906. In the 4 subsequent years, more similar cases of dementia were described, and the disease was named after Alzheimer. He described the symptoms and neuropathology of his 56-year-old female patient, Auguste Deter (Alzheimer, 1906). She showed neurodegeneration, as well as plaques and tangles, now known as the 3 main neuropathological characteristics of AD.

In 2016, there were 43.8 million people suffering from AD worldwide. The incidence of AD was 712 per 100.000 people (Nichols *et al.*, 2019). Between 1990 and 2016, the number of people suffering from AD doubled, and it is expected to rise to approximately 100 million patients in 2050 (Brookmeyer *et al.*, 2007). It has been described by several groups (reviewed in Fisher *et al.*, 2018) that AD pathology in females (humans as well as mice) is aggravated compared to males. The underlying mechanisms for this predisposition remain unclear, although several factors (e.g. sex hormones, differences in brain structure, stress-responsiveness) have been suggested (reviewed in Fisher *et al.*, 2018).

The costs of care for AD patients in Europe are estimated to add up to 630 billion euros in 2050 and rise to 770 billion euros in 2080 (Cimlér *et al.*, 2019). An important consideration however, as described by Cimlér *et al.* (2019), is that costs of care for AD patients will keep increasing if successful therapies that halt the disease progression are developed. Only if preventative treatments are discovered, there will be an economic advantage. It is therefore important to better understand the pathological development of AD and find early targeting options for treatment.

A distinction is made between 2 forms of AD: familial (presenile) and sporadic (senile) AD. Familial AD is caused by an autosomal dominant mutation in genes related to AD (different mutations have been described in families worldwide), resulting in overproduction of amyloid beta (A β), an important peptide in AD pathology. This form of AD starts early, between the age of 30 and 65 and is responsible for less than 6% of total AD cases (Von Giau *et al.*, 2019). Sporadic AD, on the other hand, starts after the age of 65 and is not related to any mutations. There have been several risk factors described for the development of sporadic AD. The Apolipoprotein E (ApoE) gene is a well-known risk factor for AD, with the ApoE2 isoform protecting against development of AD, and the ApoE4 isoform increasing the risk of AD development (Corder *et al.*, 1994; Saunders *et al.*, 1993). Other risk factors include age, family history, education, cardiovascular disease, social and cognitive engagement, depression, traumatic brain injury and smoking (reviewed in Baumgart *et al.*, 2015). Another important risk factor for the development of AD is called cognitive reserve (Stern, 2013). This principle refers

to the finding that some people are less susceptible to the brain changes caused by AD than others. There could be a complete lack of clinical symptoms in one person, whereas another person with similar neuropathological changes already experiences a loss of cognitive abilities. Underlying factors for cognitive reserve are higher education, occupational attainment, and social and intellectual participation in daily life (Stern, 2013).

Patients suffering from AD show memory deficits, but also other cognitive problems. Aphasia, changes in mood or personality, problems with planning or orientation and decreased vision can all occur as a part of AD pathology (McKhann *et al.*, 2011). The clinical development differs between patients, depending on which brain region is most strongly affected. There are 3 stages in the development of AD, as described by the National Institute on Aging and Alzheimer’s Association (Sperling *et al.*, 2011; Albert *et al.*, 2011; McKhann *et al.*, 2011) and depicted in figure 1 (Jack *et al.*, 2010). The first stage of AD is preclinical; no symptoms are occurring at this point, but there are changes in specific biomarkers in brain, blood and/or cerebrospinal fluid (CSF). These changes start to occur 20 to 30 years before the actual onset of dementia (Jansen *et al.*, 2015). The following 2 phases show changes in biomarkers, as well as behavioural deficits. Mild Cognitive Impairment (MCI), is the second phase, in which symptoms are present, but not yet interfering with the daily life of the patients. After 1-5 years, when the symptoms start to interfere with everyday activities, the third phase, called dementia due to AD, starts (Petersen *et al.*, 1999).

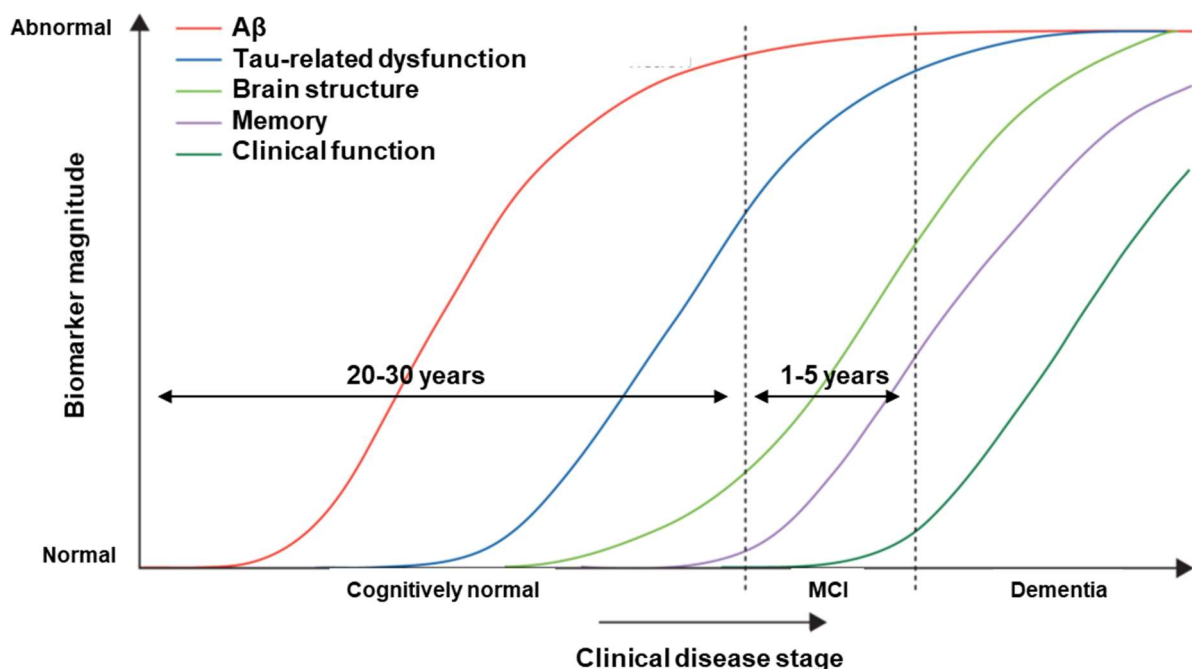


Figure 1. Development of Alzheimer’s disease. Graph shows several biomarker abnormalities during the different clinical disease stages of AD. Figure taken and adapted from Jack *et al.* (2010).

There are currently 5 drugs available on the market for AD patients: three different acetylcholinesterase inhibitors and one modulator of N-methyl-d-aspartate (NMDA) receptors,

as well as a combination of both (Hempel *et al.* 2018; Dominik *et al.*, 2019). These therapies provide relief of symptoms for a short period of time but are ineffective in halting disease progression. In 2018, there were 112 agents for AD in ongoing clinical trials, of which 26 were in phase III (Cummings *et al.*, 2018). Originally, trials were focused on patients in the stages of MCI or dementia, but currently the clinical trials are including more early-stage AD patients. The rationale for this is based on figure 1, which shows that the neuropathological changes occur far before the clinical symptoms. It thus seems important to identify patients and start treatment as early as possible.

1.2 Neuropathological hallmarks

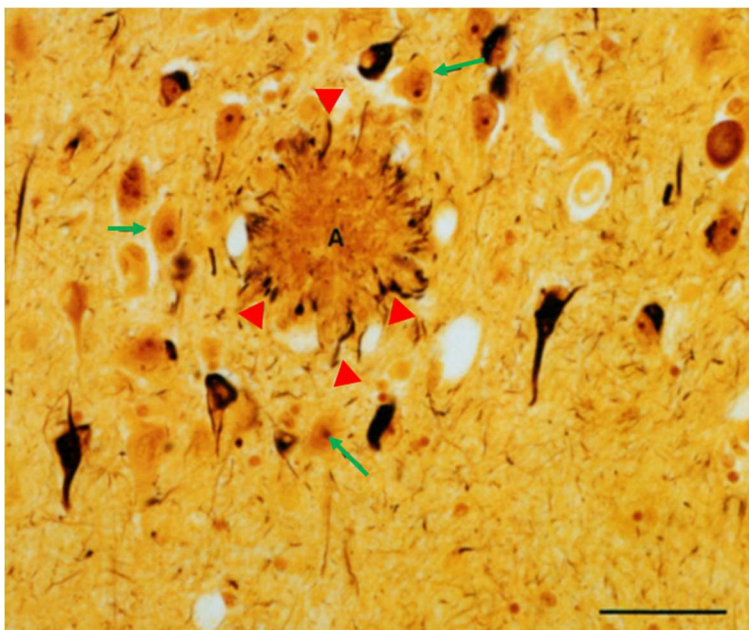


Figure 2. Neuropathology of Alzheimer's disease. Picture taken and adapted from Selkoe *et al.* (1991). Human brain tissue showing a plaque (A) with surrounding dystrophic neurites (red arrowheads). Also clearly visible are the dark brown stained neurofibrillary tangles. Green arrows point to healthy neurons. Scale bar is 50µm.

Originally, there were 3 neuropathological hallmarks described by Alois Alzheimer: plaques, tangles, and neurodegeneration. Plaques are extracellular aggregates of the peptide A β (see figure 2). They have a spherical diameter of 20-40µm, and there are 3 different types of plaques, based on their shape and density: diffuse, focal, and stellar (Duyckaerts *et al.*, 2009). Initially it was described that diffuse plaques occur first in the brain, followed by a maturation process (Iwatsubo *et al.*, 1994). The diffuse plaques

have no clear edges, and during maturation the density of the plaque core increases, and the boundaries become more pronounced. Different types of plaques are however mutually exclusive in specific brain areas and new plaques are formed in a short time span (1-2 days), staying the same size afterwards (D'Andrea *et al.*, 2004; Meyer-Luehmann *et al.*, 2008). Also, focal plaques contain a neuronal soma or neuronal debris whereas diffuse plaques are associated to projection areas of A β -producing neurons rather than cell bodies (Hartlage-Rübsamen *et al.*, 2011). Therefore, the current consensus is that different plaque types do not represent different stages of plaque development but rather are a result of different cellular mechanisms. Focal plaques are thought to be formed by the accumulation of A β in cell bodies

whereas diffuse plaques are the result of synaptic A β release (Hartlage-Rübsamen *et al.*, 2011).

A β is a cleavage product of the amyloid precursor protein (APP). Sequential cleavage of this membrane-bound protein by β -secretase and γ -secretase leads to the release of the 4kDa large A β peptide (Thinakaran & Koo, 2008) (see figure 3). Subunits of the γ -secretase are encoded by presenilin (PSEN) 1 and 2, which are common sites of mutations in familial AD. There are different isoforms of A β , varying in length between 38 and 42 amino acids, depending on the cleavage sites of the different secretases (Haass *et al.*, 2012). Although the A β_{x-40} isoform is most abundant, the A β_{x-42} isoform plays a major role in AD. Due to the 2 extra C-terminal amino acids, this isoform is more hydrophobic, and therefore prone to aggregation (Jarrett *et al.*, 1993). Physiologically, A β is important for the modulation of synaptic activity, as well as neuronal cell survival (Pearson & Peers, 2006). Additionally, A β plays a role in learning and memory (Morley *et al.*, 2008), possibly through the modulation of synaptic activity. Posed by Hardy and Selkoe (2002), the amyloid cascade hypothesis is the most important description of the development of AD pathology. The hypothesis states that the presence of high amounts of A β is the cause of all other neuropathological hallmarks of AD. The high amyloid load can be a result of overproduction of A β , caused by mutations in genes related to A β , or a result of lack of clearance of A β . It is currently thought that not the amyloid plaques, but the intermediate-sized A β oligomers are responsible for cognitive deficits (Walsh *et al.*, 2002). The formation of plaques is hypothesized to be a defence mechanism of the brain to prevent the toxic effects of soluble A β oligomers (Näslund *et al.*, 2000; Cleary *et al.*, 2005; Haass & Selkoe, 2007).

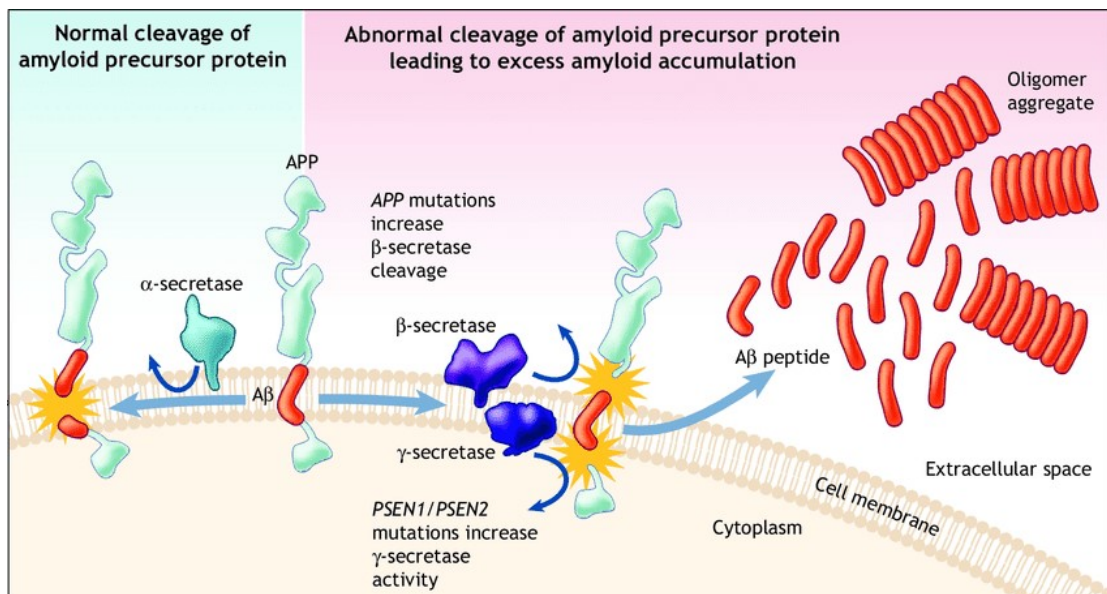


Figure 3. Cleavage of amyloid β from the amyloid precursor protein (APP). Cleavage of APP by β -secretase and γ -secretase leads to production of amyloid β . This peptide aggregates into oligomers and ultimately into plaques. Figure taken from Patterson *et al.* (2008).

Besides A β , the microtubule binding protein tau (MAPT) also aggregates in the brains of AD patients. These intracellular aggregates are called neurofibrillary tangles (NFT, see figure 2), and their presence correlates with cognitive deficits in AD patients (Giannakopoulos *et al.*, 2003). Tau tangles are one of the main pathological hallmarks of AD, but are also found in other neurodegenerative diseases, as well as in the normal aging brain. Tangles are formed when tau is hyperphosphorylated, which results in detachment of tau from the microtubules. Tau subsequently aggregates in paired helical filaments (PHF) and straight filaments (SF), which together build the NFT (Alonso *et al.*, 1996; Iqbal *et al.*, 2005). Like for A β , it is hypothesized that the formation of NFT is a protective mechanism and that a soluble species of tau is neurotoxic (Cowan & Mudher, 2013).

The physiological function of tau is induction and stabilization of microtubule formation via the microtubule binding domains in the tau molecule. Microtubules are responsible for transport inside the cell, as well as maintenance of the cell shape. Dimers of α - and β -tubulin form long strands in the cytoplasm of the cell, along which other proteins can be transported to different locations in the cell. Tau is predominantly expressed in neurons in the brain (Buée *et al.*, 2000). In adult brain, tau expression is limited to the axons, whereas during development tau is also expressed in dendrites (Su *et al.*, 1993). Normally, tau is phosphorylated at 2-3 positions in the molecule. In AD, the hyperphosphorylation process leads to a 3-fold increase in phosphorylation (Köpke *et al.*, 1993).

The gene for tau is located on chromosome 17 in humans and chromosome 11 in mice. Six different isoforms of the tau protein have been described, based on splicing variants of the mRNA (Andreadis *et al.*, 1995; see figure 4). Exon 10 codes for an additional microtubule binding domain, besides the 3 binding sites that are constitutively expressed. Therefore, isoforms including exon 10 are called 4 repeat (4R) tau, whereas isoforms excluding exon 10 are called 3 repeat (3R) tau. Splicing of exon 2 and exon 3 also results in different isoforms, with zero, one or two 29-amino acid-long N-terminal repeats. These different isoforms are therefore called 0N (exon 2⁻3⁻), 1N (exon 2⁺3⁻) and 2N (exon 2⁺3⁺). Exon 3 is spliced together with exon 2. In the human fetal brain, mostly the 0N3R isoform is expressed (Goedert *et al.*, 1989). In the human adult brain, all 6 isoforms of tau are present, with highest expression levels of the 0N isoforms. In mice, during fetal development there is also expression of 0N3R, but adult mice only express 4R tau, with the 0N isoform also being most common (McMillan *et al.*, 2008). In healthy human brain, as well as in AD, the ratio between 3R and 4R tau is equal to 1 (Boutajangout *et al.*, 2004; Ingelsson *et al.*, 2006). In other tauopathies, the ratio is changed, favouring either 3R tau (Pick's disease) or 4R tau (frontotemporal dementia, progressive supranuclear palsy, corticobasal degeneration) (Ingelsson *et al.*, 2007; Dickson *et*

al., 2011). Tangles in AD consist of both isoforms of tau (Goedert *et al.*, 1989; Jellinger & Attems, 2007).

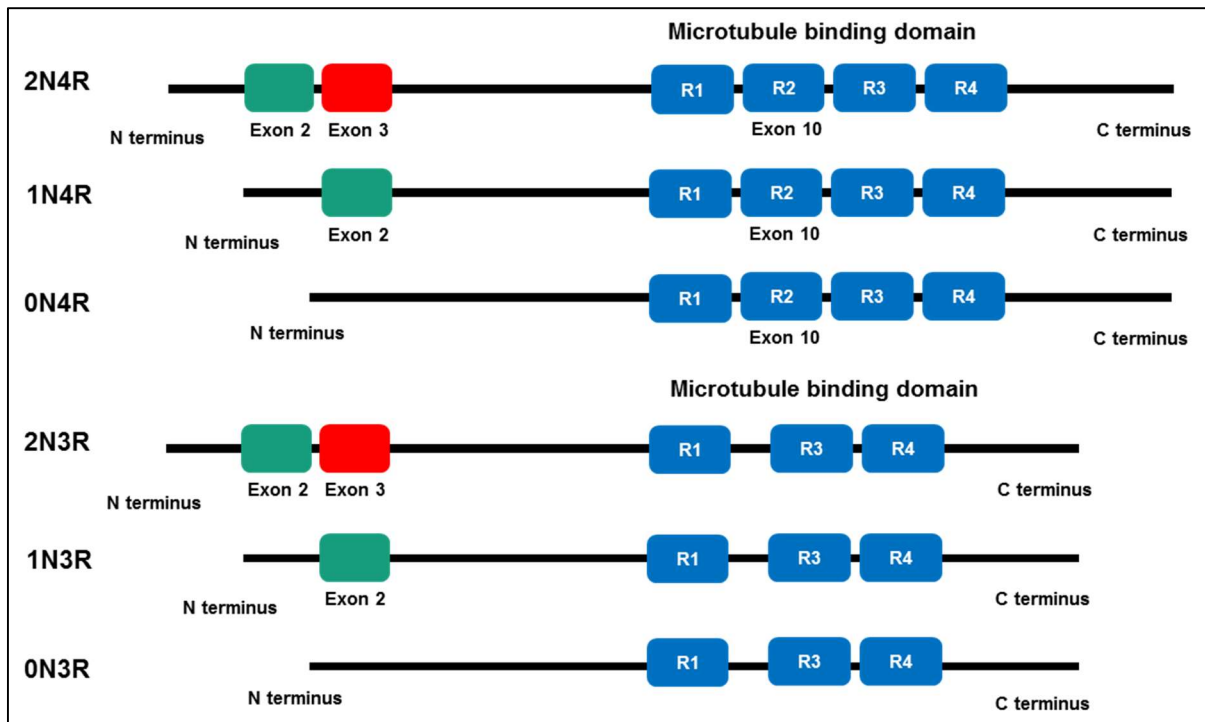


Figure 4. Different splicing isoforms of tau. The six different isoforms of tau based on splicing of exons 2, 3 and 10 are shown schematically.

Besides plaques and tangles, Alois Alzheimer also described the loss of neurons in AD brain. The loss of neurons primarily results in a decreased volume of the hippocampus in human AD patients (Fukutani *et al.*, 2000). The hippocampus is the region responsible for learning and memory and neuronal loss in this region thus results in the cognitive deficits characterizing AD. Since the discovery of AD, more hallmarks of AD have been discovered, such as the occurrence of dystrophic neurites (see figure 2; Su *et al.*, 1993; Knowles *et al.*, 1999; Sadleir *et al.*, 2016). Neurites are neuronal processes responsible for communication between the cells. Both axons and dendrites can become dystrophic in AD, which results in a distorted morphology and reduced signalling capacity of the cell due to the destruction of microtubule. As shown in figure 2, these dystrophic neurites are found around plaques and stain positively for pathological tau markers (Su *et al.*, 1993; Dickson *et al.*, 1999; Knowles *et al.*, 1999). Furthermore, there is pronounced astro- and microgliosis in AD brains (Itagaki *et al.*, 1989). Astroglial activation is the activation of astrocytes in the brain in response to pathological changes in the central nervous system (CNS)

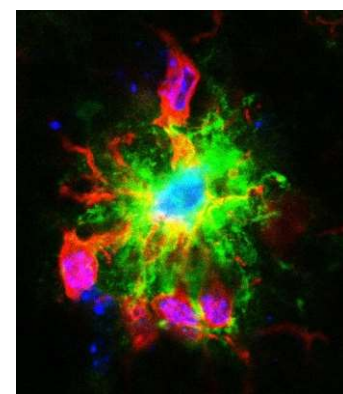


Figure 5. Microgliosis in an AD mouse brain. Microglia (red) are clustering around an Aβ plaque (green) in the brain of a 6-month-old female 5xFAD mouse. Blue stains are nuclei.

(Itagaki *et al.*, 1989). Similar activation has been described for the immune cells of the brain (microglia) in response to a pathogenic insult. This was first shown by Itagaki *et al.* (1989), who described human leukocyte antigen (HLA)-positive cells surrounding compact plaques. Figure 5 shows an example of microgliosis in a mouse AD brain, where microglia (red) are clustering around the plaque (green).

1.3 Immune cells in AD

The contribution of activated immune cells to AD pathology has been a matter of debate. Since the discovery of the triggering receptor expressed on myeloid cells (TREM2) as a risk factor for late onset AD by 2 separate groups simultaneously (Guerreiro *et al.*, 2013; Jonsson *et al.*, 2013) and the finding that the use of non-steroidal anti-inflammatory drugs (NSAIDs) may be preventive for the development of AD (reviewed in Imbimbo *et al.*, 2010), the focus on immune cells in AD has grown enormously. It is therefore important to understand the functioning of these cells in the context of AD. Microglia are the immune cells of the brain, making up 5-12% of the total population of brain cells (Lawson *et al.*, 1999). During development, microglia have important functions in pruning of synapses and clearance of superfluous neurons. In adult brain, microglia are important for the immune defence of the brain and play a role in the regulation of neurogenesis (Tremblay *et al.*, 2011). They can phagocytose dead cells and pathogens and release cytokines to regulate the inflammatory status in the brain. Microglia develop out of haematopoietic progenitor cells in the yolk sac and populate the brain around prenatal day 8 (Ginhoux *et al.*, 2010; Mizutani *et al.*, 2012). There they form a stable self-renewing population, without any replenishment by haematopoiesis (Askew *et al.*, 2017).

The morphology of microglia is highly dependent on the activation state. During the non-activated, so-called 'resting' state, microglia have a small soma and highly arborized processes (see figure 6), with which they continuously scan their environment. When a pathogen or dying neuron is found, microglia retract their processes, and the soma moves toward the site of injury (see figures 5 and 7). In this active state, microglia can phagocytose the malefactor and additionally release several pro-inflammatory cytokines (Nimmerjahn *et al.*,

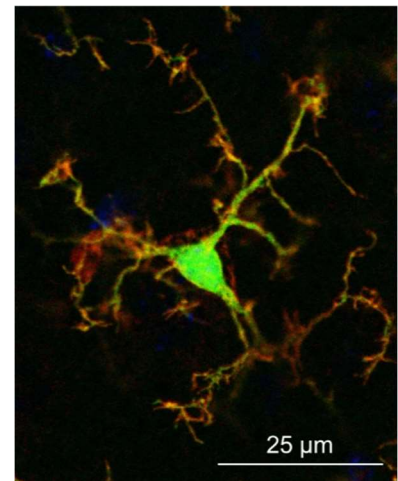


Figure 6. *In vivo* ramified morphology of microglial cell.

2005; Hanisch and Kettenmann, 2007). Several groups have shown that microglia are able to phagocytose A β , and therefore act neuroprotective during AD (Bolmont *et al.*, 2008; Lee *et al.*, 2010). Interestingly, microglia are associated specifically to focal plaques, not to diffuse plaques (D'Andrea *et al.*, 2004). It is hypothesized that this is due to the different mechanisms of formation of both plaque types. Focal plaques are thought to be remnants of dead neurons,

which contain different signalling factors to which microglia respond. Besides the neuroprotective effect of phagocytosis of A β , long-lasting activation of microglia can be detrimental to neuronal health, by resulting in a continuous release of inflammatory cytokines (Akiyama *et al.* 2000). Microglia are therefore described as a ‘double-edged sword’ in AD pathology (Naert & Rivest, 2013). One publication showed that upregulation of interleukin (IL)-1b resulted in increased neuroinflammation and a dramatic decrease of plaque pathology in AD mice (Shaftel *et al.*, 2008). Total ablation of microglia in another mouse model however showed no effect on plaque pathology, suggesting that microglia are less important in AD than anticipated (Gratwohl *et al.*, 2009) and other immune cells might play a role. In this regard, an important but unclear factor in this field of research is the contribution of putatively infiltrating immune cells originating from haematopoietic stem cells to AD pathology.

In 1968, van Furth and Cohn postulated a theory about the development of monocytes and macrophages, called the mononuclear phagocyte system theory (van Furth & Cohn, 1968).

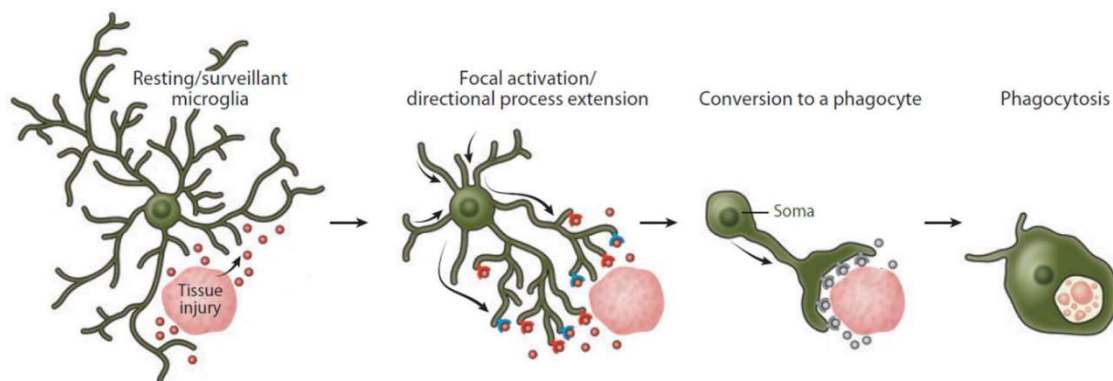


Figure 7. Activation of microglial cell and phagocytosis in response to tissue injury. Picture adjusted from Nayak *et al.*, 2014.

They hypothesized that all tissue macrophages develop from blood monocytes that are derived from bone marrow haematopoietic stem cells. Later findings showed that, although the general idea of the theory was correct, many details were different. After derivation from bone marrow cells, monocytes are stored in the spleen (Swirski *et al.*, 2009). Only a small proportion of monocytes circulates continuously in the bloodstream. Monocytes make up approximately 10% of white blood cells in human blood, and 4% in mouse blood (Auffray *et al.*, 2009). In case of inflammation, monocytes exit the spleen into the bloodstream and travel towards the site of infection. After entering the affected organ, they differentiate into macrophages (Geissman *et al.*, 2010). These cells can phagocytose pathogens and cellular debris and secrete both cytokines and growth factors.

Microglia were originally described as a population of infiltrated macrophages, until their separate yolk-sac derived lineage was discovered (Ginhoux *et al.*, 2010). Many other organs also contain resident macrophages independent of bone marrow derived monocytes, such as

the liver (Kuppfer cells), skin (Langerhans cells), spleen, lung, pancreas, and kidney (Schulz *et al.*, 2012; Yona *et al.*, 2013).

After these discoveries of separate populations of immune cells in specific organs, the consensus was that the blood brain barrier (BBB) prevented peripheral immune cells from entering the brain and microglia were solely responsible for the immune status of the CNS. In case of disease, however, peripheral immune cells can enter the brain and play a role in disease progression (El Khoury *et al.*, 2007; Ajami *et al.*, 2011). The production of the monocyte chemoattractant protein 1 (MCP-1, also called CCL2) by microglia confirms this process, because there are no cells present in healthy brain that express the receptor for this signalling factor: the C-C chemokine receptor type 2 (CCR2) (Saederup *et al.*, 2010; Mizutani *et al.*, 2012). The common hypothesis is therefore that CNS-produced CCL2 binds to CCR2 on peripheral immune cells, thereby attracting them to the brain to assist in the immune response. The upregulation of CCL2 in AD brain was shown in both human patients and mouse models (Ishizuka *et al.*, 1997; Simard *et al.*, 2006; Naert & Rivest, 2011). In addition, upregulation of CCL2 can cause a disruption of the BBB (Roberts *et al.*, 2012). Based on the important function of the CCL2-CCR2 axis, a reporter mouse line was created, which expresses red fluorescent protein (RFP) instead of CCR2 (CCR2^{+RFP}) (Mizutani *et al.*, 2012). The underlying idea is that the infiltrating immune cells in these mice are coloured red due to the production of RFP and can thereby easily be distinguished from the resident microglia. Simultaneously, there is a reduced expression of CCR2 in heterozygous CCR2^{+RFP}, or a knock-out in homozygous CCR2^{RFP/RFP} mice. This mouse line has since been used to investigate infiltration of immune cells in the brain in different disease models. In Tg2576 mice, overexpressing human APP with the Swedish mutation, a complete knock out of CCR2 had detrimental effects (El Khoury *et al.*, 2007): a higher mortality rate and increased A β levels were found, in a CCR2 gene-dose dependent manner. The authors hypothesized that the lack of CCR2 resulted in a lack of microglial accumulation. As described above, however, it has been found since then that microglia do not express CCR2 and the knock-out of this receptor is thus probably affecting the infiltration of peripheral immune cells, rather than microglial functioning. Naert and Rivest (2011) performed a similar study with another AD mouse model, APP_{Swe}/PS1. They found increased cognitive deficits and plaque pathology with a knock-out of CCR2 in this model and thus hypothesized that peripheral monocytes are important to contain AD pathology. Oppositely, other studies revealed increased A β pathology/accelerated cognitive deficits when CCL2 was overexpressed and decreased pathology/rescued cognitive performance when CCL2 was blocked (Yamamoto *et al.* 2005; Kiyota *et al.*, 2009a, 2009b). These studies suggest that reduced activation of immune cells has a protective effect against AD. Clearly, more research is required to understand the underlying mechanisms and elicit the role of both resident microglia and peripheral immune cells in AD mouse models.

1.4 Mouse models for AD

Animal models are used to discover target proteins for therapy and to test treatments for AD. Mice are most often used, because they can easily be genetically manipulated, and because they possess a high reproduction rate. Although many groups are investigating AD, and there is a high number of clinical studies ongoing (Cummings *et al.*, 2018), the treatments options for AD are currently limited. Almost all therapies that seemed effective in preclinical studies, failed in later clinical studies (Cummings, 2018). From the several hundred candidates that entered clinical trials, only 5 agents were brought onto the market. A possible explanation is the discrepancy between animal models that are used in preclinical studies, and human AD patients. The current animal models do not fully recapitulate the pathology seen in humans (Myers & McGonigle, 2019). The target discovery based on these animal models is therefore inefficient and leads to the failure of promising drugs in a clinical setting. Different mouse models have been generated over the past decades, which all recapitulate aspects of human AD pathology. Most models focus on A β pathology due to the strong influence of the amyloid cascade hypothesis and the well-described mutations in A β -related genes (Myers & McGonigle, 2019). It is known that plaques are not formed naturally in the mouse brain due to the differences between human and mouse APP. There is a homology of 96% between human and mouse APP protein, but 3 amino acids are different inside the A β primary sequence (Kirschner *et al.*, 1989; Podlisney *et al.*, 1991). The result is a lack of aggregation of mouse A β , whereas human A β is forming higher order aggregates. Therefore, mouse models for AD are generated by placing a mutated version of the APP and/or PSEN gene inside the mouse genome. These mutations, as explained in paragraph 1.1 and shown in figure 3, lead to an overproduction of A β (or a change in A β_{42} /A β_{40} ratio), which results in the formation of plaques in the murine brain and ultimately causes cognitive deficits.

A commonly used model, the 5xFAD mouse model, was generated by Oakley *et al.* (2006). Five familial AD mutations were combined to generate this model: the Swedish (K670N/M671L), London (V717I) and Florida (I716V) mutations in the human APP gene, as well as 2 mutations in human PSEN1 (M146L and L286V). The genes are overexpressed and controlled by the brain specific Thy1 promoter. Together, these 5 mutations result in a high amyloid load in the brains of 5xFAD mice as early as 2 months after birth.

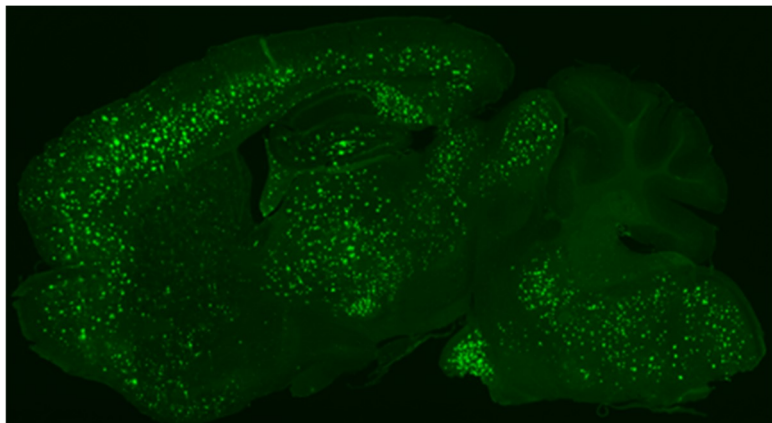


Figure 8. Plaques in the brain of a 5xFAD mouse. A sagittal brain slice of a 12-month-old female 5xFAD mouse was stained for A β (green, 6E10) and clearly shows a high plaque load spread throughout the brain.

The mice gradually develop plaque pathology, similar to human AD pathology (see figure 8). Cognitive deficits are first identified at an age of 6 months in these mice, for example in Y-maze (Oakley *et al.*, 2006; Ohno *et al.*, 2007) and Morris water maze (Urano & Tohda, 2010; Xiao *et al.*, 2013; Tang *et al.*, 2016). No tangles are formed in the brains of these mice, although hyperphosphorylation of tau is found already at an early age (Kanno *et al.*, 2014). In addition, the 5xFAD mouse line recapitulates the strong activation of microglia in AD (see figure 5) and is one of the few models exhibiting neuron loss at an early age (Oakley *et al.*, 2006; Wirths & Bayer, 2010).

Besides amyloid-based models, there are also several mouse models mimicking tau pathology. Since there is no known AD-related mutation in the tau gene, many models are based on the P301L or P301S mutations, which are related to frontotemporal dementia (Hutton *et al.*, 1998). Mice carrying this mutation develop tangle pathology, but no plaques, for example the JNPL3 line (Lewis *et al.*, 2000) and the htau.P301S line (Allen *et al.*, 2002). These mice show progressive motor deficits, rather than cognitive deficits, and therefore do not accurately model human AD. Importantly, many models currently on the market use overexpression of (mutated) human tau, by placing several copies of the human tau gene randomly inside the mouse genome. Furthermore, the original mouse tau gene is usually still present and also expressed at regular levels. These models therefore have unphysiologically high expression levels of tau. In addition, the presence of mouse tau seems to have a rescuing effect on AD pathology, both *in vitro* and *in vivo* (Ke *et al.*, 2012).

All these factors together might be an important reason for the failure of tau-based clinical studies (Cummings *et al.*, 2018). Treatments that are highly efficient in mouse models during preclinical studies, do not translate well to human AD patients, since the development of AD pathology is obviously still different in humans compared to mouse models. To better understand AD and find biologically relevant targets for the development of tau-directed medication, it is therefore important that mouse models with higher translational predictability are developed.

2. Goals of the thesis

There are currently no mouse models available that accurately model tau pathology in AD. This might be an important reason for the gap between successful preclinical studies and failure of clinical studies. We therefore generated a new mouse model for AD using whole gene replacement: the human tau knock-in (htau-KI) mouse line expresses the human wild-type (WT) tau gene instead of the murine tau gene, but under the same promoter. The model therefore possesses physiological tau expression without mutations, as seen in most of human AD patients. After successful generation, the following goals were defined:

- Characterization of the htau-KI mouse model.
- Crossing htau-KI mice with the well-known 5xFAD mouse model to study physiological levels of human tau under progressing cerebral amyloidosis and investigate the interplay between A β and tau.
- Investigating the immunological aspects of the newly generated model and the cross-bred model with 5xFAD.
- Confirming the importance of CCL2-CCR2 signalling in AD pathology and the infiltration of peripheral immune cells in 5xFAD mice.

Together, these investigations will help to understand AD pathology, both at the level of A β and tau, as well as at the level of neuro-immunology. The findings from this thesis might in future lead to the discovery of new targets for AD therapy development.

3. Materials & methods

Mice

In collaboration with Taconic Biosciences (Cologne, Germany), a human tau knock-in (htau-KI) mouse model was generated. Whole gene replacement was performed, as displayed in figure 9. The bacterial artificial chromosome RP11-111I23 was used to generate a targeting vector, which was transfected into mouse ES cells from the C57BL6/NtTac strain. Two validated ES clones were used to generate chimeric mice. Eight males and ten females were used as founders for breeding of the colony. Based on coat colour, the highest chimeric mice were picked and bred with C57BL6/N females. Germline transmission was confirmed by the birth of black offspring. Mice were subsequently genotyped to check the presence of the human tau and mouse tau genes (see primers in table I) and backcrossed to a C57BL6/J background. Subsequently, the htau-KI (homozygous) mouse line was cross bred with 5xFAD (Oakley *et al.*, 2006, commercially available from Jackson Laboratory (Bar Harbor, USA)) to generate groups for behavioural analysis. 5xFADxhtau-KI^{+/+} mice were compared to htau-KI^{+/+}, 5xFAD and WT mice. 5xFADxhtau-KI^{+/+} and htau-KI^{+/+} mice were generated by mating a 5xFADxhtau-KI^{+/-} mouse with a htau-KI^{+/+} mouse. WT controls and 5xFAD mice were generated by mating a 5xFAD mouse with a WT mouse. All 5xFAD mice were bred heterozygous. Age-matched phenotyping groups were generated using timed matings of 4 days.

The 5xFAD mouse line was also cross bred with the CCR2^{RFP/RFP} line (Saederup *et al.*, 2010, commercially available at Jackson Laboratory). WT, CCR2^{+/RFP} and CCR2^{RFP/RFP} mice were used as controls. Again, all mice had a had a C57BL6/J background and all 5xFAD mice were bred heterozygous.

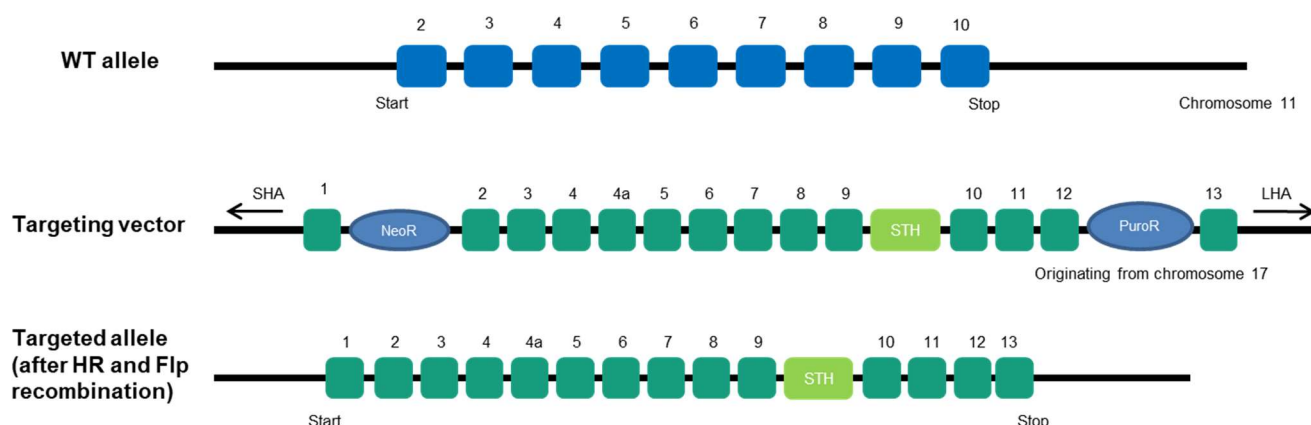


Figure 9. Targeting vector used to generate the htau-KI mouse line.

Housing

All experiments were performed in compliance with the directive 2010/63/EU, current German law and authorized under the following approval number: 42502-2-1371 MLU (Landesverwaltungsamt Halle, Saxony-Anhalt, Germany). Mice were group housed (maximum

5) in individually ventilated Type II long cages, with a regular 12-hour dark-light cycle. Food and water were available *ad libitum*. For electrophysiology, mice were bred in Halle (Germany) and transported to KU Leuven (Belgium) a minimum of 2 weeks ahead of testing. Mice were group housed in open cages in Leuven. Housing and animal procedures were approved by the KU Leuven Ethical Committee (project P181/2017). We confirm that all animal handling procedures were carried out in accordance with directive 2010/63/EU of the European Parliament and of the Council on the protection of animals used for scientific purposes, the Belgian and German Animal Protection Acts and recommendations from the Federation of European Laboratory Animal Science Associations (FELASA).

Genotyping

At the age of 19-21 days, ear punches were taken from each mouse as biopsy material for genotyping. After sacrificing the mice, tail tips were taken for confirmation of the genotype. DNA was isolated from the ear punches/tail tips using the 1-Step kit (Nexttec, Leverkusen Germany) according to manufacturer's protocol. The DNA was analysed for the presence of 5xFAD and htau genes using the GoTaq DNA Polymerase (Promega, Wisconsin, USA) to run a RT-PCR. Primers were specific for the different genes, and sequences are shown in table I. Samples were afterwards loaded onto a 1.6% agarose (VWR, Radnor, USA) gel in TAE buffer with ethidium bromide (Carl Roth, Karlsruhe, Germany) to visualize the PCR products. A 100bp DNA ladder (Fermentas, Waltham, USA) was used to estimate the size of the PCR products and a UV-Transilluminator Bio Doc-It™ Imaging System (VWR) used to visualize bands.

Buffer preparation

PB Buffer – 12.13g $\text{Na}_2\text{HPO}_4 \cdot 2\text{H}_2\text{O}$ and 3.1g NaH_2PO_4 were dissolved in approximately 800mL ultrapure water. pH value was adjusted to 7.4 using NaOH. 25mL sodium azide (1% aqueous, VWR) was added and volume filled up to 1L with ultrapure water.

PBS – 8g NaCl, 0.2g KCl, 1.44g $\text{Na}_2\text{HPO}_4 \cdot \text{H}_2\text{O}$ and 0.24g KH_2PO_4 (all Carl Roth) dissolved in 1L ultrapure water.

TBS – 8.766g NaCl and 6.057g Tris were dissolved in approximately 800mL ultrapure water. pH value was adjusted to 7.4 using HCl and the total volume subsequently filled up to 1L with ultrapure water.

Tris buffer – 6.057g Tris was dissolved in approximately 800mL ultrapure water. pH value was adjusted to 7.6 using HCl and the total volume filled up to 1L with ultrapure water.

4% PFA – 16% PFA (Life Technologies) diluted 4x in PBS (Life Technologies).

Behavioural studies

Mice were subjected to behavioural experiments in the light phase. The experimenter was blinded to the genotype of the mice for the complete duration of the tests, as well as the subsequent analysis of the videos. Behavioural experiments were performed in the order described below, sorted by increasing stress levels caused by the different tests.

Primary screening

Before starting full behavioural analysis, all mice were screened for general health. Weight, vision, hearing, grip strength, and mobility were tested.

Pole

To investigate motor skills and fear-related behaviour, mice were placed on a pole (height 50cm, diameter 19mm) in a type III cage filled with animal bedding. The pole was completely wrapped in anti-slipping tape, and a ball (diameter 2.5cm) was placed on top. Mice were placed on this pole in a vertical position, with the head pointing upwards, positioned just below the ball, or with the front paws on the ball. In a maximum period of 120 seconds, mice were supposed to turn around (head downwards, all 4 feet in a vertical position) and reach the floor. Mice performed 5 trials directly after another, with 10 seconds between the single trials, and 20 seconds prior to the first trial to explore the test cage. The average time over 5 trials (for turning around and reaching the floor) was compared between sex and genotype. If the mouse fell, or climbed down without completely turning around first, the time was set at 120 seconds.

Open Field

The mice were placed in 1 corner of the open field (Biobserve GmbH, Bonn, Germany) and allowed to explore freely for 10 minutes. Movement was recorded using an infrared camera (Biobserve) and the animal was tracked using the Biobserve Viewer system.

The open field was a square area of 53.8 x 53.8 cm, with walls of 50 cm. The floor was covered with animal bedding. An area of 10.5 cm along all 4 walls was considered as area close to the walls, the square of 32.8 x 32.8 cm in the middle was considered centre area. Percentage of time spent in the centre area was compared between genotypes and sexes as a measurement of anxiety.

Y-maze

The Y-maze set up (Biobserve) is a maze shaped like a Y, with different markings on each arm (see figure 10). The floor of the maze was covered with animal bedding. The mice were placed in arm A of the Y-maze set up and allowed to explore freely during a period of 10 minutes. Mice were recorded



Figure 10. Y-maze set up. The three arms of the y-maze are marked with different patterns, allowing the mice to orientate.

using an infrared camera (Biobserve) and the videos analysed manually. Subsequently, the percentage of perfect triads was calculated and compared between groups. A perfect triad means the mouse sequentially entered arms A, B and C in any order, without repeats.

Elevated plus maze

The setup was a plus-shaped maze with arms of 40 x 7.5 cm, placed 70 cm above the ground. Two of the arms had walls with a height of 20 cm (closed arms), the other two arms did not have walls (open arms). The floor of each arm was covered with animal bedding. Mice were placed in one of the closed arms and allowed to explore freely for 10 minutes. Movement was recorded using an infrared camera (Biobserve) and the animal was tracked using Biobserve Viewer software. The percentage of time spent in the open arms was compared between genotypes and sexes.

Rotarod

The rotarod protocol consisted of two days. On the morning of day 1, the mice went through a training phase. The rod rotated with a continuous speed of 4 rpm. As soon as the mouse was placed on the rod, a timer was started. The animals passed the training when they managed to stay on the rod for 60 consecutive seconds. A maximum of 16 training trials was performed, with a break of at least 15 minutes after the first 8 training trials. Mice that did not pass the training still performed the following testing sessions, but this was noted for analysis purposes. On the afternoon of day 1, the first testing session was performed. Two more testing sessions were performed on the morning and afternoon of day 2, with a 1-hour break between the two sessions. A testing session consisted of three runs per mouse, with an hour between each individual run. During these runs, there was a linear increase of rotation speed from 4rpm until 40rpm, over a time of 5 minutes. The maximum distance walked by each mouse in these 9 trials was compared between groups.

Morris Water Maze

The Morris water maze consisted of a round pool (diameter 120 cm) with white walls. A platform (diameter 10 cm) covered with white sports tape (thereby invisible) was placed inside, 8 mm below water level. The water temperature was 26°C ($\pm 0.5^\circ\text{C}$). Four differently coloured/shaped 3D environmental cues were attached to the side of the pool, to allow the mice to orientate. The protocol consisted of four days, with 4 swimming trials each day. The platform was always in the same position in the pool. For each trial, a mouse was placed in the pool, and allowed 60 seconds to swim and find the platform. If the mouse did not find the platform within 60 seconds, the experimenter led the mouse to the platform. When the mouse was on the platform (either by finding it or placed by the experimenter), it was left there for 10 seconds to orientate. The mice were subsequently dried with paper and warmed under a heat lamp for 5 minutes, followed by the next trial. Each trial, the mouse started in a different quadrant of the pool. The platform was in quadrant 3. During trial 1 and 4 of each test day, the

mice started in quadrant 1, opposite from the platform. The second trial the mice started in quadrant 2, and the third trial in quadrant 4. Movement of the mice was recorded using an infrared camera (Biobserve), and the animal was tracked using the Biobserve Viewer system. A learning curve over all 16 trials was drawn for each mouse (see figure 29) and the area under the curve was calculated. Average learning curves were compared between sexes and genotypes.

Fear conditioning

The fear conditioning protocol was performed using the automated fear conditioning system by TSE Systems (Bad Homburg, Germany). The system consists of a white box, with a grid-floored square area and replaceable walls inside. For the conditioning, plastic walls were used, and the mice were placed directly on the grid floor. The mice explored the area freely for 3 minutes, followed by a continuous sound for 28 seconds, followed by a 2 second foot shock (0.7 mA). Twenty-four hours later, two tests were performed to measure the strength of conditioning. First, mice were placed in the same area (plastic walls, grid floor) for 3.5 minutes. Secondly, mice were placed in an area with black floor and black walls, and after free exploration for 3 minutes, exposed to the continuous tone for 3 minutes. In both trials, the freezing duration of the mice was measured by the fear conditioning software (TSE Systems) and compared between genotypes and sexes.

Organ collection

After performing all behavioural experiments, mice were euthanized using CO₂ inhalation and perfused with 20mL PBS (Life Technologies, Carlsbad, USA). Whole blood was collected in lithium-heparin tubes (Sarstedt, Nümbrecht, Germany) and centrifuged for 10 minutes at 1920xg and 4°C, after which plasma was collected and fresh frozen on dry ice. Liver and spleen were collected and fresh frozen on dry ice. Tail tip was collected for confirmation of the genotype. The brain was collected and divided into two hemispheres; the left hemisphere was fresh frozen on dry ice, and the right hemisphere fixed in 4 % PFA. All fresh frozen samples were subsequently stored at -80°C. Spleens of WT, CCR2^{+RFP} and CCR2^{RFP/RFP} mice were collected fresh for splenocyte isolation or fresh frozen for RNA isolation.

Electrophysiology

Detailed methods are described in Barendrecht *et al.* (in preparation). In short, mice were sacrificed, the hippocampus immediately isolated and cut into 300 µm-thick slices using a custom-made tissue chopper for field potential recordings. The part of the right hemisphere containing medial hippocampus was cut into 400 µm-thick slices using a vibratome (Microm HM 650 V, ThermoFisher Scientific) for whole-cell recordings.

For extracellular recording of field potentials, hippocampal slices were afterwards placed in an incubation chamber (Warner Instruments, Hamden, Connecticut) and a multi-electrode array (MEA) system (Multi Channel Systems, Reutlingen, Germany) was used as described before (Bhattacharya *et al.*, 2017). Stimulation and recording were performed using a stimulus generator (SG 4002), MEA1060-BC amplifier, temperature controllers (TC, PH01) and software (MEA_Select, MC_Stimulus, MC_Rack) from Multi Channel Systems. A single electrode located at the level of the Schaffer collaterals in the CA1 region was selected for biphasic constant voltage stimulation and the evoked signal was measured in the electrode adjacent to the stimulation electrode (in anterograde direction of the Schaffer collaterals). An input/output curve was established using increasing stimulation intensities ranging from 0.5 to 4 V (at 0.5 V intervals). The intensity leading to 35% of the maximum of the input/output curve was calculated and subsequently used for all stimulations. Next, a series of paired-pulse stimulations with intervals of 10, 20, 50, 100, 200 and 500 ms was applied. Last, after obtaining a stable baseline, LTP was induced by 3xTBS (10 trains of 4 pulses at 100 Hz, with 200 ms intervals and 200 μ s pulse-width: 10-minute interval). Field extracellular postsynaptic potentials (fEPSPs) were recorded for at least 120 minutes after LTP induction. For analysis, raw data were extracted using MC_Rack software. fEPSP slope values were obtained with the region of interest set from peak-to-peak (10-90%), and all groups of 3 subsequent sweeps were averaged. Paired-pulse ratios were calculated by dividing the slope of the second fEPSP by the slope of the first. LTP recordings were normalized to the average baseline slope.

Whole-cell voltage clamp recordings of CA1 pyramidal cells were performed at RT using a MultiClamp 700B patch-clamp amplifier and pClampTM software (Molecular devices, San José, California), as previously described (Bhattacharya *et al.*, 2017). First, mini (m)EPSPs were recorded at the reversal potential for GABA_A receptor-mediated events (-60 mV), after which mini inhibitor postsynaptic potentials (mIPSPs) were recorded at the reversal potential for glutamatergic currents (+10 mV) with tetrodotoxin (1 μ M) present in the bath medium. To verify that mEPSPs were indeed glutamatergic, they were blocked at the end of the experiments by applying 20 μ M 6-cyano-7-nitroquinoxaline-2,3-dione (CNQX) and 10 μ M d-aminophosphonovalerate (d-APV). Similarly, mIPSPs were verified by blocking them with 100 μ M picrotoxin, a GABA_A receptor antagonist. Data were low pass filtered at 2 kHz and acquired at 10 kHz using Digidata 1440 and pClampTM 10 software. Offline analysis of mEPSP and mIPSP was performed using MiniAnalysis software (v.6.0.7, Synaptosoft, Decatur, Georgia). All electrophysiology experiments were performed by collaboration partners from the KU Leuven.

Isolation and cultivation of primary microglia

Primary microglia were isolated from brains of newborn (postnatal day 1-3) WT mice of the C57BL/6J strain. Mice of both sexes were used. Microglia were isolated using the shaking protocol as described by Barger and Basile (2001) with minor adaptations. In short, newborn mice were sacrificed by decapitation. Subsequently, brains were isolated, and meninges removed with sterile tools. Brains were homogenized using trypsin, and several triturating and washing steps. Homogenate of 2-3 brains was seeded in a 75 cm² cell culture flask coated with poly-L-ornithine (PLO) in DMEM:F12 with 10 % Fetal bovine serum (FBS) and 0.5 % Gentamycin (all Life Technologies). Flasks were washed after overnight incubation and stimulated with L929 conditioned medium (medium collected from regular culturing of L929 cells, see below) after 1 week. A cell layer of glia cells developed in the flask, on which microglia proliferated under the influence of the L929 conditioned medium. Microglia were collected by shaking the flasks for 5.5 hours at 70rpm and subsequently collecting the medium. Highly pure microglia were then seeded with 1x10⁶ cells per well in a 6-well plate for subsequent RNA isolation. Medium was changed after 30 minutes to remove dead cells. After culturing for 24 hours, microglia were lysed using lysis buffer from the Macherey Nagel RNA XS isolation kit. Alternatively, microglia were seeded with 250.000 cells per well in a 24-well plate for A β stimulation assay.

Culturing of L929 cells

L929 fibroblasts were seeded into a 75cm² cell culture flask (0.4x10⁶ for four days or 0.8x10⁶ for three days). The cells were grown in RPMI medium (Life Technologies) with 10 % FBS at 37°C and 5 % CO₂. Supernatant was collected every second day and whenever cells were passaged. The collected medium was filtered (20 μ m, cellulose acetate) and stored at -20°C. For passaging, flasks were washed with 10 mL warm PBS. After aspirating PBS, cells were detached by incubation with 3 mL trypsin for three minutes (37°C, 5 % CO₂). Live cell counts were performed using a cell counter (CASY, Schärfe System).

A β stimulation of primary microglia

Primary microglia isolated according to the protocol described above were seeded with 250.000 cells per well in a 24-well plate. After 30 minutes incubation at 37°C and 5 % CO₂, medium was changed to remove dead cells. Recombinant A β ₁₋₄₂ was provided by the Protein and Drug Biochemistry Unit of the Fraunhofer IZI. The peptide was dissolved in hexafluoroisopropanol (HFIP, 2,5 mg/mL). The organic solvent was evaporated using nitrogen. A solution of 22.2 μ L 0.1 M NaOH in PBS was utilized to resuspend 50 μ g peptide. The solution was diluted with 180 μ L medium with 0.5 % Gentamycin. Further on, an appropriate volume of medium containing 0.5 % Gentamycin was added to the diluted solution to yield a 5 mM A β ₁₋

⁴² solution. 500 µL of the diluted solution was added to each well and the cells incubated for 24 hours (37°C, 5% CO₂). Subsequently, the medium was collected for a CCL2 ELISA.

CCL2 ELISA

An ELISA, established by the Protein and Drug Biochemistry Unit of the Fraunhofer IZI-MWT, was performed to determine the concentration of CCL2 in the culture medium of primary microglia. A multiwell plate (MaxiSorp, VWR) was coated overnight at 4°C with rabbit anti-rat MCP1 antibody (Lifespan Biosciences, Seattle, USA; diluted 1:666.7 in PBS). The next day, wells were blocked with 200 µL PBS with 0.05 % Tween20 and 10 % FBS (2h, RT). Subsequently, wells were washed three times with 200 µL TBS-T. Samples were applied to the wells at a dilution of 1:50 in PBS containing 0.05 % Tween20 and 10 % FBS. After two hours incubation at 4°C, wells were washed three times with 200 µL PBS. 4 µg biotinylated rabbit anti-rat MCP-1 antibody (Peprotech, Rocky Hill, USA) and 8 µg Streptavidin-Peroxidase Polymer (Sigma Aldrich) were incubated (15 minutes RT). Subsequently, the mixture was diluted 1:200 in PBS with 0.05 % Tween20 and 10 % FBS. Next, 100 µL of the diluted detection complex was added to each well and incubated for one hour at 4°C, followed by 3 washing steps. 100 µL SureBlue (VWR) was added per well (30 minutes RT) and the reaction was terminated with 50 µL 1 M sulfuric acid per well. The CCL2 levels were determined photometrical (Sunrise Microplate Reader, Tecan, Männedorf, Switzerland) with a standard curve of murine pE1-MCP-1.

Isolation of bone marrow cells

Isolation of murine bone marrow cells was performed according to the protocol by Madaan *et al.* (2014). Briefly, a C57BL6/J mouse was euthanized by CO₂ inhalation. Both tibiae were removed, muscle tissue was cleaned away and the joints on both ends were removed to expose the interior marrow shaft. Subsequently, all bone marrow was flushed out of the medullar cavity with HBSS and collected in a 50 mL centrifugation tube. Clusters were disintegrated by vigorous pipetting. Afterwards, the cell suspension was diluted by adding 20 mL HBSS and washed three times (centrifugation at 200xg, 8 minutes, 4°C, followed by aspiration of the supernatant and resuspension in 20 mL HBSS). After the last washing step, the cell number was determined using trypan blue and a Fuchs-Rosenthal chamber. Subsequently the cell suspension was centrifuged (200xg, 8 minutes, 4°C) and the cell pellet resuspended in an appropriate volume of 1:1 mixture of sterile filtered, conditioned L929 medium and RPMI 1640 Medium, containing 10 % FBS and 0.5 % Gentamycin. Cells were seeded into a 24-well plate (7.5×10^5 cells/well) and cultivated. Medium was changed after 3 days and cells were lysed on day 6 of cultivation using lysis buffer from the Macherey Nagel RNA XS isolation kit. Purity of BMDM was confirmed with FACS analysis.

Splenocyte preparation

Whole spleen was extracted from WT (C57BL6/J), CCR2^{+RFP} and CCR2^{RFP/RFP} mice and cut into small pieces. Tissue was stored in ice-cold HBSS and transported to sterile working bench. Spleen pieces were transferred to 50 mL tube and incubated with 20 mL digestion buffer (PBS with 1 mg/L collagenase IV, 50 µg/mL DNase I and 1 % FBS) for 45 min at RT. Subsequently, solution was filtered through a 70 µm cell strainer and tissue pushed through using a 5 mL syringe plunger and strainer flushed with additional 10 mL of digestion buffer. Filtrate was centrifuged for 10 min (1400 rpm, 4°C) and supernatant discarded. Pellet was resuspended in 10 mL RBC lysis buffer and incubated for 5 min at RT, followed by another centrifugation (1400 rpm, 4°C, 10 min). Pellet was then resuspended in 10 mL FACS buffer (PBS with 3 % FBS) and cells were counted using trypan blue and a Fuchs-Rosenthal chamber. Splenocytes were diluted in an appropriate volume of FACS buffer (2×10^6 cells/mL) and measured using FACSCalibur (BD Biosciences, Franklin Lakes, USA). Results were analysed using FlowJo (BD Biosciences).

RNA isolation & qRT-PCR

RNA was isolated from small piece of fresh frozen left prefrontal cortex (after removal of olfactory bulb) or small piece of fresh frozen spleen tissue. The Nucleospin RNA kit (Macherey Nagel, Düren, Germany) was used according to manufacturer's protocol with some minor adjustments. TCEP (included in kit) was used instead of β-mercaptoethanol in the lysis step. Furthermore, RNA was eluted in 40 µL RNase free H₂O instead of 60 µL, and the eluate was loaded onto the spin column twice to retrieve higher RNA yield.

RNA was isolated from primary microglia and peripheral macrophages using the Macherey Nagel RNA XS isolation kit according to manufacturer's protocol, with similar minor adaptations. TCEP was used to supplement the lysis buffer and 500 µL lysis buffer was used per sample. In addition, the centrifugation after the last washing step was prolonged to 4 minutes and in the final elution step, the eluate (12 µL instead of 15 µL) was loaded onto the spin column twice to increase RNA yield. RNA concentrations were measured using Nanodrop 2000 (Thermo Fisher scientific, Waltham, USA). The cDNA was synthesized with random primers using the Superscript II kit (Invitrogen, Carlsbad, USA), according to manufacturer's protocol. For quantification of 3R- and 4R tau isoforms, 300 ng total RNA was used. Primers were specific for 3R- and 4R tau isoforms, as described in Ingelsson *et al.* (2006) and shown in table I. For quantification, a standard curve of double stranded 3R- and 4R tau DNA was generated. The double stranded DNA was ordered at Metabion (Planegg, Germany) and the sequences are shown in table I. Specificity of the primers and cDNA was confirmed by a lack of signal when 3R primers were incubated with 4R cDNA, and vice versa. A standard curve ranging from 30-300.000 molecules/µL was prepared. Two biological replicates were prepared

for each standard curve and the standard curve best fitting a linear equation ($R^2 > 0.98$) was used to calculate the respective numbers of 3R- and 4R tau molecules in each brain sample. The rotor-gene 3000 system (Corbett research, Mortlake, Australia) was used, and the SYBR Green kit (Applied Biosystems, Foster City, USA) according to manufacturer's protocol. For quantification of inflammation-related gene expression in spleen and brain tissue, qRT-PCR was performed with primers shown in table I. CT values were used to perform statistical comparisons, whereas $\Delta\Delta Ct$ values (normalized over control sample) were plotted for clarity of figures. $\Delta\Delta Ct$ values were calculated as described in Pfaffl (2001). For each biological replicate, three technical replicates were performed, and a maximum difference of 0.4 CT was allowed between technical replicates. If the difference was > 0.4 CT, the technical replicate was excluded. If the difference between all 3 technical replicates was > 0.4 CT, the biological replicate was excluded. Additionally, samples with an amplification rate below 1.6 or above 2.0 were excluded. If n was reduced to 1 due to exclusion of samples based on qRT-PCR results, sample was excluded from statistical analysis.

NanoString

The NanoString mouse AD panel (NanoString Technologies, Seattle, USA) was used to analyse the expression levels of 770 AD specific genes in 48 different mice. WT mice were compared to 5xFAD, htau-KI and 5xFADxhtau-KI mice. We investigated mice of 7 and 13 months of age, of both sexes, n=3. RNA from prefrontal cortex was isolated with the Macherey Nagel Nucleospin RNA isolation kit, as described above. First, the NanoString panel required an overnight hybridization step. 100-150 ng of RNA was incubated with the reporter and capture probes for 16.5 hours, as described in the NanoString protocol. After hybridization, the samples were placed in the NanoString Prep station and run with high sensitivity settings. Finally, the cartridge was prepared in the Prep station and read in the analyzer, with MAX data resolution. The NanoString panel was performed at the institute of human genetics of the MLU Halle with the help of Kerstin Körber-Ferl.

Mouse-human co-expression data comparison

In collaboration with JAX, the data from our NanoString panel were compared to data from *post-mortem* human AD brains, according to the detailed methods described in Barendrecht *et al.* (in preparation). In short, differential gene expression analysis was performed for each genotype and sex compared to female WT mice. These values were correlated to data from over 2,000 human brain samples from three independent late-onset AD cohorts. The data is subdivided into 30 AMP-AD modules, which are divided over 5 specific consensus clusters consisting of overlapping co-expression modules associated with specific AD related changes across studies and brain regions

The correlation between changes in expression (log fold change) was computed for each gene in each specific expression module with each mouse model, sex, and age. Correlation coefficients were obtained using `cor.test` function built in R as:

$$\text{cor.test}(\text{LogFC}(h), \text{LogFC}(m)) \quad (1)$$

where $\text{LogFC}(h)$ is the log fold change in transcript expression of human AD patients compared to control patients and $\text{LogFC}(m)$ is the log fold change in expression of mouse transcripts compared to control mouse models. To determine the age-, genotype-, and sex-specific effects, a multiple linear regression analysis was performed.

Gene Set enrichment analysis in mouse and human data

Additionally, gene set enrichment analysis based on the method proposed by Subramanian *et al.* (2005) was performed using the cluster profiler package in the R software environment for the KEGG pathway database. Briefly, human data with log fold changes for the seven AMP-AD brain regions was obtained through synapse (<https://www.synapse.org/#!/Synapse:syn14237651>). Only orthologous genes on the NanoString Mouse AD panel were selected and KEGG pathway enrichment was performed for each brain region independently to identify significantly up- and downregulated gene sets. For the mouse data, differential expression analysis between the 5xFAD and 5xFADxhtau-KI models was performed to obtain a list of fold changes highlighting genes that are either up- or downregulated in the presence of htau on the 5xFAD background. Enrichment scores for all significantly associated KEGG pathways were computed to compare relative expression on the pathway level between *post-mortem* brain samples and the 5xFADxhtau-KI mouse model. Finally, we extracted the leading-edge gene set which identified the genes that appeared in the ranked list at or before the point at which the running sum reaches its maximum deviation from zero. This leading-edge subset can be interpreted as the core that accounts for the gene set's enrichment signal. The comparison of our mouse data to human co-expression modules, including all statistical analyses, was performed by collaboration partners at Jackson Laboratories.

Immunohistochemistry

The right hemisphere was fixed in 4 % PFA for 2 days at 4°C, followed by incubation in 30 % sucrose solution at 4°C. After a minimum of 2 days, the organs were washed in PBS, and subsequently frozen in Tissue-Tek O.C.T. (Sakura Finetek, Alphen aan den Rijn, the Netherlands) in plastic moulds. Sagittal slices (30 µm) of the hemisphere were prepared using a cryomicrotome (Cryostar NX70, Thermofisher Scientific), starting in the centre of the brain. Slices of the hippocampal region were collected in 24-well plates and stored at 4°C in PB buffer

containing 0.025 % sodium azide until staining. Immunohistochemical staining for the newly generated htau-KI mouse model was performed by Stefanie Geissler.

For free-floating 3,3'-diaminobenzidine (DAB) staining, the slices were washed in TBS (5 min, RT), after which the endogenous peroxidase was blocked by incubation with 1 % H₂O₂ in 60 % MeOH (30 min, RT). Subsequently, the slices were washed 3 times in TBS, followed by blocking with 5 % goat serum in 0.3 % Triton-X TBS (30 min, RT). For mouse on mouse staining, M.O.M. reagent (Vector Laboratories, Burlingame, California) was added during the blocking step. The primary antibodies (see table II) were diluted in 5 % goat serum 0.1 % Triton-X TBS, and the slices incubated overnight at 4°C in a humidified chamber. The following day, slices were washed in TBS 3 times, followed by incubation with the respective secondary antibodies (see table II), which were diluted in 2 % BSA TBS (1h, RT). After another 3 washes in TBS, slices were incubated with ExtrAvidin® Peroxidase (Sigma Aldrich, St. Louis, USA), diluted 1:1000 in 2 % BSA TBS (1h, RT), followed by 2 times washing in TBS, and 1 time in Tris buffer. DAB staining was performed by incubating slices in 0.05 % DAB 0.015 % H₂O₂ in Tris buffer (8 min, RT). Subsequently, the slices were washed once in Tris buffer and once in TBS, followed by placing the slices on glass slides, coated with protein glycerol (Carl Roth). After air drying the sections, the slides were dehydrated by submersion in ethanol absolute twice, followed by submersion in ROTI®-Histol (Carl Roth). Finally, the slices were embedded using Permount mounting media (Fisher Scientific, Hampton, New Hampshire) and closed with cover slips. Slides were stored at RT. For free-floating immunofluorescent staining, the protocol was the same as for DAB staining, with the following exceptions: there was no blocking of endogenous peroxidases on day 1. On day 2, after the secondary antibody incubation, the protocol was as follows: two times washing in TBS, followed by one washing step in aqua dest. Slices were then counterstained with DAPI (Life Technologies, 1 µg/mL), in ice cold methanol (2 min, RT, in the dark). After washing 2 times in TBS, the slices were placed on slides, dehydrated, and embedded as described for the DAB staining. Slices were recorded with a BZ-9000E microscope (Keyence, Osaka, Japan) and subsequent quantification of plaques was performed using the BZ-II-Analyzer software (Keyence).

Biochemical analyses

Fresh frozen left-brain hemispheres were homogenized using the following protocol: Frozen brain was transferred to a dounce tissue homogenizer, after which 1 mL of cell extraction buffer (Invitrogen) was added. Brain was mechanically homogenized, followed by incubation on ice for 30 minutes. Every 10 minutes, the homogenate was vortexed and resuspended. Subsequently, the samples were centrifuged for 30 minutes at 13000xg and 4°C. The supernatant was collected in a fresh tube, and both supernatant and pellet were stored at -20°C until further use. Human primary cortical neurons (used as a Western blot control) were

differentiated from human neuronal progenitor cells purchased from a commercial vendor (Axol Bioscience, Cambridge, United Kingdom) according to manufacturer's protocol. Mouse primary neurons (also used as a Western blot control) were isolated from embryonic brain tissue (embryonic day 13) and cultured for 4 days in Neurobasal medium + B-27 supplement + 0.05 % Gentamicin (ThermoFisher Scientific). Pellets of both cell types were homogenized in cell extraction buffer according to manufacturer's protocol and stored at -20°C until further use.

Western blot

Brain homogenates (supernatants from step described above) were thawed, and protein concentration measured using the Pierce Bradford assay (Thermo Fisher Scientific) according to manufacturer's protocol. Selected brain extracts were also dephosphorylated using lambda phosphatase as described elsewhere (Saito *et al.*, 2019). SDS Page was performed using the NuPage system and reagents (Thermo Fisher Scientific), according to manufacturer's protocol. The PAGERuler plus prestained protein ladder, 1.0mm Bis Tris gels with 12 wells and MES SDS running buffer (all Thermo Fisher Scientific) were used and the gel was run for approximately 35 minutes at 200V. For splitting different tau isoforms on a gel, a 4-20 % Tris glycine gel (Serva Electrophoresis GmbH, Heidelberg, Germany) was run for 4 hours at 80 V with a tau ladder (Sigma Aldrich). For subsequent western blotting, the semi dry system by Galileo Biosciences (Cambridge, USA) was used according to manufacturer's instructions. Proteins were blotted on 0.2 µm nitrocellulose membranes (Amersham Biosciences, Little Chalfont, UK) for 90 minutes at 38 mA. Afterwards, the membrane was blocked while floating for 30 minutes in a box with 5 % milk (Carl Roth) 0.05 % Tween TBS, under continuous shaking. The membrane was then placed in a 50 mL tube, with the protein side to the inside. The primary antibody was dissolved in 5 % milk 0.05 % Tween TBS and the membrane incubated overnight at 4°C on a roller bank. Different antibodies and concentrations are shown in table II. The following day, the membrane was washed 3 times 5 minutes with 0.05 % Tween TBS, after which it was incubated with the secondary antibody, also diluted in 5 % milk 0.05 % Tween TBS (1 hour at RT, on roller bank). Subsequently, the membrane was washed twice with 0.05 % Tween TBS, and once with TBS (all washes 5 min, RT, on a roller bank). For protein detection, the SuperSignal West Femto or Pico kit (Thermo Fisher scientific) was used according to manufacturer's protocol. The Fusion system (Vilber, Collégien, France) was used to visualize protein bands.

Statistics

All graphs were made using Graphpad Prism 6 (Graphpad Software, San Diego, USA). Statistics were performed using either Graphpad Prism 6 for one-way ANOVA or JASP 0.9.2.0 (University of Amsterdam, the Netherlands) or Microsoft Excel for non-parametric two-way

ANOVA. A one-way ANOVA was used to compare 3R- and 4R gene expression levels and area of 3A1 staining between different mice. A two-way ANOVA was used to compare inflammation-related gene expression in brain and behavioural results. First, Levene's test was used to check for equal variances, and Q-Q plots were analysed to check for a normal distribution. Data sets that failed the assumption of equal variances, or were not normally distributed, were transformed: a log transformation was used for pole turn and pole down time (12M), and a square root transformation was used for the elevated plus maze (12M). A two-way ANOVA with post hoc Tukey's was subsequently used to examine the effects of genotype and sex on the different behavioural outcome parameters. When the assumptions were still not met after transformation (weight, pole turn time and pole down time (6M) and open field and rotarod (6 and 12M)), an ordered logistic regression was used, with the help of Dr. Robby Schönfeld. When statistically significant differences were found, post hoc Tukey's test was used. When multiple significant differences of different factors were found, a pre-processing step was used to align the data, according to Bortz (2008), with the help of Dr. Robby Schönfeld.

For electrophysiology, statistical analysis was performed by our collaboration partners in Leuven, as described in Barendrecht *et al.* (in preparation). In short, time series were tested using two-way repeated measures (RM-)ANOVA and Tukey's or Dunnett's multiple comparisons test in GraphPad Prism 8. Because of significant differences in variance between samples of mEPSPs and mIPSPs, they were analysed by Welch's One-way ANOVA test using the two-stage linear step-up procedure of Benjamini, Krieger and Yekutieli to correct for multiple testing. The Kolmogorov-Smirnov test was used to compare cumulative distribution functions of mEPSPs and mIPSPs.

For comparison of the NanoString gene expression data to human *post-mortem* tissue, statistical analysis was performed by our collaboration partners from Jackson laboratories, as described in Barendrecht *et al.* (in preparation). In short, all counts were log-transformed from normalized count values. Differential gene expression analysis was performed using the voom-limma package in R to test the differences between each mouse model and sex. The correlation between changes in expression (log fold change) across species was computed for each gene in a given expression module with each mouse model, sex and age. As described above, the `cor.test` function in R was used to obtain correlation coefficients for all co-expression module comparisons. Gene set enrichment analysis was performed by the collaboration partners from Jackson Laboratories using the clusterprofiler package in R for the KEGG pathway database.

Table I - Primers

All used primers and double stranded cDNA were ordered at Metabion.

Gene	Forward primer (5' - 3')	Reverse primer (5' - 3')
Human 4R tau	GAA GCT GGA TCT TAG CAA CG	GAC GTG TTT GAT ATT ATC CT
Human 3R tau	AGG CGG GAA GGT GCA AAT AG	TCC TGG TTT ATG ATG GAT GTT
Mouse GAPDH	ACT CCA CTC ACG GCA AAT TC	TCT CCA TGG TGG TGA AGA CA
5xFAD tg	CTA GGC CAC AGA ATT GAA AGA TCT	GTA GGT GGA AAT TCT AGC ATC ATC C
5xFAD int. contr.	AAT AGA GAA CGG CAG GAG CA	GCC ATG AGG GCA CTA ATC AT
Human tau	CTT GTC CCC AAC TCC ATA CC	GGA GAA CAC AGA CTG TGC TCC
Mouse tau	CTT GTC CCC AAC TCC ATA CC	ACT GCT TGA GTT ATC TTG GCC
CCR2	CCT GCA AAG ACC AGA AGA GG	CAA GGC TCA CCA TCA TCG TA
CCL2	AGG TCC CTG TCA TGC TTC TG	TCT GGA CCC ATT CCT TCT TG
IL1a	CGC TTG AGT CGG CAA AGA AAT C	GTG CAA GTC TCA TGA AGT GAG C
IL1b	CAG GCA GGC AGT ATC ACT CA	AGC TCA TAT GGG TCC GAC AG
TNFa	GAA CTG GCA GAA GAG GCA CT	AGG GTC TGG GCC ATA GAA CT
3R cDNA	CCAGCCGGGAGGCGGGAAGGTGCAAATAGCTACAAACCAGTTGACCTGAGCAAGG TGACCTCCAAGTGTGGCTCATTAGGCAACATCCATCATAAACCAGGAGGTGGCCAG	
4R cDNA	AATTAATAAGAAGCTGGATCTTAGCAACGTCCAGTCCAAGTGTGGCTCAAAGGATAA TATCAAACACGTCCCGGGAGGC	

Table II - Antibodies

Antibody	Concentration		Product number	Manufacturer
	WB	IHC		
Human tau (7e5)	1µg/mL	-	847-0102006301	Analytik Jena (Jena, Germany)
Total tau (Tau-5)	1:1000	-	AHB0042	Life technologies
GAPDH	1:1000	-	21185	Cell signaling (Danvers, USA)
3R tau (RD3)	1:2000	1:100	05-803	Merck (Burlington, USA)
4R tau	1:2000	1:250	CAC-TIP-4RT-P01	Cosmo Bio (Tokyo, Japan)
PHF1	-	1:250	-	Peter Davies
MC1	-	1:50	-	Peter Davies
CP13	-	1:150	-	Peter Davies
Amyloid β (3A1)	-	1:1000 (DAB) 1:100 (IF)	825201	Biologend (San Diego, USA)
Amyloid β (6E10)	-	1:1000	SIG-39320	Biologend
GFAP	-	1:2500 (DAB) 1:1000 (IF)	Z 0334	Dako Agilent (Santa Clara, USA)
Iba1	-	1:1000 (DAB) 1:500 (IF)	019-19741	Wako Chemicals (Osaka, Japan)
MHCII	-	1:500	14-5321-81	Thermofisher Scientific
Cy3 rabbit IgG	-	1:500 (GFAP/Iba1)	111-165-144	Dianova (Hamburg, Germany)
Cy2 mouse IgG	-	1:100 (3A1, 6E10)	115-225-166	Dianova
Cy5 rat IgG	-	1:200 (MHCII)	712-175-153	Dianova
HRP mouse IgG	1:2000 (7e5/3R/Tau-5)	-	7076	Cell signaling
HRP rabbit IgG	1:1000 (GAPDH) 1:2000 (4R)	-	7074	Cell signaling
Biotin Mouse IgG1	-	1:100 (PHF1/MC1/CP13) 1:1000 (3A1)	115-065-205	Dianova
Biotin Mouse IgG	-	1:100 (3R)	A16076	Invitrogen
Biotin Rabbit IgG	-	1:100 (4R) 1:1000 (GFAP/Iba1)	A16108	Invitrogen

4. Results

Analysis of tau gene and protein expression in newly generated htau-KI mice

htau-KI mice were generated by whole gene replacement as described in the methods section. To confirm the knock-in of human tau and the simultaneous knock-out of mouse tau, a reverse transcriptase polymerase chain reaction (RT-PCR) with primers specific for mouse and human tau was performed to test DNA isolated from ear biopsies of different mice. As shown in figure 11a, the homozygous htau-KI mouse does not have mouse tau, but only human tau. Additionally, a Western blot with a human tau specific antibody (7E5) revealed a positive signal for all htau-KI mice and no signal for a WT mouse (figure 11b), confirming the success of the model at protein level. Finally, the protein expression level of tau was equal between WT mice and htau-KI mice as shown using a pan-tau antibody (Tau-5) on Western blot (figure 11c and d), confirming the endogenous expression levels in the newly generated htau-KI mice.

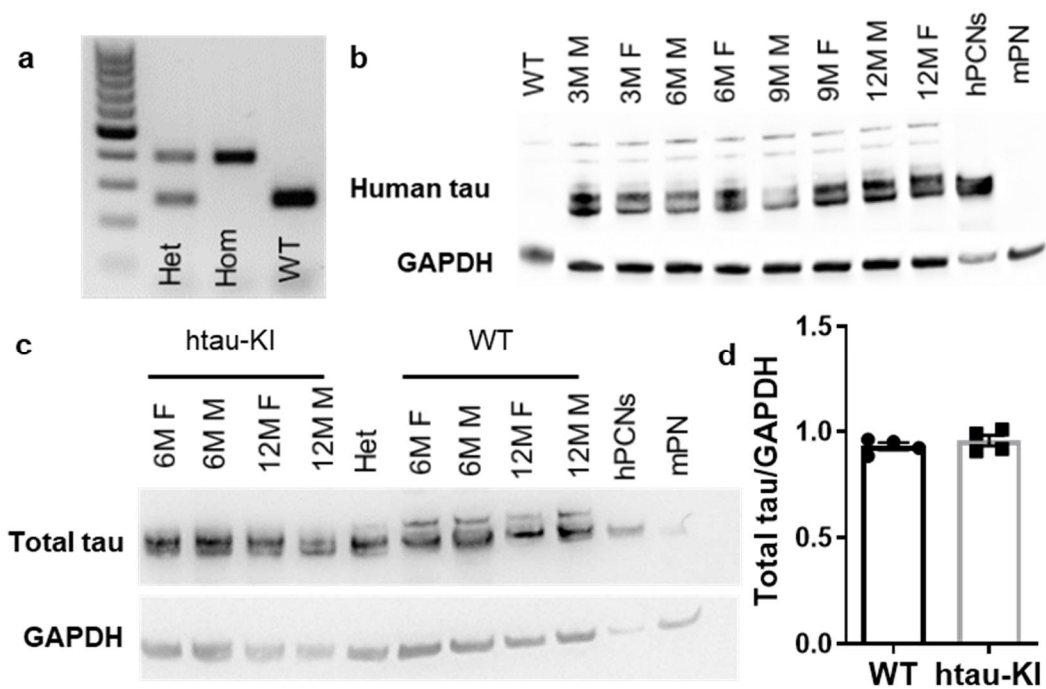


Figure 11. Confirmation of gene- and protein expression of human tau. (a) RT-PCR confirmed the loss of the mouse tau and the presence of the human tau gene. Het = heterozygous, Hom=homozygous. (b) Western blot with 7E5 showed protein expression of human tau. hPCNs = human primary cortical neurons, mPN = mouse primary neurons, xM = age in months, M = male, F = female. (c,d) A Western blot with Tau-5 and subsequent quantification of Tau-5 staining over GAPDH staining confirmed the endogenous expression levels of tau in htau-KI mice. Graph shows mean \pm SEM, n=4.

Analysis of the expression of tau isoforms

Various methods were subsequently used to investigate the expression of different isoforms of tau in htau-KI mice. First, immunohistochemistry showed 3R- and 4R tau expression in the brains of htau-KI mice (figure 12a), while WT mice only express 4R tau. Western blots with 3R- and 4R tau specific antibodies revealed that the htau-KI mice express all 6 isoforms of tau, as seen by the 3 bands in each blot in figure 12b. There was again no signal for 3R tau in WT mice and there seemed to be an increase in 3R tau expression with aging. Interestingly, human primary cortical neurons were used as a positive control but did not show 4R tau expression. Finally, using isoform specific primers as well as a standard curve of double stranded DNA, (described by Ingelsson *et al.*, 2006), the mRNA expression of 4R tau was quantified in mouse brains. The results in figure 13a revealed that 4R tau expression is significantly different between groups ($F_{15,31}=53.57$, $p<0.0001$). Post hoc testing showed a decreased expression of 4R tau in htau-KI and 5xFADxhtau-KI mice compared to WT and 5xFAD. Furthermore,

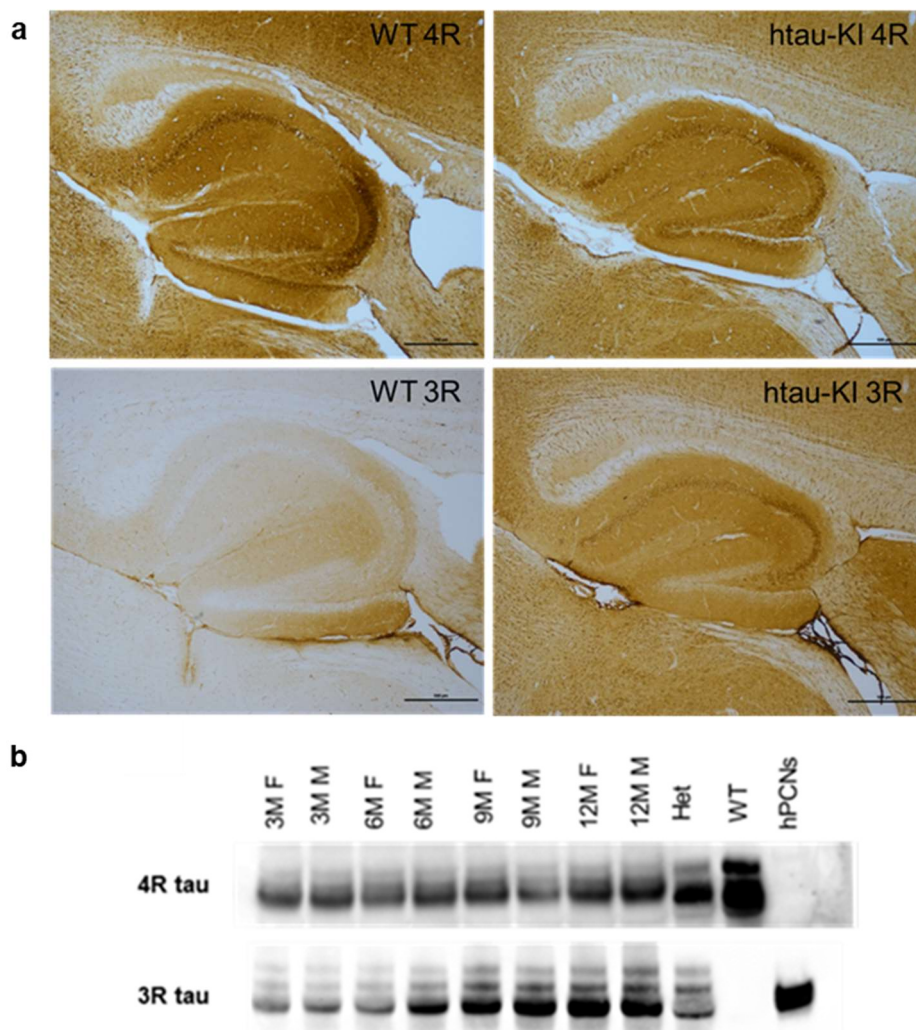


Figure 12. 3R- and 4R tau expression in htau-KI mice. (a) Immunohistochemistry showed only 4R expression in WT mice (left) and both 3R and 4R expression in htau-KI mice (right). Brains shown are 13-month-old female mice. (b) A Western Blot revealed that all 6 isoforms of tau are expressed in htau-KI mice and only 4R tau isoforms are expressed in WT mice.

significantly higher 4R tau expression was found in young WT mice than in old WT and all 5xFAD mice. Subsequently, isoform specific primers and a standard curve of double stranded DNA were also used to quantify 3R tau expression in htau-KI and 5xFADxhtau-KI mice. WT and 5xFAD mice were also tested but gave no signal in qRT-PCR due to the lack of 3R expression, as shown already in figure 12, as well as in literature. The results of the 3R tau quantification revealed no significant differences between genotypes, sexes, or ages (figure 13b). Another important outcome measurement is the ratio of 4R- to 3R isoforms. The exact quantification of the number of molecules allowed a calculation of the ratio of 4R/3R in htau-KI and 5xFADxhtau-KI mice (figure 13c). No significant differences were found and a ratio of approximately 0.05 for all samples. This means there is a 20-fold overexpression of 3R tau mRNA compared to 4R tau in htau-KI and 5xFADxhtau-KI mice.

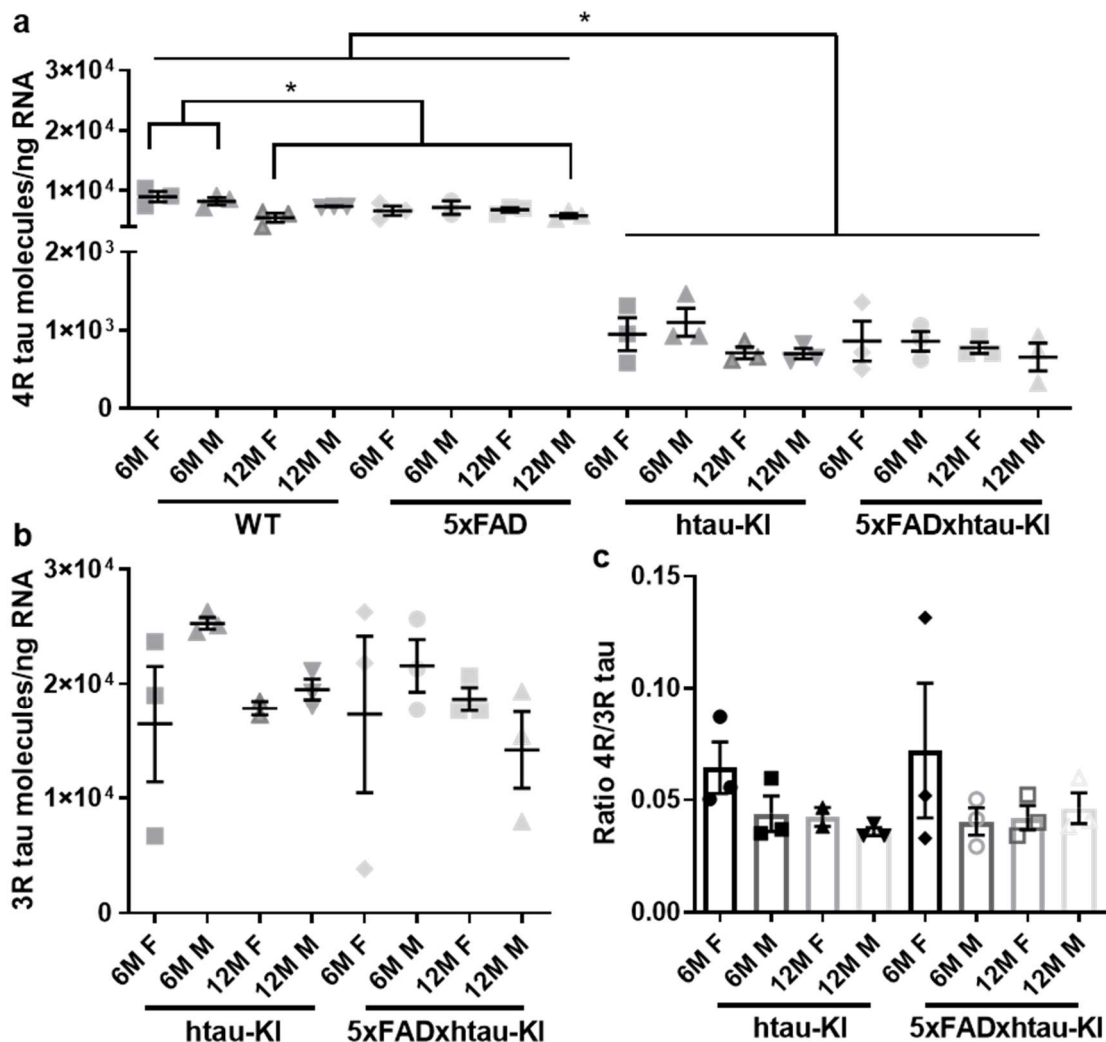


Figure 13. Quantification of 3R- and 4R tau mRNA expression in htau-KI mice. (a) qRT-PCR with isoform specific primers and a standard curve of double stranded DNA was used to quantify 4R tau molecules in WT, 5xFAD, htau-KI, and 5xFADxhtau-KI mice of both sexes and at the ages of 6- and 12-months. (b) The same approach was used to quantify 3R tau molecules in htau-KI and 5xFADxhtau-KI mice, whereas no signal was found for WT and 5xFAD mice for 3R tau. (c) The ratio of 4R/3R was calculated based on the exact quantification shown in a and b. n=2-3, One-way ANOVA was used to compare samples. *p<0.05.

Subsequently, several attempts were made to quantify the protein expression levels of 3R- and 4R tau, to investigate whether this 20-fold overexpression of 3R tau was also translated to protein level. Because different antibodies were used for the blots in figure 12, with possibly different binding propensities, no quantification could be based on these blots. Staining of all tau isoforms with the same antibody was therefore attempted by using a ladder of tau isoforms (figure 14). Additionally, the brain lysates were dephosphorylated to allow the distinction between the isoforms on Western blot. As shown in figure 14a, although the six tau isoforms in the ladder were split, the tau in brain lysates appeared as a smear using 7E5 staining. Similarly, 4R tau staining revealed 3 clear bands for the tau ladder in figure 14b, whereas the brain lysates did not show such a clear distinction. Further optimization of the Western blot conditions is thus required to allow quantification of the different tau isoforms at protein level.

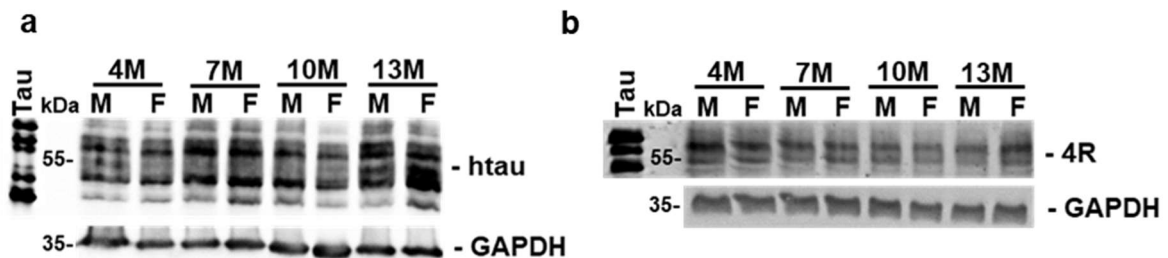


Figure 14. Expression of different tau isoforms in dephosphorylated brain extracts analysed by Western blot. Analysis of tau isoforms in male (M) and female (F) htau-KI mice at different ages and in comparison to a tau marker using the human tau-specific antibody 7E5 (a) and a 4R tau specific antibody (b). Some individual tau bands are visible after dephosphorylation of the protein extract by lambda phosphatase, but not sufficiently to quantify the level of protein expression. GAPDH was used as a loading control.

Immunohistochemical characterization of tau and A β pathology

To investigate the levels of tau phosphorylation and pathology under progressing amyloid pathology in htau-KI mice, immunohistochemistry was performed on brain tissue of 7 and 13-month-old mice. Different types of phosphorylated tau were stained, but no tangle pathology was found. Dystrophic neurites, which stained positive for phosphorylated tau, were found specifically around amyloid deposits (see figure 15). Interestingly, specific regions showed a high load of dystrophic neurites: superior colliculus, brain stem, striatum, hypothalamus, and cingulate gyrus (see figure 15a).

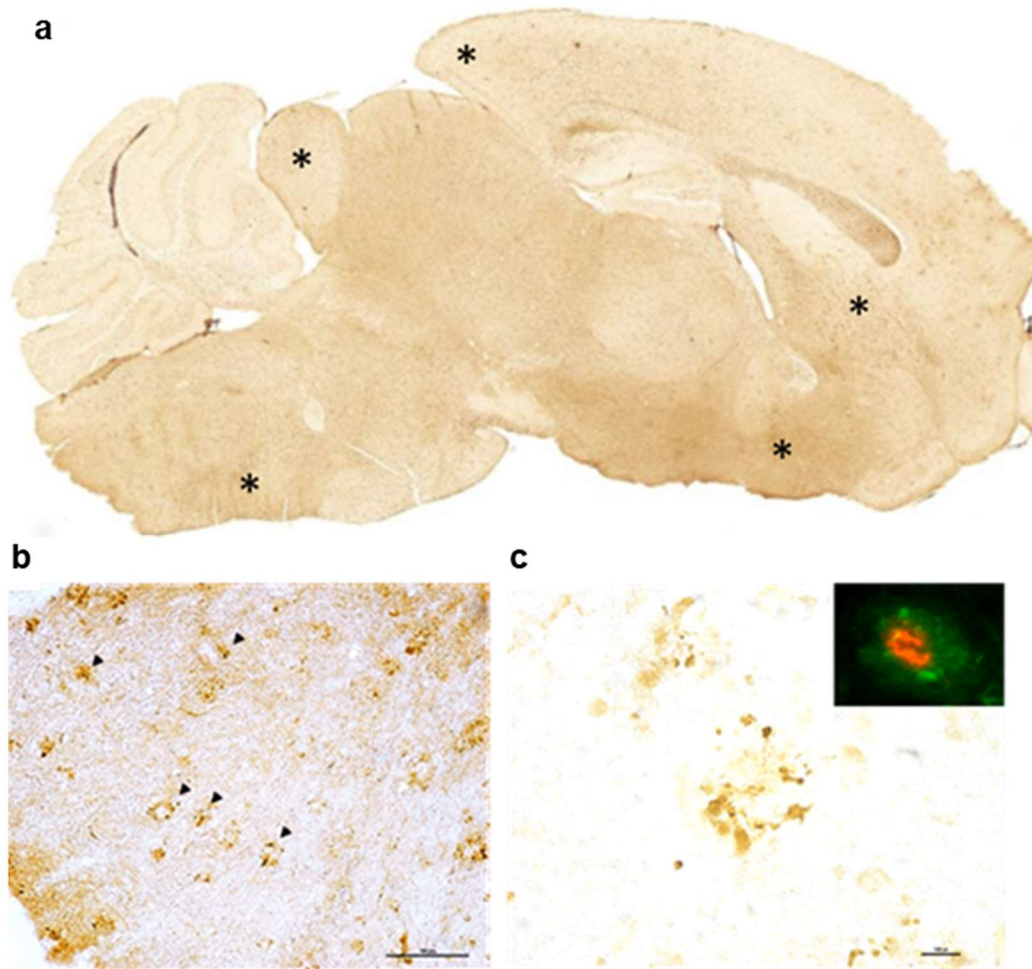


Figure 15. Dystrophic neurites in 5xFAD and 5xFADxhtau-KI mice. Plaque-associated dystrophic neurites were positive for PHF1 and CP13 in several brain areas in 13-month-old mice. (a) sagittal slice of a 17-month-old 5xFADxhtau-KI female stained with PHF1. * areas with high load of dystrophic neurites. (b) Higher magnification image (DAB: 20x) of the superior colliculus of a 13-month-old female 5xFAD mouse. PHF-1⁺ neurites are depicted by arrow heads. Scale bar: 100 μ m (c) DAB staining (magnification: 60x) of CP13⁺ material in the hypothalamus of a 13-month-old female 5xFADxhtau-KI mouse. Scale bar: 35 μ m. Inset confirms that the dystrophic neurites are plaque related (red = A β , green = PHF1).

Both 5xFAD and 5xFADxhtau-KI mice revealed PHF1 (phospho-Ser396/Ser404) and CP13 (phospho-Ser202) positive dystrophic neurites, which were plaque-related (figure 15b and c). WT and htau-KI mice showed no signal for PHF1 and CP13 (results not shown). Interestingly, staining with the antibody MC1 (confirmation specific tau antibody) revealed specific staining in htau-KI and 5xFADxhtau-KI mice only at the age of 13 months (figures 16-21). Hypothalamus, brain stem, and cortex of female and male mice of all 4 genotypes were stained at the age of 7 and 13 months. In the hypothalamus at the age of 7 months (figure 16), there was a stronger signal for MC1 in htau-KI and 5xFADxhtau-KI, especially in females. In males the staining was only visible in 5xFADxhtau-KI in small clusters (see arrowheads in figure 16). At 13 months of age (figure 17), the hypothalamus was strongly MC1-positive in both male and female htau-KI and 5xFADxhtau-KI. In 5xFADxhtau-KI, the staining was clustered, probably around amyloid plaques, whereas the staining was more widespread in htau-KI mice,

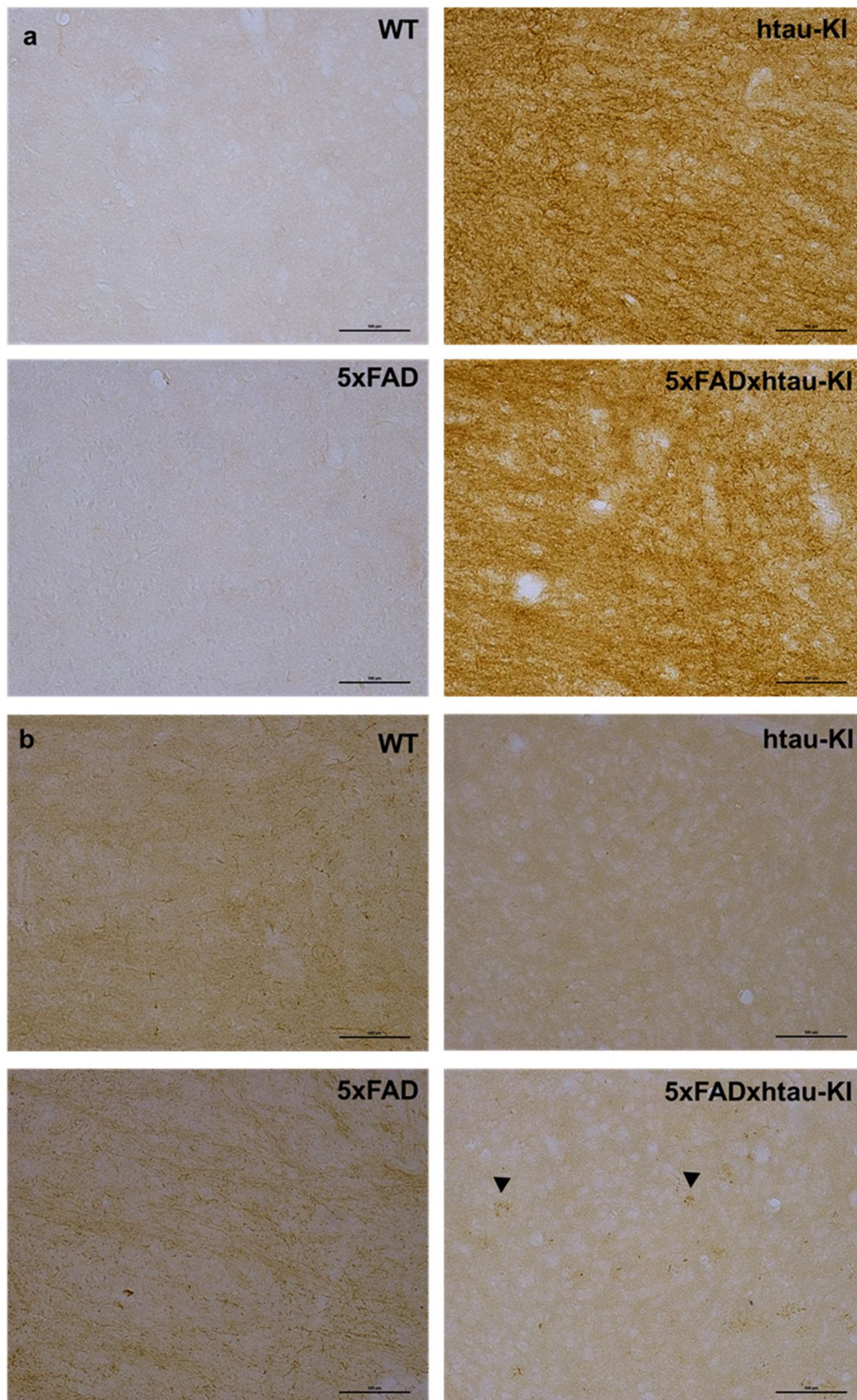


Figure 16. MC1 staining in hypothalamus at 7 months of age. (a) female mouse brains of all genotypes (b) male mouse brains of all genotypes. Arrowheads point to MC1⁺ dystrophic neurites. Scale bars are 100 μ m.

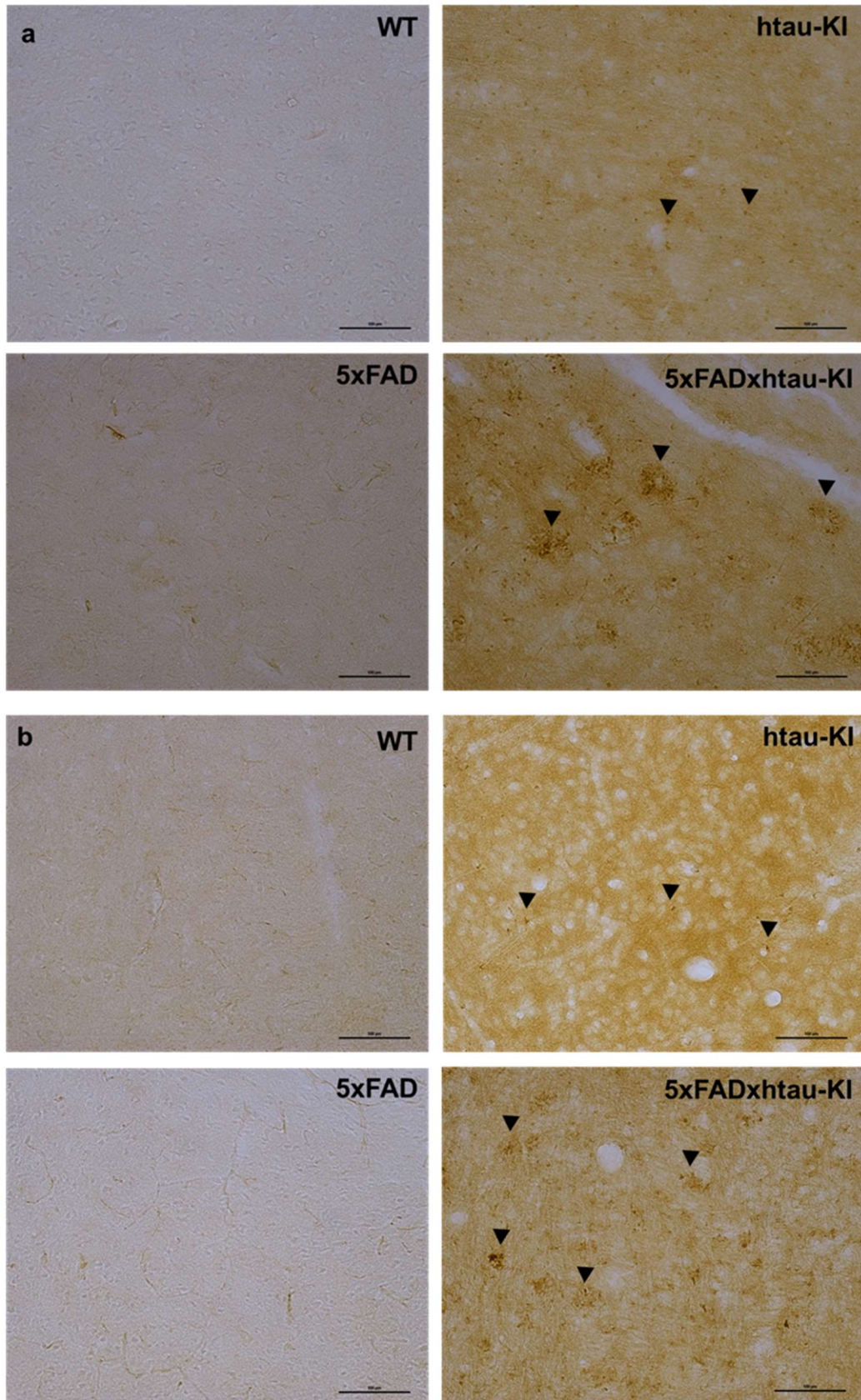


Figure 17. MC1⁺ dystrophic neurites specifically in hypothalamus of 13-month-old htau-KI and 5xFADxhtau-KI mice. (a) female mouse brains of all genotypes (b) male mouse brains of all genotypes. Arrowheads point to (clusters of) MC1⁺ dystrophic neurites. Scale bars are 100 μ m.

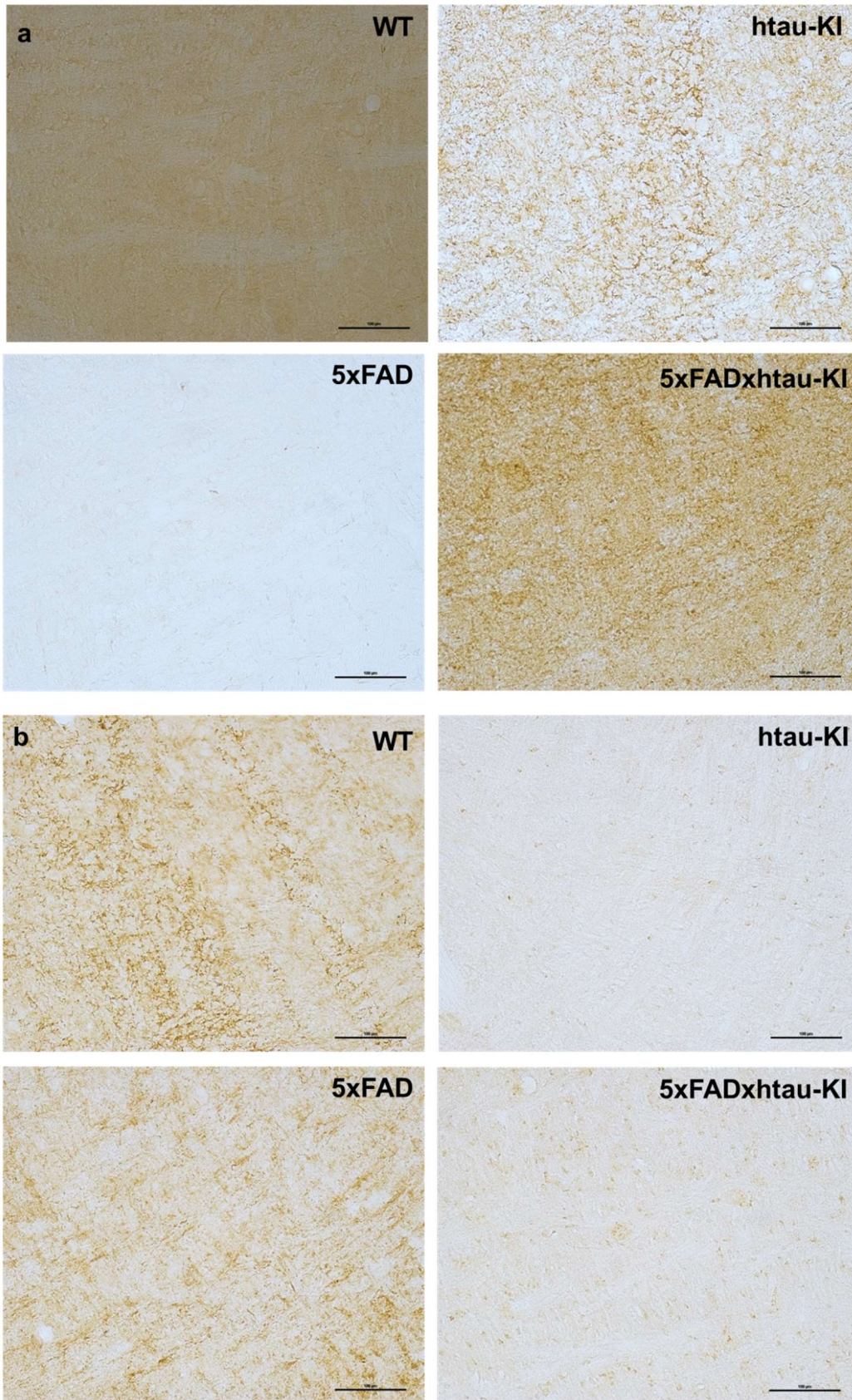


Figure 18. MC1 staining in brain stem of 7-month-old mice. (a) female mouse brains of all genotypes (b) male mouse brains of all genotypes. Scale bars are 100µm.

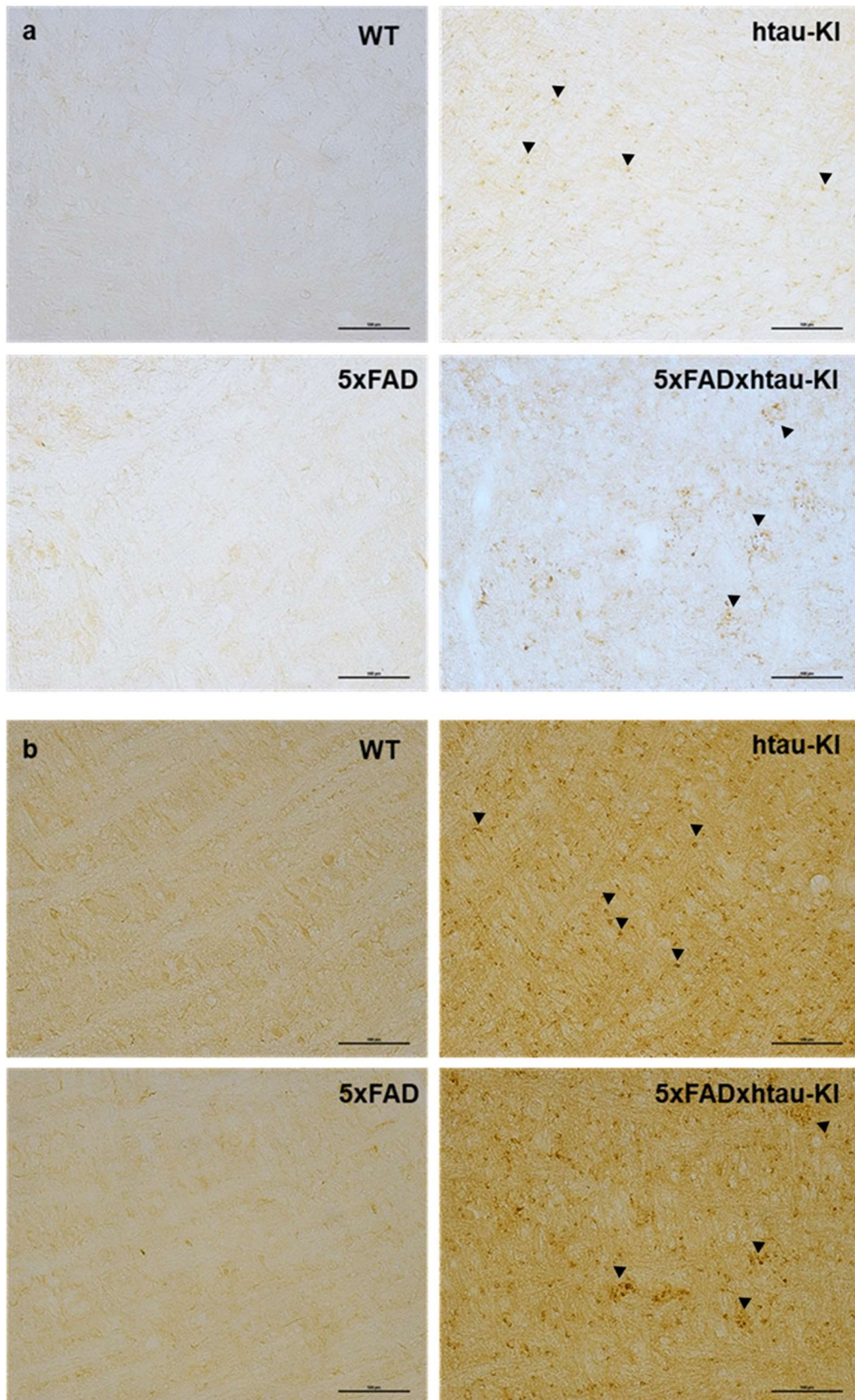


Figure 19. MC1⁺ dystrophic neurites specifically in brain stem of 13-month-old htau-KI and 5xFADxhtau-KI mice. (a) female mouse brains of all genotypes (b) male mouse brains of all genotypes. Arrowheads point to (clusters of) MC1⁺ dystrophic neurites. Scale bars are 100 μ m.

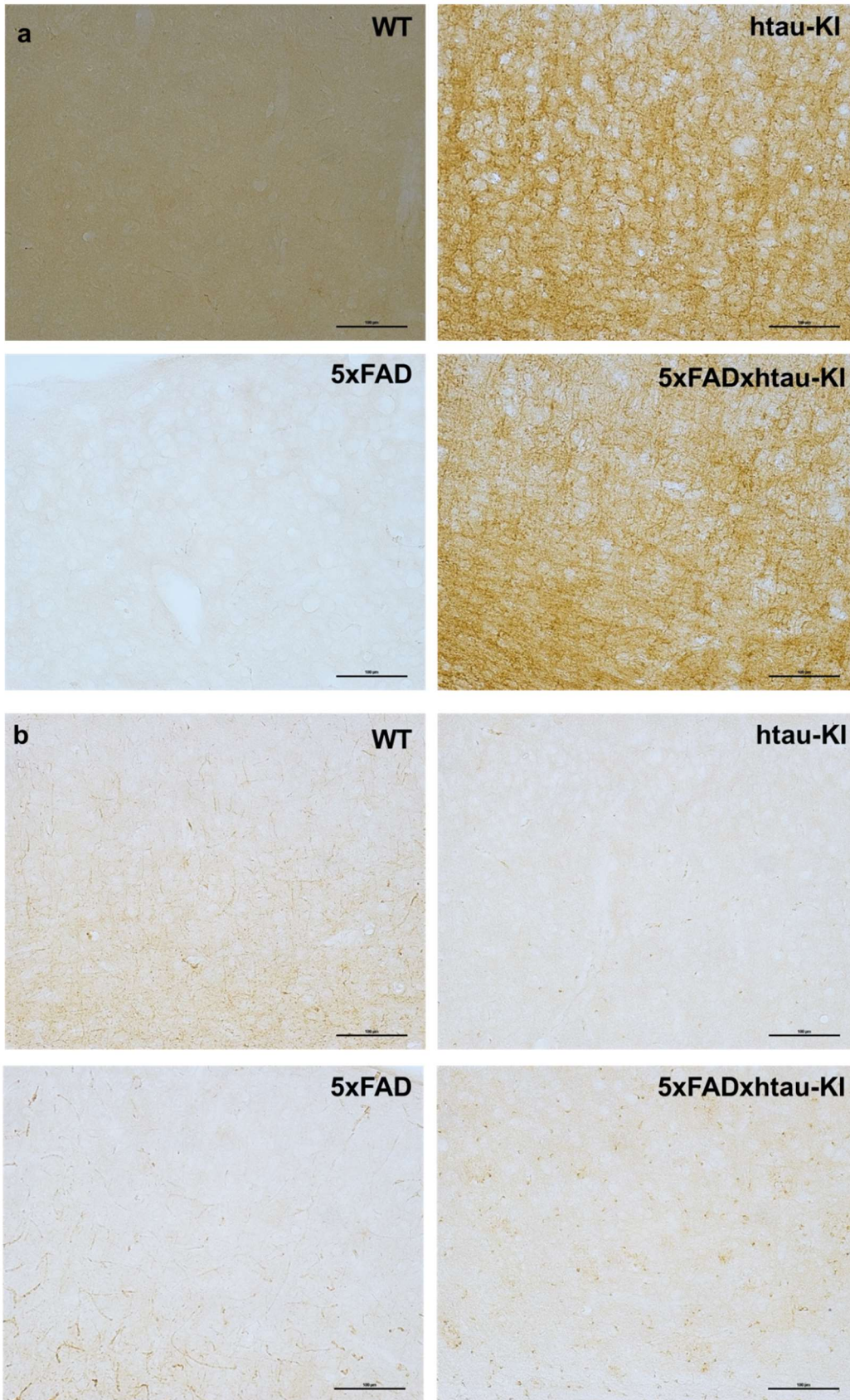


Figure 20. MC1 staining in cortex of mice at 7 months of age. (a) female mouse brains of all genotypes (b) male mouse brains of all genotypes. Scale bars are 100µm.

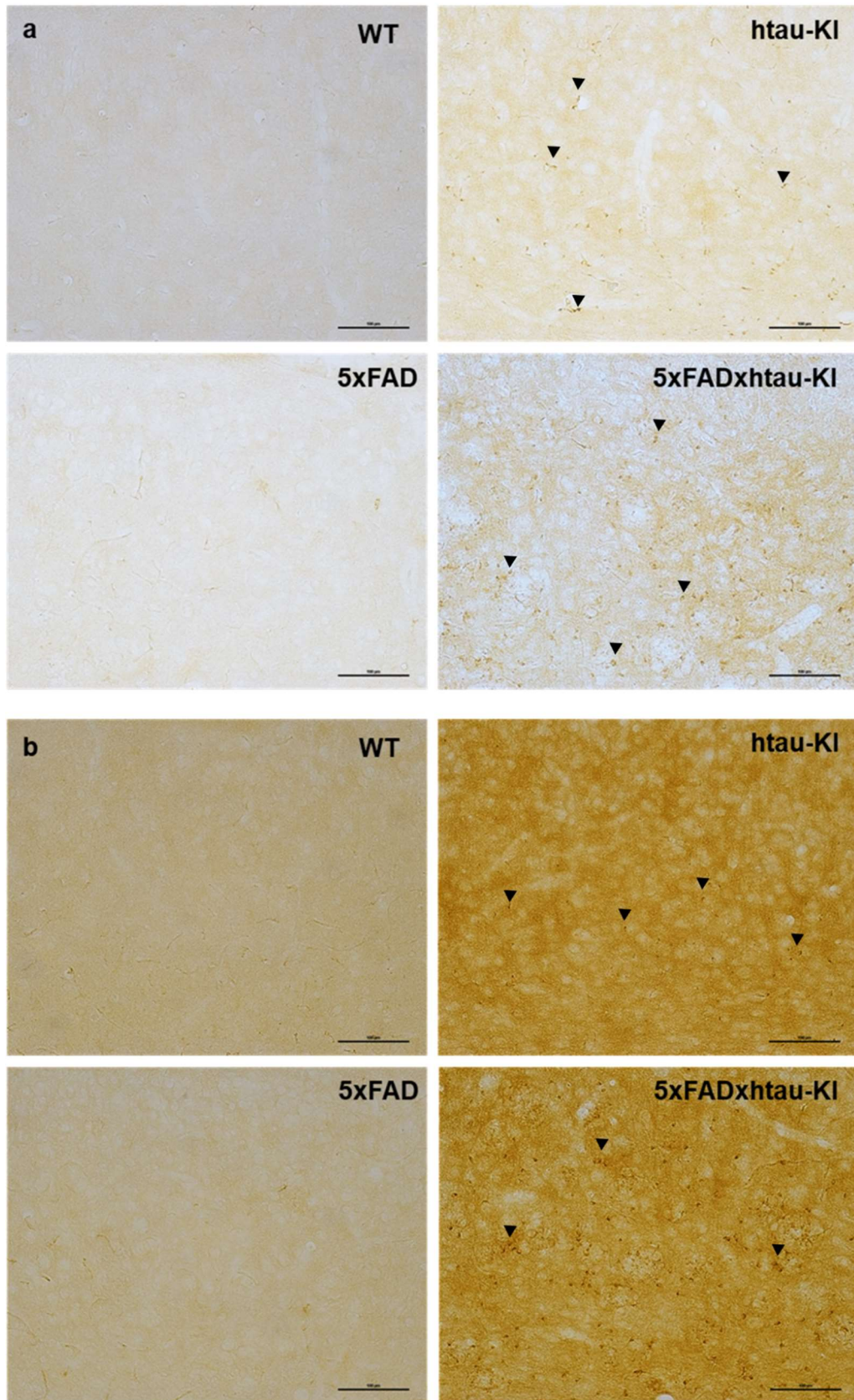


Figure 21. MC1⁺ staining specifically in cortex of 13-month-old htau-KI and 5xFADxhtau-KI mice. (a) female mouse brains of all genotypes (b) male mouse brains of all genotypes. Arrowheads point to (clusters of) MC1⁺ dystrophic neurites. Scale bars are 100µm.

suggesting general neurite staining. Co-staining with other markers is however required to confirm these hypotheses. In brain stem at 7 months (figure 18), a clear effect of sex was visible. In female htau-KI and 5xFADxhtau-KI mice a net-like staining was seen throughout the brain stem and female WT and 5xFAD mice showed no signal. In male mice this was completely reversed (figure 18b). At the age of 13 months, although the staining in male mice appeared stronger than in female mice in general, the same effects were seen as in hypothalamus: htau-KI and 5xFADxhtau-KI mice showed specific MC1⁺ structures, which were more clustered in 5xFADxhtau-KI mice (figure 19). A weak signal was seen in WT and 5xFAD. Finally, the cortex was also compared between genotypes, sexes, and age groups (figures 20 and 21). At 7 months, there was again a clear sex difference, with a net-like staining in female htau-KI and 5xFADxhtau-KI mice throughout the cortex and male mice showing only background staining. Both in female and male WT and 5xFAD mice, there was no signal. At 13 months (figure 21), again the same result was found as in other brain regions. The cortex of htau-KI and 5xFADxhtau-KI mice of both sexes revealed many MC1⁺ neurites, with larger, probably plaque-related, clusters visible in 5xFADxhtau-KI. Overall, these results suggest that there is an age-dependent increase in MC1-specific pathological formations of tau, which is specific for human tau and independent of A β .

In addition to staining for tau, plaque pathology was also analysed by staining for A β with 3A1, as shown in figure 22a. The complete 3A1⁺ area, as well as the 3A1⁺ area specifically in cortex and hippocampus were compared between genotypes and sexes at 7 (figure 22b) and 13 months (figure 22c). Cortex and hippocampus are important for memory and cognitive functions and both regions are affected early by plaque pathology (Thal *et al.*, 2002). These regions are therefore quantified and compared separately between genotypes and sexes. No significant differences were found, either in complete brain or hippocampus or cortex. When comparing figure 22b to 22c, a clear increase in plaque pathology with age is visible, as expected (no statistical comparison). The results also confirm that hippocampus and cortex are strongly affected by plaque pathology, as shown by the increased area compared to total brain, both in figure 22b and c (note the differences in Y-axes, no statistical comparison). Finally, at the age of 13 months in complete brain, a trend was visible for a higher plaque load in 5xFAD compared to 5xFADxhtau-KI mice, as well as for a higher plaque load in female compared to male mice.

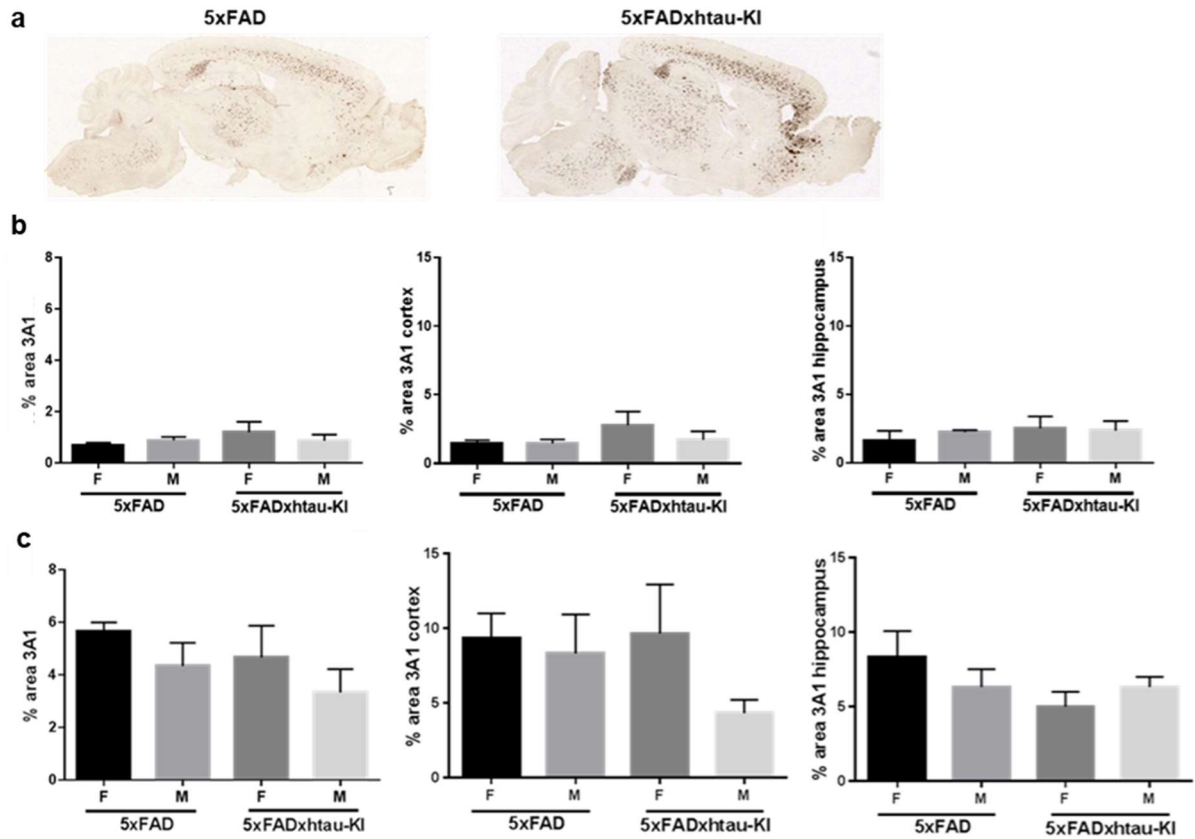


Figure 22. Plaque quantification in 7- and 13-month-old 5xFAD and 5xFADxhtau-KI mice. (a) Sagittal brain slices were stained with 3A1 ($A\beta$) and area of plaques quantified, examples show 7-month-old females of both genotypes. At 7 (b) and 13 (c) months of age, total area, area in the cortex and in the hippocampus were quantified and compared with one-way ANOVA, $n=3$.

Since the immune system plays such an important role in AD, the response of glia cells was also investigated. Microglia (Iba1, ionized calcium binding adaptor molecule 1) and astrocytes (GFAP, glial fibrillary acidic protein) were stained to obtain an overview of the neurological immune status of mice of all genotypes. As expected, clear microgliosis and astrogliosis were visible in the brains of 5xFAD and 5xFADxhtau-KI mice, but not in WT and htau-KI mice (see figure 23a). Double-immunofluorescent staining was subsequently performed to provide more details. As shown in figure 23b, microglia clustered around amyloid deposits. Figure 23c illustrates the stellar, activated morphology of astrocytes.

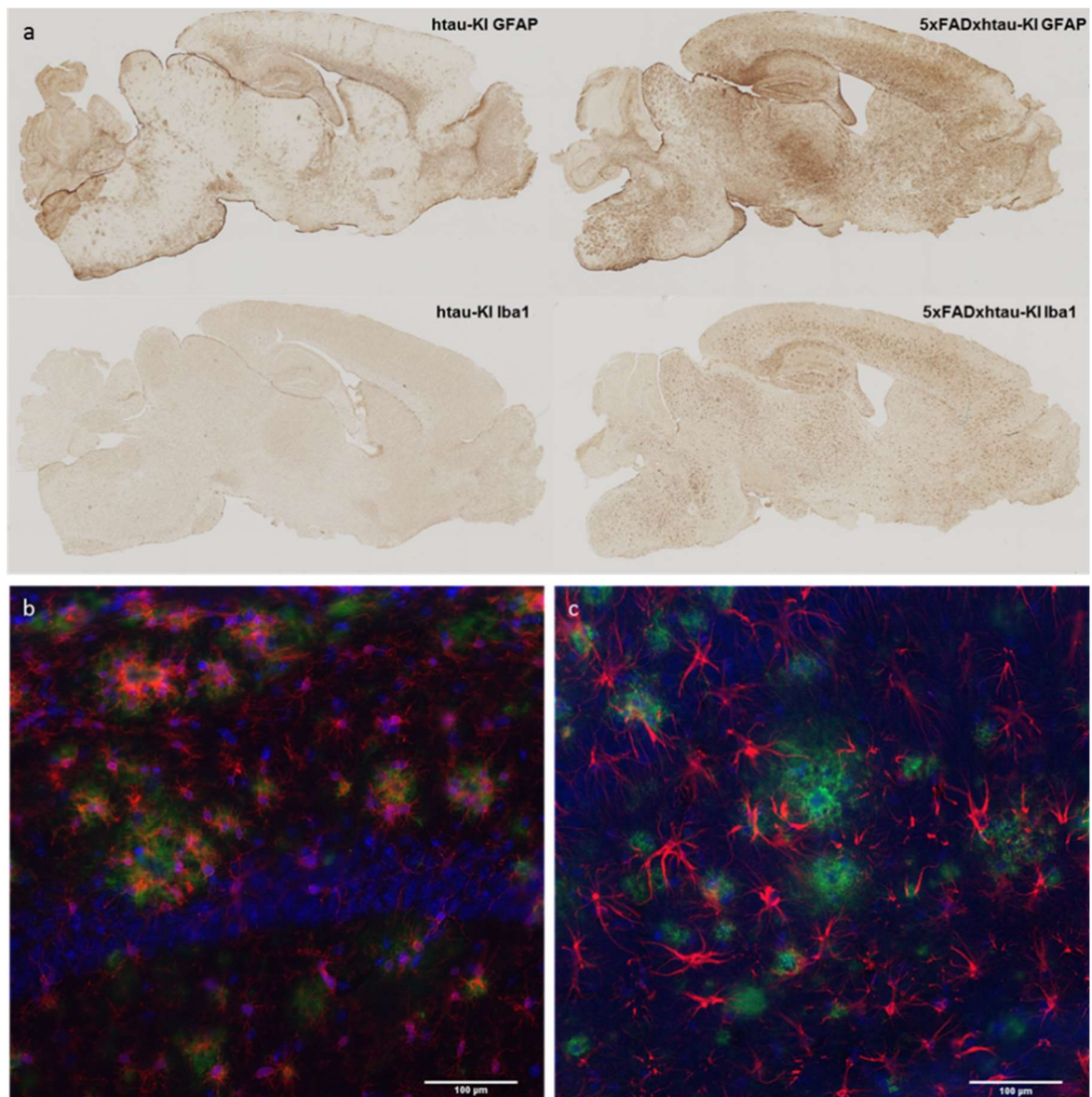


Figure 23. Microgliosis and astrocytosis in 13-month-old 5xFADxhtau-KI mice, but not in htau-KI mice. (a) Staining for astrocytes (GFAP, top) and microglia (Iba1, bottom) in sagittal brain slices of 13-month-old female htau-KI (left) and 5xFADxhtau-KI (right) mice revealed clear activation of these cell types in response to 5xFAD pathology, but an equal distribution in htau-KI mice. Pictures of htau-KI are representative for WT, whereas 5xFAD mice resemble 5xFADxhtau-KI. (b,c) Double immune-fluorescence in a 13-month-old 5xFADxhtau-KI female mouse showed that the activation of microglia and astrocytes was plaque-related. Pictures are representative for 5xFAD mice as well. Green = 3A1, A β . Red = Iba1, microglia (left) or GFAP, astrocytes (right). Blue = DAPI. Scale bars in b are 100 μ M.

Analysis of AD-related gene expression

The nCounter Mouse AD gene expression panel was used to measure the expression levels of 770 AD-specific genes in the prefrontal cortex of 48 different mice. Males and females of all 4 genotypes were compared, at the age of 7 and 13 months. No differences were found between htau-KI and WT mice, except for the loss of mouse tau (MAPT) expression in htau-KI mice, which confirmed the correctness of the NanoString data (see figure 24). Similarly, no significant differences were found between 5xFAD and 5xFADxhtau-KI except for the loss of mouse tau in 5xFADxhtau-KI (see figure 25a). Several genes were differentially expressed between 5xFADxhtau-KI and WT mice (see figure 25b). Besides the loss of mouse tau in 5xFADxhtau-KI, two other genes (Bex1 and Zbtb33) were downregulated in these mice, and 23 genes were upregulated in 5xFADxhtau-KI mice compared to WT mice (see detailed list in supplementary table I). Mostly the same genes were upregulated in 5xFAD compared to WT mice (see supplementary table II). Most of the upregulated genes found in 5xFAD and 5xFADxhtau-KI mice were related to the immune system, specifically microglia. The complement system (C1qa, C1qb and C1qc), as well as several other genes expressed by microglia (Tyrobp, Tgfr1 and Tgfr2) are significantly higher expressed in response to overexpression of A β (see figure 25b).

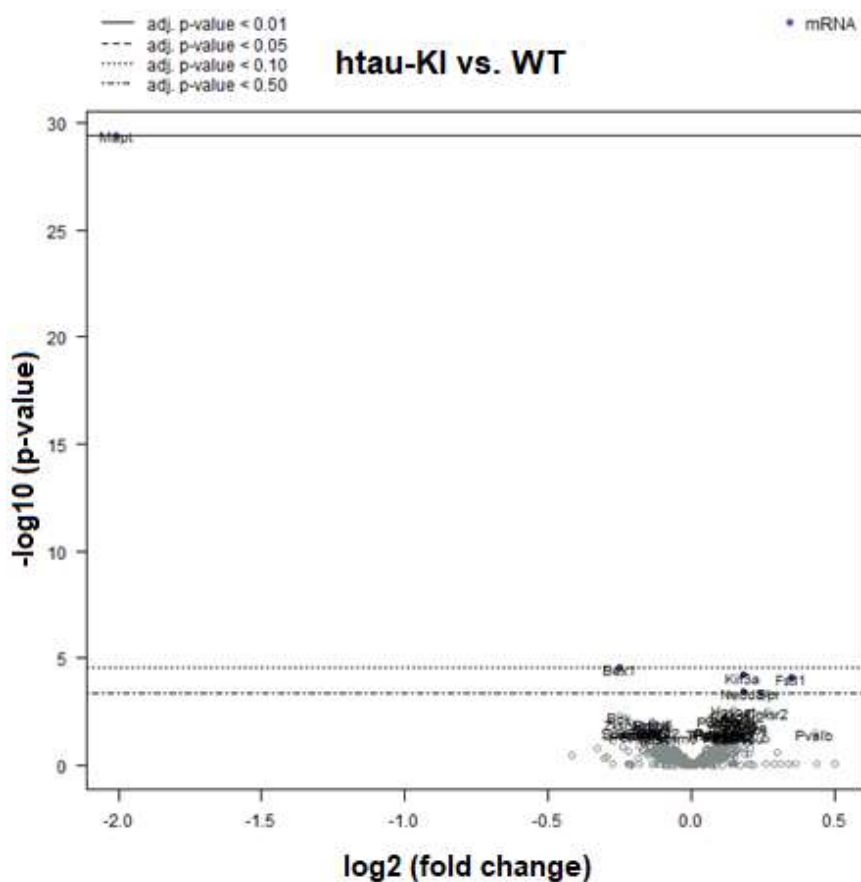
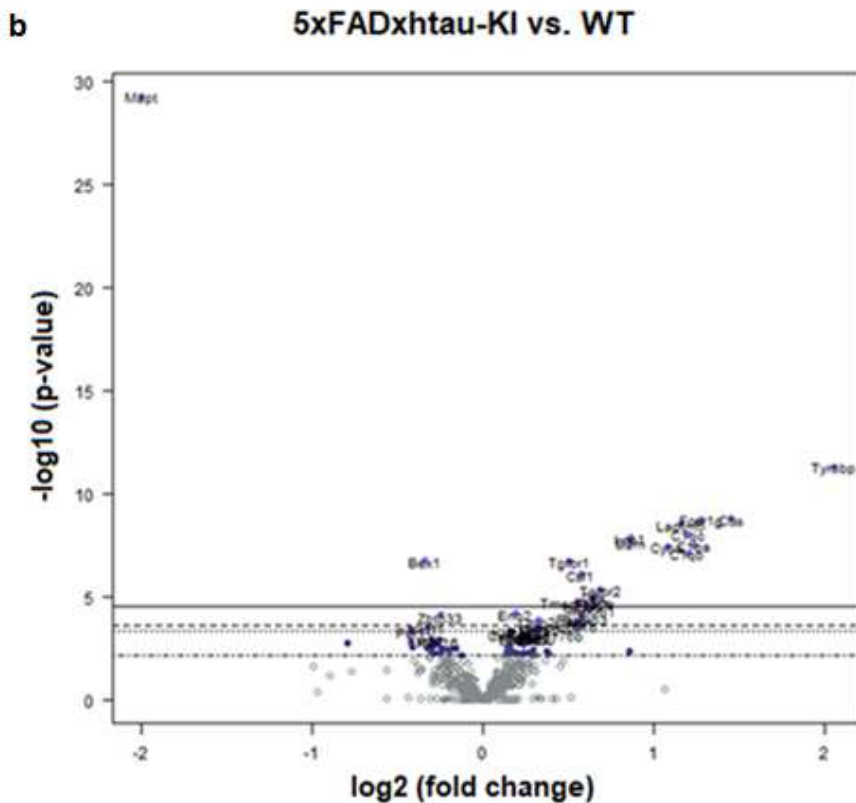
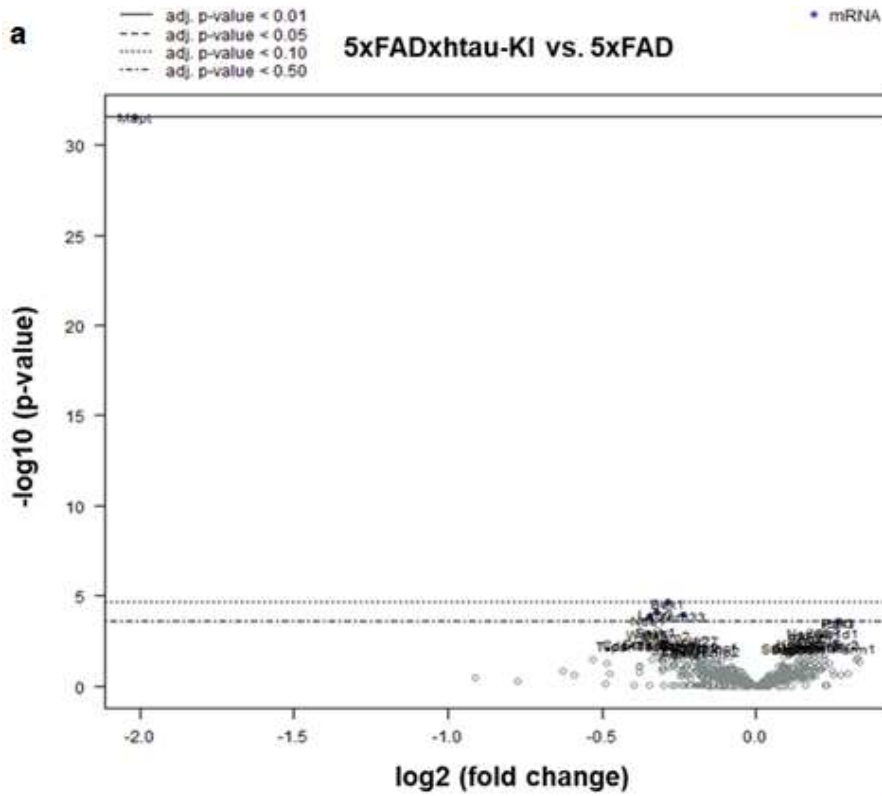


Figure 24. Differentially expressed genes in htau-KI mice compared to WT in the Nanostring mouse AD panel. Volcano plot of differentially expressed genes in htau-KI mice compared to WT.



Gene name	Log2 fold change
Mapt	-2
Tyrobp	2.05
Ctss	1.45
Fcer1g	1.28
Laptm5	1.16
C1qc	1.2
Lcp1	0.864
B2m	0.868
C1qa	1.24
Cyba	1.08
C1qb	1.2
Bex1	-0.337
Tgfb1	0.505
Csf1	0.568
Tgfb2	0.687
Grn	0.651
Tmem176a	0.552
Pros1	0.643
Itgb5	0.602
Slco2b1	0.629
Eno2	0.193
Zbtb33	-0.244
Rasgrp3	0.58
Lmo2	0.323
Srgn	0.555
Arpc1b	0.539

Figure 25. Differentially expressed genes in 5xFADxhtau-KI mice compared to 5xFAD and WT mice in the NanoString mouse AD panel. (a) Volcano plot of differentially expressed genes in 5xFADxhtau-KI mice compared to 5xFAD mice. (b) Volcano plot of differentially expressed genes in 5xFADxhtau-KI mice compared to WT. (c) List of significantly up- (orange) or down- (blue) regulated genes in 5xFADxhtau-KI mice compared to WT. n=12.

This finding is underlined by the severe microgliosis found in immunohistochemical staining shown in figure 23. A pathway analysis on the NanoString data furthermore revealed that there was an upregulation of the lysosomal pathway. The NanoString data revealed no differentially expressed genes between males and females, and only 1 gene (Samd12) that was upregulated in 7-month-old mice compared to 13-month-old mice (see supplementary figure 1).

Comparison to human co-expression modules

In collaboration with the Jackson Laboratory (Maine, USA), we have investigated the correlation of our mouse gene expression data to *post-mortem* human AD brain tissue. As displayed in figure 26, 5xFAD mice at the ages of 7 and 13 months show positive correlations (correlation coefficients: 0.38-0.67, $p < 0.01$) with CBEturquoise (cerebellum), STGblue (superior temporal gyrus) and IFGturquoise (inferior frontal gyrus) of human AD tissue in cluster B, related to the immune system. This finding again underlines the importance of the immune system in AD and confirms that the 5xFAD mouse model is mimicking the neuro-immunological status of AD patients quite well. Interestingly, the results in cluster E for 5xFAD and 5xFADxhtau-KI mice are completely reversed. While there are positive correlations with 5xFAD at the age of 7 months, there are clear significant negative correlations (correlation coefficients -0.23 - -0.49, $p < 0.01$) with 5xFADxhtau-KI. These effects are no longer visible at the age of 13 months. The AMP-AD modules with the strongest negative correlation, FPbrown (frontal pole) and PHGblue (parahippocampal gyrus) primarily contain genes related to

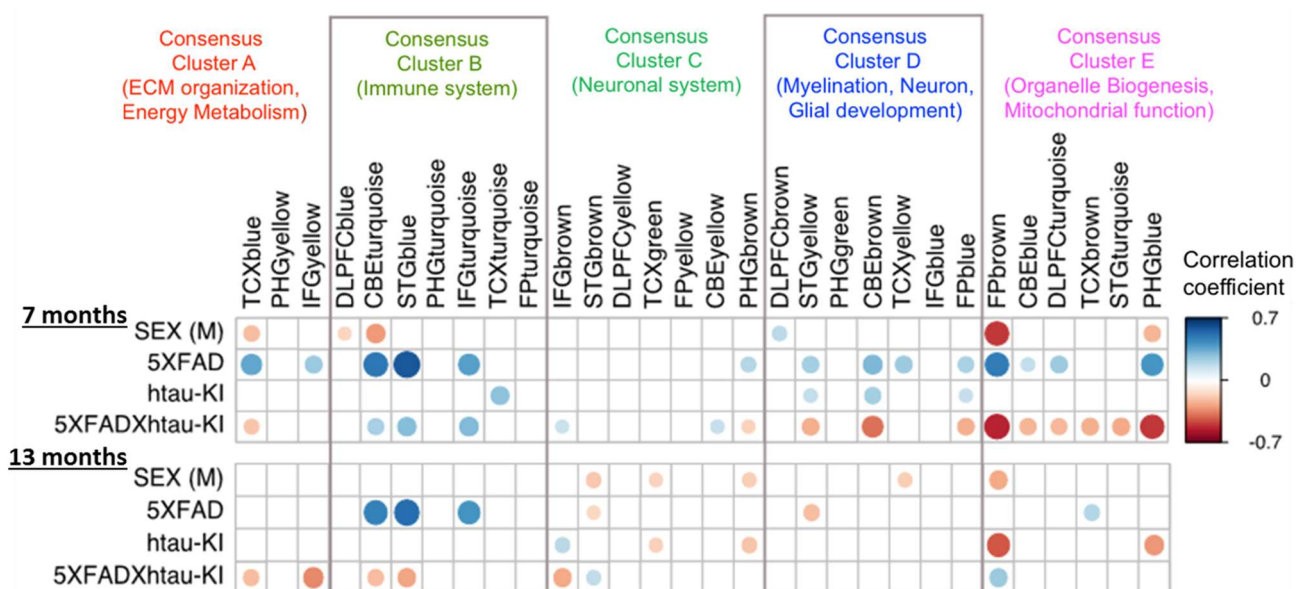


Figure 26. Correlation of NanoString gene expression data of mice with data on *post-mortem* human brain regions reveals a protective effect of human tau in 5xFADxhtai-KI mice. The correlation coefficient of each model with human *post-mortem* brain tissue is shown for 30 AMP-AD modules, divided in 5 clusters. The results in cluster E suggest a protective effect of human tau in a 5xFAD background.

mitochondrial functioning and oxidative phosphorylation. The data suggests that the presence of human tau at an early age somehow provides protection against the changes induced by overproduction of A β in 5xFAD in these modules. This hypothesis led us to take a closer look at the differences between 5xFADxhtau-KI and 5xFAD at gene expression level. More detailed information was obtained by performing gene set enrichment analysis. This analysis uses the aggregate per gene statistics to identify small but consistent changes in transcription in specific pathways. At 7 months of age, the oxidative phosphorylation pathway was significantly upregulated in 5xFADxhtau-KI mice (mmu190, enrichment score= 0.69, adjusted p-value= 0.0058) (Figure 27a), whereas this pathway was significantly downregulated in AD patients (hsa190, enrichment score= -0.59, adjusted p-value= 0.0025) (Figure 27b). Comparison of 5xFAD and htau-KI to WT separately revealed no differential gene expression in this pathway (Figure 27c), confirming that there is a synergistic effect of A β and human tau, specifically in

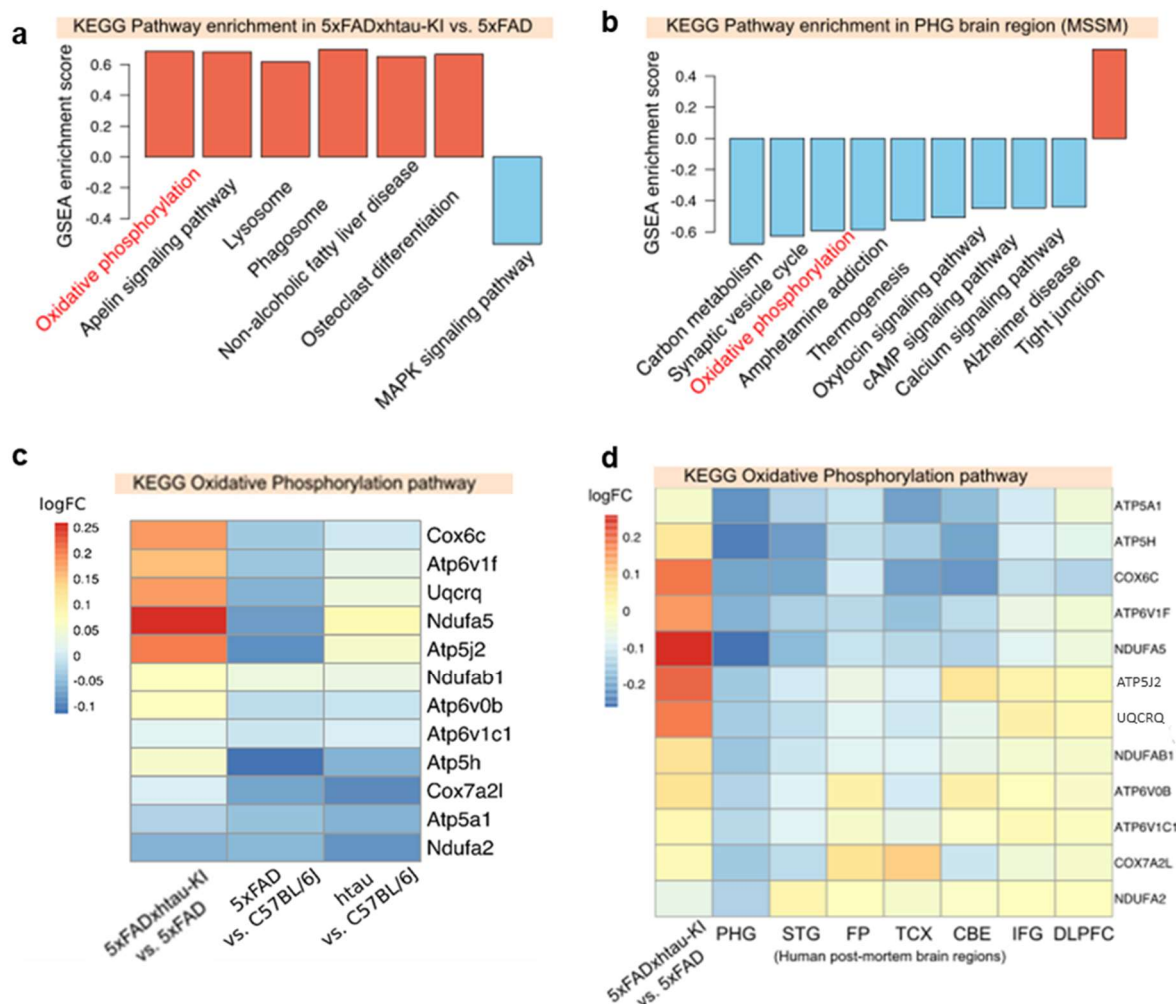


Figure 27. Gene set enrichment analysis of 5xFADxhtau-KI mice compared to 5xFAD at 7 months of age. (a) Pathways with significant up (red) or down (blue) regulation in 5xFADxhtau-KI mice compared to 5xFAD mice. (b) Pathways with significant up (red) or down (blue) regulation in the parahippocampal (PHG) region of human *post-mortem* AD brain tissue compared to controls. Interestingly, the oxidative phosphorylation pathway shows opposite effects. (c) Differential expression of genes in the oxidative phosphorylation pathway in the different mouse genotypes tested. (d) Differential expression of genes in the oxidative phosphorylation pathway in 5xFADxhtau-KI compared to different human brain regions.

5xFADxhtau-KI mice. As shown in figure 27d, the genes related to this pathway are downregulated across all human brain regions. In the data from 13-month-old mice, another pathway was revealed: the extracellular matrix (ECM)-receptor interaction pathway was significantly downregulated in 5xFADxhtau-KI mice compared to 5xFAD mice (Figure 28a). This pathway was upregulated in AD patients compared to controls (Figure 28b). Again, these differences were not visible in 5xFAD mice alone (Figure 28c). Figure 28d shows the upregulation of genes involved in the ECM-receptor interaction pathway specifically in the temporal cortex of AD patients, whereas these genes are downregulated in 5xFADxhtau-KI mice.

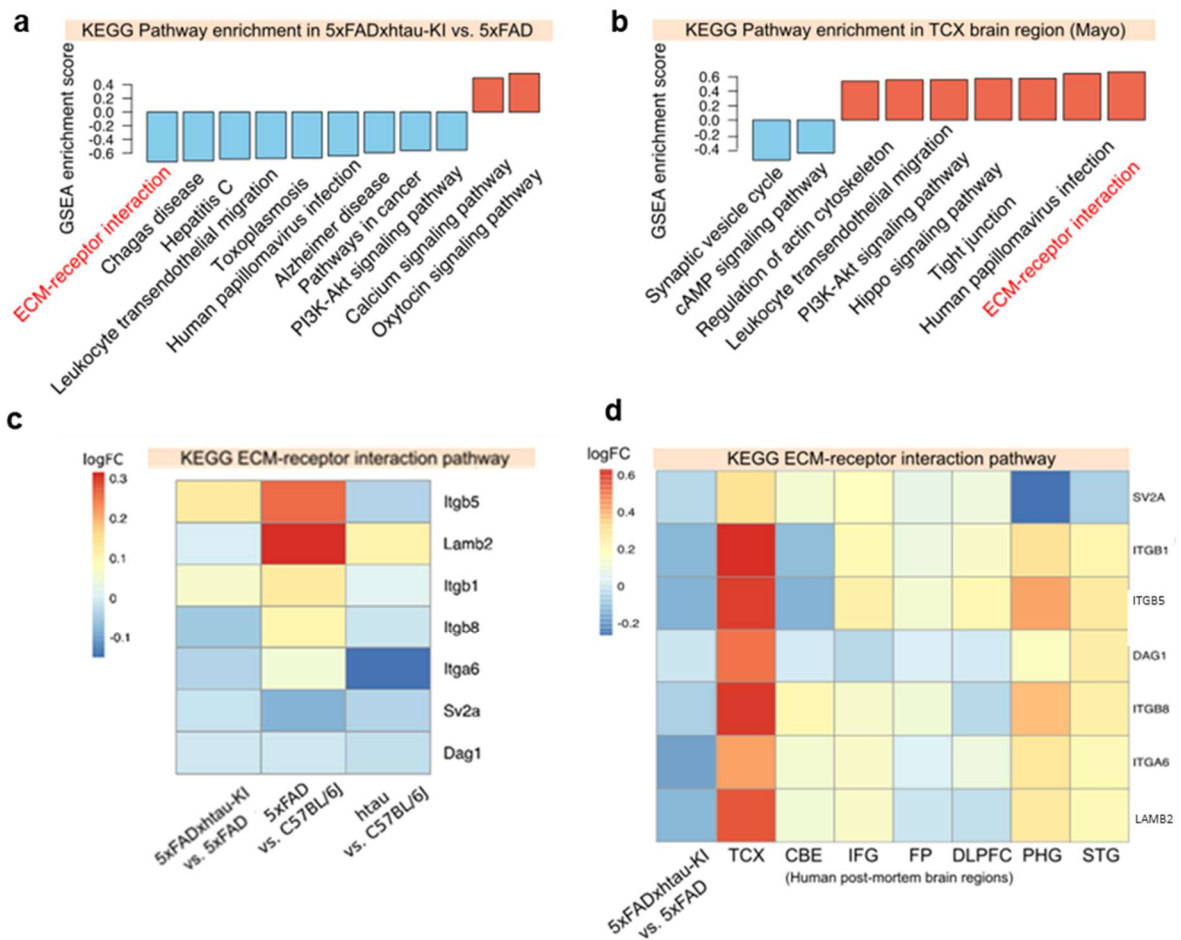


Figure 28. Gene set enrichment analysis of 5xFADxhtau-KI mice compared to 5xFAD at 13 months of age. (a) Pathways with significant up (red) or down (blue) regulation in 5xFADxhtau-KI mice compared to 5xFAD mice. (b) Pathways with significant up (red) or down (blue) regulation in the temporal cortex (TCX) region of human *post-mortem* AD brain tissue compared to controls. Interestingly, the ECM-receptor interaction pathway shows opposite effects. (c) Differential expression of genes in the ECM-receptor interaction pathway in the different mouse genotypes tested. (d) Differential expression of genes in the ECM-receptor interaction pathway in 5xFADxhtau-KI compared to different human brain regions.

Immune cells in 5xFAD brains

Next, in a supplementary analysis, we were interested in the types of immune cells activated in 5xFAD brains. For this purpose, 5xFAD mice were cross bred with CCR2^{RFP/RFP} mice to distinguish between resident microglia and infiltrating peripheral monocytes. First, the importance of CCL2-CCR2 signalling in AD was confirmed. For this purpose, a CCL2 ELISA was performed on the supernatant of primary microglia exposed to 5µM Aβ for 24 hours. As shown in figure 29, there is a significant increase in CCL2 after Aβ stimulation (t=3.071, df=10, p=0.0118). This confirms that CCL2 is upregulated in microglia in response to Aβ.

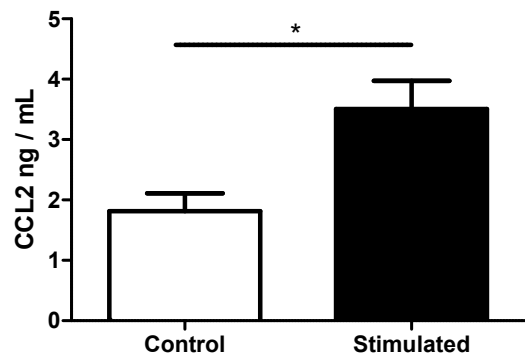


Figure 29. CCL2 ELISA of culture supernatant of control and Aβ-stimulated primary microglia. Primary microglia were stimulated with 5µM of recombinant Aβ₁₋₄₂ for 24 hours. Supernatant was analysed using a CCL2 ELISA. Mean±SEM displayed, n=6, unpaired t-test, *p<0.05

Subsequently, the expression of CCR2 was investigated. CCR2 could not be shown in spleen using commercial antibodies, but RFP expression was seen in a CCR2^{RFP/RFP} mouse spleen (figure 30a). Furthermore, a flow cytometric analysis of splenocytes of a WT, CCR2^{+RFP}, and CCR2^{RFP/RFP} mouse revealed that the RFP production was gene-dose dependent (figure 30b). The gene-dose dependent reduction of CCR2 was also confirmed at mRNA level using qRT-PCR (figure 30c). Finally, the lack of CCR2 expression in the CNS could be confirmed at cellular level by RNA isolation of cultured primary microglia and bone marrow derived peripheral macrophages (BMDM). Using qRT-PCR, we showed that peripheral macrophages express high levels of CCR2, whereas primary microglia do not express CCR2 (see figure 30d). Due to lack of good antibodies, CCR2 could not be stained at the protein level. None of the tested antibodies gave a signal in a positive control.

Infiltration of peripheral immune cells in AD brain

After confirming that CCL2 is upregulated in response to Aβ and that CCR2 is not expressed in the healthy mouse brain, the infiltration of peripheral immune cells in AD was investigated. In brain tissue of 5xFADxCCR2^{+RFP} mice, immunohistochemistry was used to check for RFP expression. As shown in figure 31, no RFP⁺ cells were found. There are several possible hypotheses to explain this finding: (1) a lack of infiltrating cells, (2) a downregulation of CCR2/RFP expression by peripheral cells upon entering of the brain, or (3) a loss/fading of the RFP signal after isolation of the tissue. Therefore, another marker for peripheral immune cells was used to investigate the infiltration of peripheral cells: major histocompatibility complex II (MHCII) is expressed by dendritic cells, macrophages and B lymphocytes (Hohl, 2015).

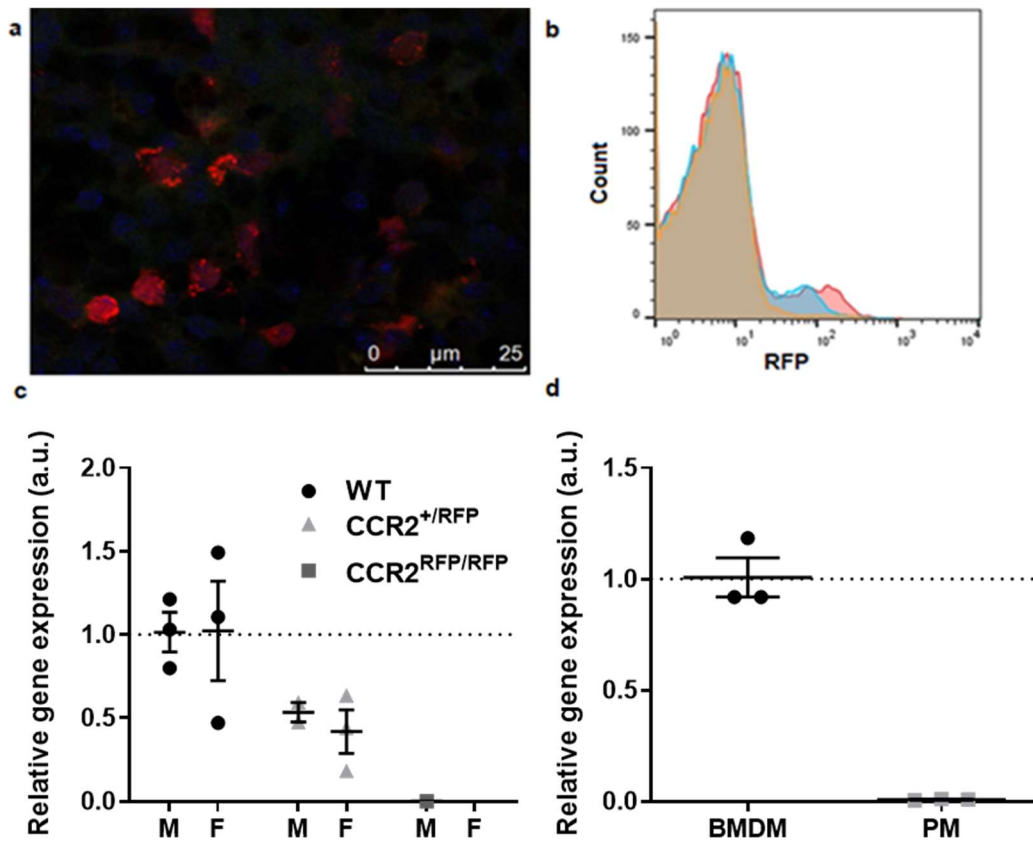


Figure 30. Gene-dose dependent RFP/CCR2 expression in spleen tissue of WT, CCR2^{+/RFP} and CCR2^{RFP/RFP} mice and lack of expression in microglia. (a) RFP production in spleen tissue of a CCR2^{RFP/RFP} mouse shown by immunohistochemistry. Red granular staining is RFP. (b) Flow cytometry showed a gene-dose dependent red fluorescent signal in WT (orange), CCR2^{+/RFP} (blue) and CCR2^{RFP/RFP} (red) mouse splenocytes. (c) qRT-PCR revealed a gene-dose dependent reduction of CCR2 mRNA expression in splenocytes of WT, CCR2^{+/RFP}, and CCR2^{RFP/RFP} mice, both male and female. n=1-3, 3 technical replicates performed for each sample, female CCR2^{RFP/RFP} mice showed no detectable signal for all 3 samples. (d) qRT-PCR confirmed the lack of CCR2 mRNA expression in primary microglia (PM) whereas bone marrow derived macrophages (BMDM) showed high expression. Mean ± SEM is displayed, n=3.

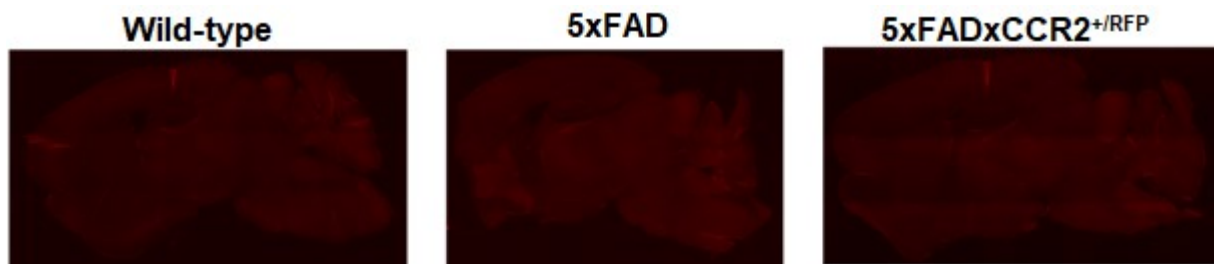


Figure 31. Lack of RFP production in WT, 5xFAD and 5xFADxCCR2^{+/RFP} mouse brain. WT (left) and 5xFAD (middle) mouse brain showed no RFP expression, as expected. But there was also no RFP expression detected in the brain of a 5xFADxCCR2^{+/RFP} mouse (right).

An MHCII antibody was used to stain WT, 5xFAD, and 5xFADxCCR2^{+/RFP} mouse brains and revealed that there was indeed infiltration of peripheral cells in response to amyloid overexpression (figure 32a).

Co-staining of MHCII and Iba1 revealed that only a small percentage of Iba1⁺ cells was also MHCII⁺ (figure 32b and c). This suggests that there is a specific cell type that appears in the

brain in response to AD pathology and expresses MHCII. It seems unlikely that microglia are becoming MHCII⁺, since many Iba1⁺ cells are MHCII⁻. We therefore hypothesize that microglia (Iba1⁺), in response to amyloid pathology, produce CCL2, which binds to CCR2⁺MHCII⁺ peripheral monocytes, which travel to the CNS and play a role in AD pathology. Clearly, additional analyses (and the development of good CCR2 antibodies) are required to confirm this hypothesis.

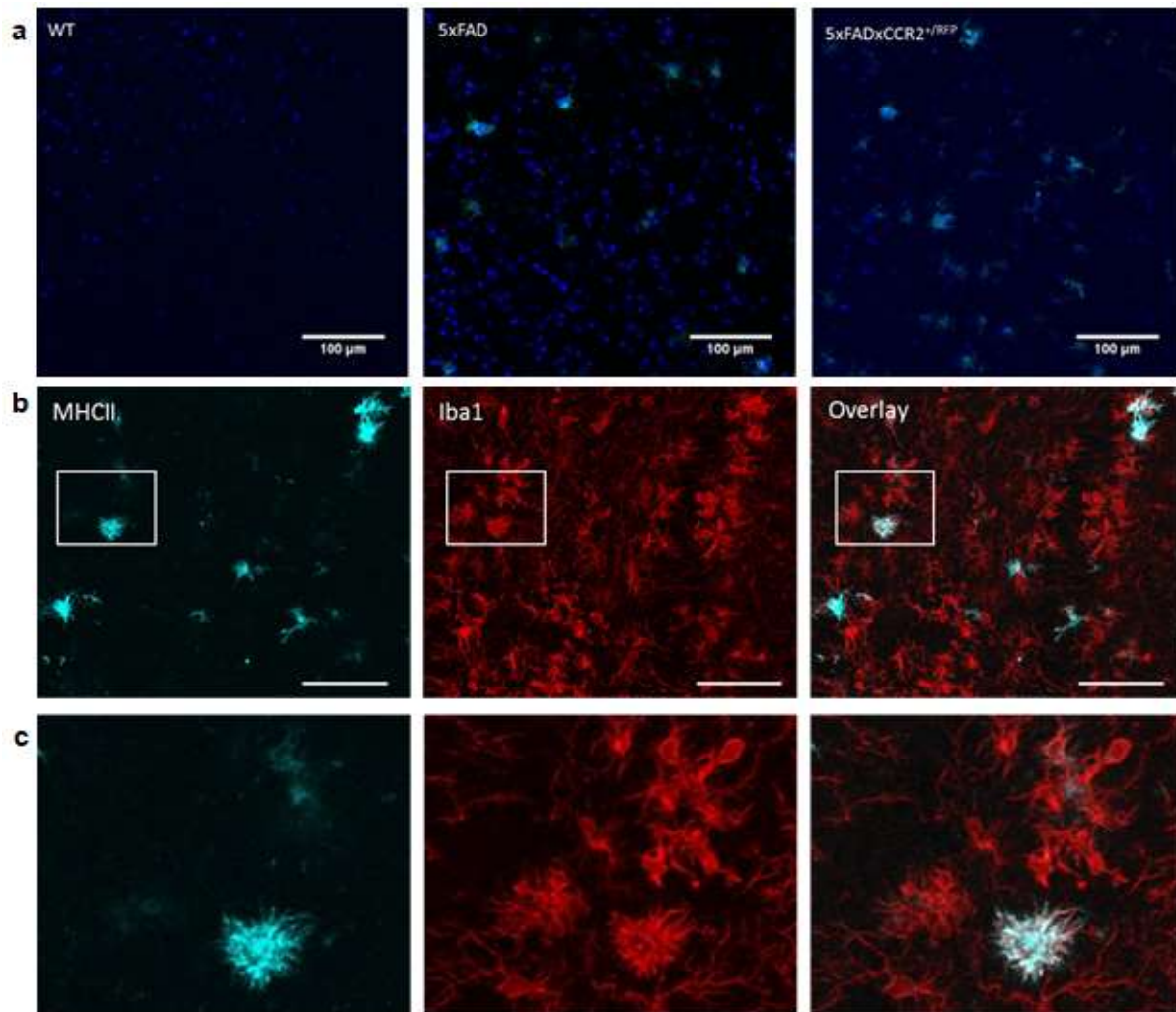


Figure 32. Occurrence of MHCII⁺ cells in the CNS in response to AD-like pathology and co-staining with Iba1. (a) Immunohistochemical staining revealed no MHCII⁺ cells in a WT mouse brain (left), whereas multiple MHCII⁺ cells were found in 5xFAD (middle) and 5xFADxCCR2^{+/RFP} (right) mouse brain. Dark blue staining = nuclei (DAPI), light blue = MHCII. (b) Co-staining of MHCII⁺ and Iba1⁺ immune cells. Staining is of a 12-month-old female 5xFAD mouse brain. Light blue (left) is MHCII, red (middle) is Iba1, right panel shows an overlay. Scale bar is 100μm, inlay in b marks area enlarged in c.

Effect of heterozygous knock-out of CCR2

After confirming that peripheral cells infiltrate the brain in AD through CCL2-CCR2 signalling, the effect of a heterozygous knock-out of CCR2 on AD pathology was investigated. In literature, CCR2^{+RFP} mice are used as a reporter line, but investigations on the effect of the loss of one allele of CCR2 are lacking. Some preliminary experiments were therefore performed to compare CCR2^{+RFP} mice to WT, and 5xFADxCCR2^{+RFP} mice to regular 5xFAD mice. First, using immunohistochemistry, plaque pathology and infiltration of immune cells in the brains of 5xFAD and 5xFADxCCR2^{+RFP} mice were compared (figure 33). These data showed some trends, which could however not be statistically analysed and should therefore be considered very carefully. The sample size differed between 1 and 5 for all experiments

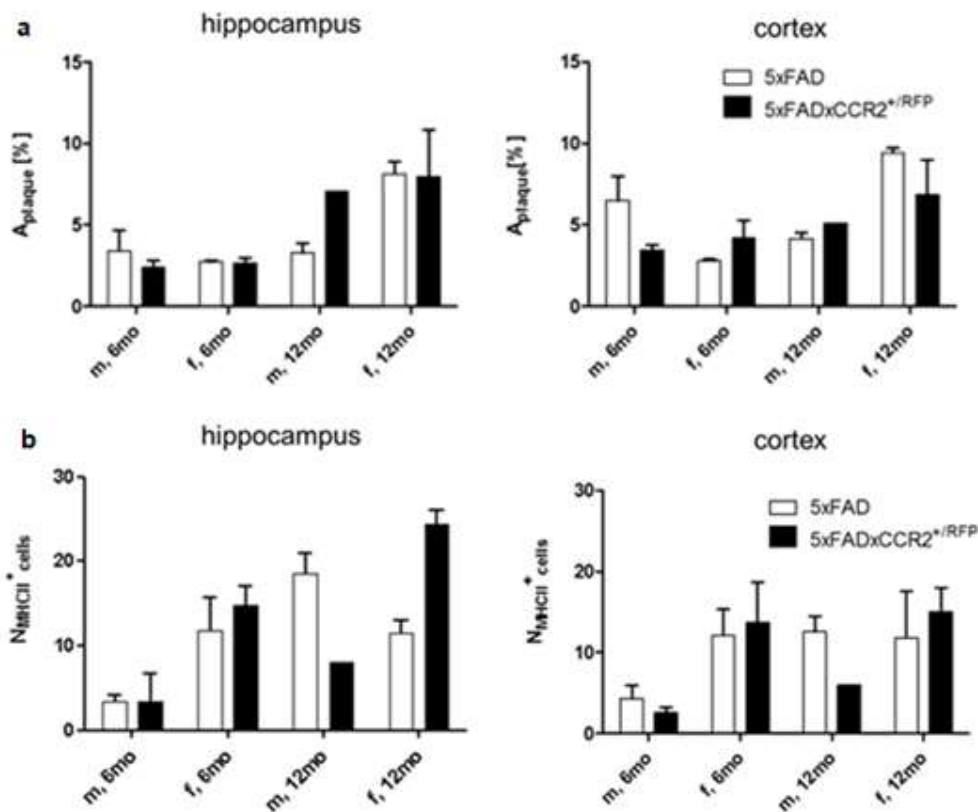


Figure 33. Neuropathology in 5xFAD and 5xFADxCCR2^{+RFP} mice. (a) Immunohistochemistry with 6E10 (A β) was performed to quantify area of plaques in hippocampus and cortex of 5xFAD and 5xFADxCCR2^{+RFP} at the age of 6 and 12 months, in male (M) and female (F) mice. (b) Immunohistochemistry was performed to quantify number of MHCII⁺ cells in hippocampus and cortex of 5xFAD and 5xFADxCCR2^{+RFP} at the age of 6 and 12 months, in male (M) and female (F) mice. (a,b) n=1-5, no statistical analyses possible due to low sample sizes.

described here, which is too low to draw any conclusions about immunohistochemistry. The staining for plaque pathology revealed no differences between genotypes, but a larger area of plaques in 12-month-old mice compared to 6-month-old mice, as expected (see figure 33a). In addition, a trend was found that revealed a larger plaque area in female than in male mice, especially in 12-month-old mice. Similar results were found in the preliminary quantification of infiltrating immune cells; a trend for an age-dependent increase in the area of MHCII⁺ cells was

found, as well as a trend for a higher area of MHCII⁺ cells in female compared to male mice (figure 33b).

Subsequently, to look deeper into the immune status of the brains, qRT-PCR was used to test the mRNA expression of several inflammatory cytokines in prefrontal cortex at the age of 6 and 12 months. The expression of CCL2 was investigated to confirm the *in vitro* findings mentioned above and to compare to findings in literature showing an upregulation of CCL2 in AD mouse models (Janelsins *et al.*, 2005; Simard *et al.*, 2006, Naert & Rivest, 2011). In addition, two cytokines of the IL1-family were investigated because it is known that these cytokines play an important role in AD pathology and can work both beneficial as well as detrimental (reviewed in Shaftel *et al.*, 2008). Two specific isoforms of IL1 were tested, IL1a and IL1b. Although some studies have revealed a link between polymorphisms in both isoforms of IL1 and increased risk of AD, this could not be confirmed by meta analyses (reviewed by Tanzi & Bertram, 2005). IL1b was upregulated in an AD mouse model (Simard *et al.*, 2006), as well as in CSF of human AD patients (Blum-Degen *et al.*, 1995). Another study showed no difference in CSF-IL1b between AD patients and controls but found a significant positive correlation between IL1b and MMSE-scores (Tarkowski *et al.*, 2003). Finally, tumour necrosis factor alpha (TNF α) was investigated, because this proinflammatory cytokine was upregulated in AD mice (Janelsins *et al.*, 2005) as well as in CSF of AD patients (Tarkowski *et al.*, 2003) and is even seen as an important target for AD therapy (reviewed in Chang *et al.*, 2017). Using a two-way ANOVA to investigate the effect of both genotype and sex, significant differences were found between genotypes at 6 months for IL1b ($F_{3,8} = 19.48$, $p=0.0005$) and at 12 months for CCL2 ($F_{3,13} = 6.756$, $p=0.0055$), IL1b ($F_{3,15} = 13.34$, $p=0.0002$), IL1a ($F_{3,15} = 4.744$, $p=0.0161$) and TNF α ($F_{3,13} = 16.16$, $p=0.0001$). Post hoc testing revealed that 5xFAD (females only) and 5xFADxCCR2^{+RFP} mice showed significantly higher expression of IL1b than WT mice at the age of 6 months (see figure 34). At the age of 12 months, 5xFADxCCR2^{+RFP} mice showed significantly higher expression of CCL2 (males only), IL1b, IL1a (females only) and TNF α (females only) compared to WT mice. There were no significant differences between WT and 5xFAD mice and no significant differences were found between 5xFAD and 5xFADxCCR2^{+RFP} mice, in any age or sex. Only for CCL2 expression at the age of 12 months, there was a trend visible for higher expression in 5xFADxCCR2^{+RFP} mice compared to 5xFAD. Also, for several genes a trend was visible for higher expression in females than in males in 5xFAD and 5xFADxCCR2^{+RFP} mice. Finally, no differences were found between CCR2^{+RFP} and WT mice.

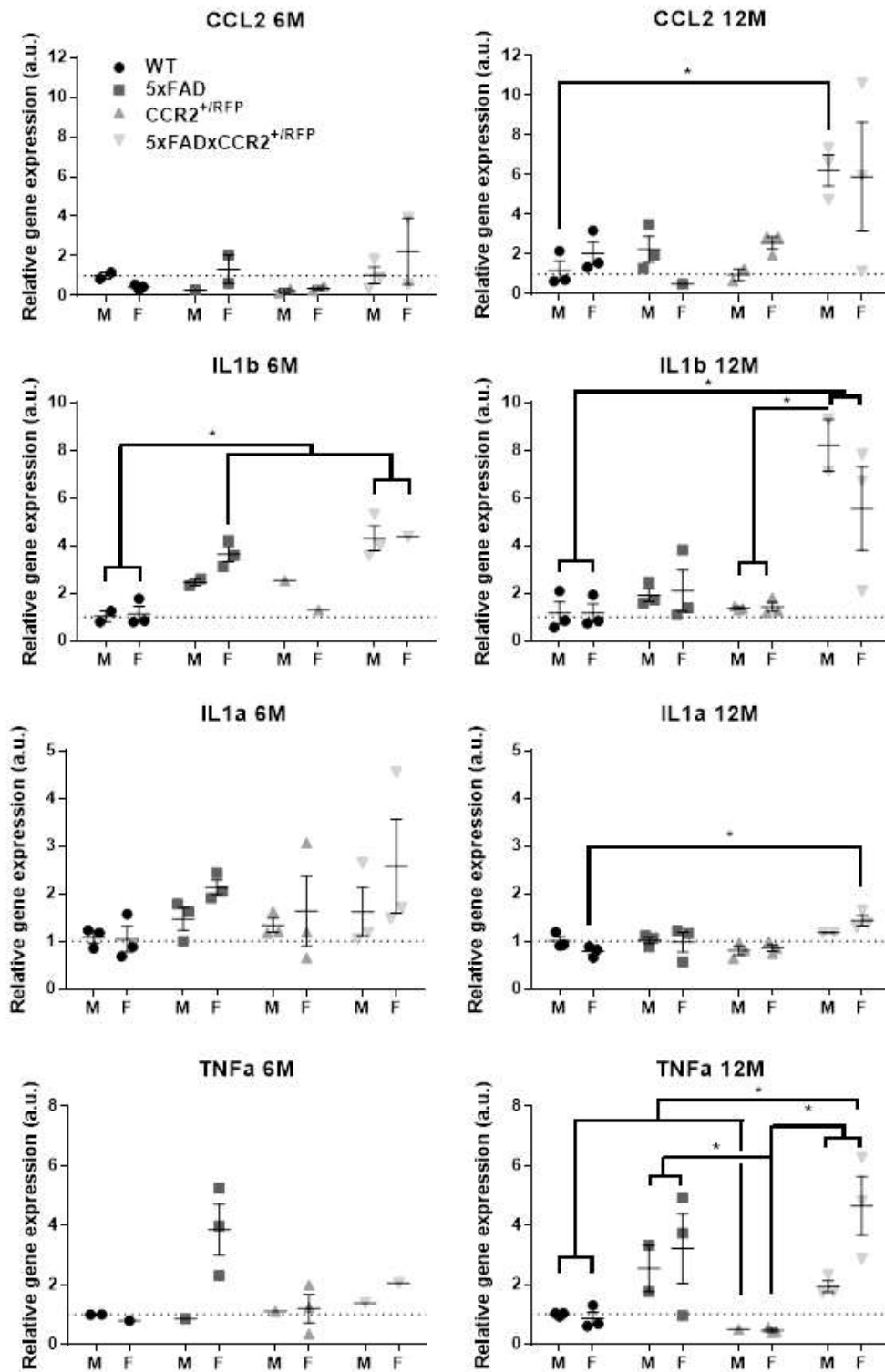


Figure 34. Gene expression of immune-related factors in prefrontal cortex of mouse brains. qRT-PCR was performed on prefrontal cortex tissue from WT, 5xFAD, CCR2^{+/RFP} and 5xFADxCCR2^{+/RFP} at the age of 6 and 12 months, in male (M) and female (F) mice. Two-way ANOVA with post hoc Tukey's, n=1-3, *p<0.05.

Behavioural studies

In addition to plaques, tangles, and immune-related changes, poor cognitive performance is another important characteristic of AD. To investigate this, and other possible changes in behaviour resulting from the knock-in of human tau, or the interplay between A β overexpression and human tau, behavioural studies were performed. WT mice were compared to htau-KI, 5xFAD, and 5xFADxhtau-KI mice. For each genotype, both sexes were compared at the ages of 6 and 12 months.

6 months

At the age of 6 months, the weight was significantly different between sexes, for all genotypes ($H = 62.104$, $df = 1$, $p < 0.05$), as shown in figure 35. Males have a higher weight than females. There were no differences in weight between genotypes.

In the rotarod, which tests motor skills and learning ability, a significant effect of sex ($H = 20.866$, $df = 1$, $p < 0.05$) was found. As visible in figure 35, females performed better than males, especially for the 5xFAD.

The pole test measures both motor skills and fear-related behaviour and revealed a significant effect of genotype both for the turn time ($H = 15.385$, $df = 3$, $p < 0.05$) and the down time ($H = 17.009$, $df = 3$, $p < 0.05$). Post hoc testing revealed that WT mice were significantly faster than 5xFADxhtau-KI mice (figure 35).

The open field and elevated plus maze are both used to measure anxiety-related behaviour in mice. When more time is spent in the centre of the open field or on the open arms of the elevated plus maze, mice are hypothesized to be less anxious. Both paradigms showed no significant differences between sexes or genotypes at the age of 6 months.

Spatial working memory is tested in mice using the Y-maze, with a higher percentage of perfect triads suggesting a better working memory. At 6 months, a significant sex effect was found in the Y-maze ($F(1,81) = 16.8$, $p < 0.001$), as well as an interaction effect between sex and genotype ($F(3,81) = 2.92$, $p = 0.039$). No effect of genotype alone was found. Post hoc testing showed a significant difference between male and female 5xFADxhtau-KI mice, with males performing better than females.

In the Morris water maze, the time to platform over 16 trials was plotted for each genotype and sex (see figure 36). Faster learning or better memory results in a steeper learning curve. Therefore, the area under these learning curves was compared as a measurement of cognitive abilities. At 6 months, a significant effect of genotype was found in this test ($F(3,82) = 7.14$, $p < 0.001$), but no effect of sex or an interaction effect (figure 35). The genotype effect was due to a significant difference between 5xFAD compared to WT and htau-KI mice, as well as a significant difference between 5xFADxhtau-KI and htau-KI. The difference between WT and

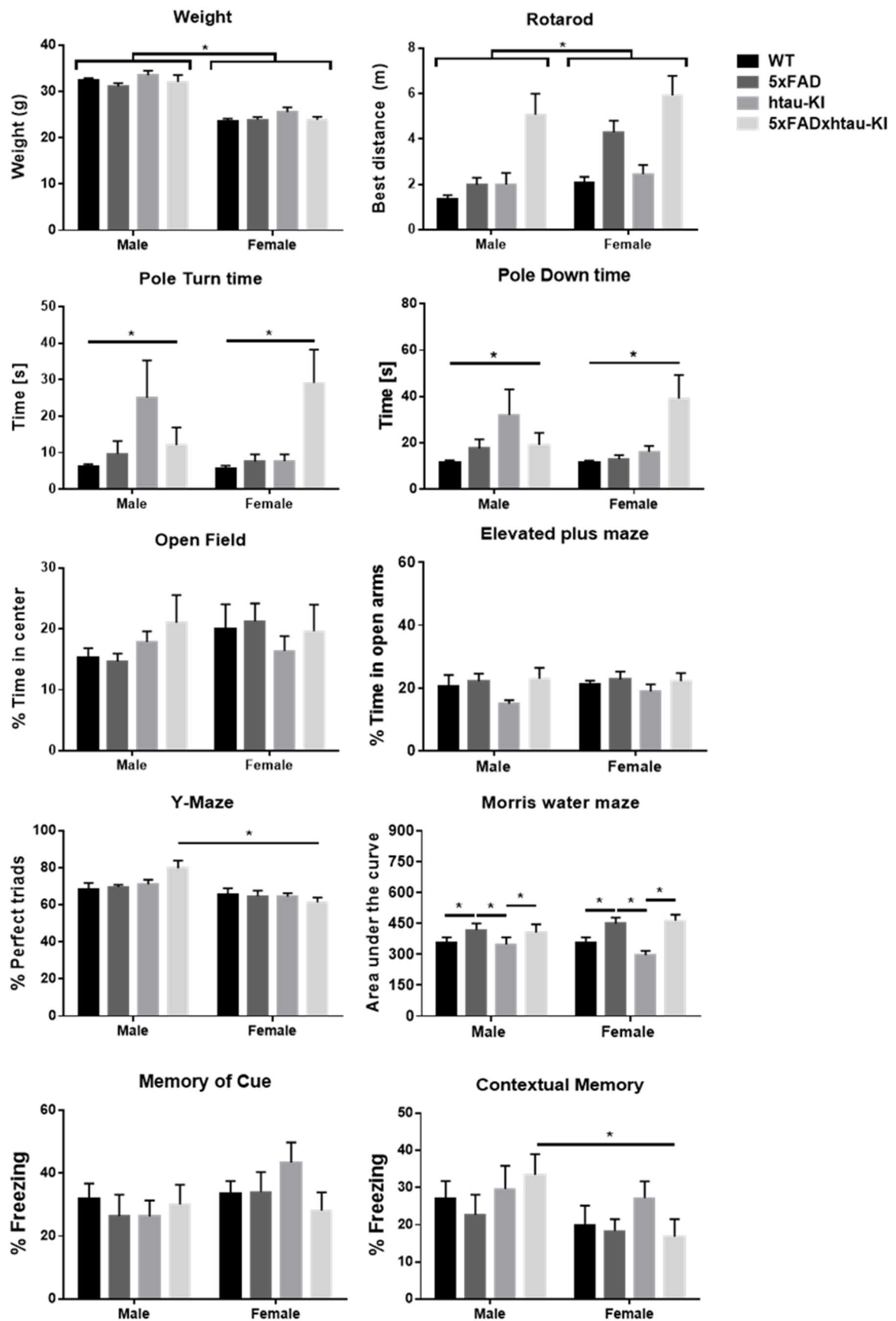


Figure 35. Behavioural data at 6 months of age. Results of all phenotyping experiments performed at the age of 6 months in WT, 5xFAD, htau-KI, and 5xFADxhtau-KI males and females. Two-way ANOVA or ordered logistic regression were used, with post hoc Tukey's, mean + SEM is shown, *p<0.05, n=8-14.

5xFADxhtau-KI is only slightly above the significance level ($p = 0.053$). Both 5xFAD and 5xFADxhtau-KI mice had a larger area under the curve than httau-KI mice (and WT mice), which means their cognitive performance was hampered.

Fear conditioning is another paradigm to measure cognitive performance. Increased freezing behaviour suggests better memory, either cue- or context-related. In the fear conditioning at 6 months, no significant differences were found for the memory of cue. In the contextual memory, a significant sex effect was found ($F(1,82) = 4.66$, $p = 0.034$), which was due to a difference between male and female 5xFADxhtau-KI. Male mice were freezing more in response to the environment, and thus showed better memory.

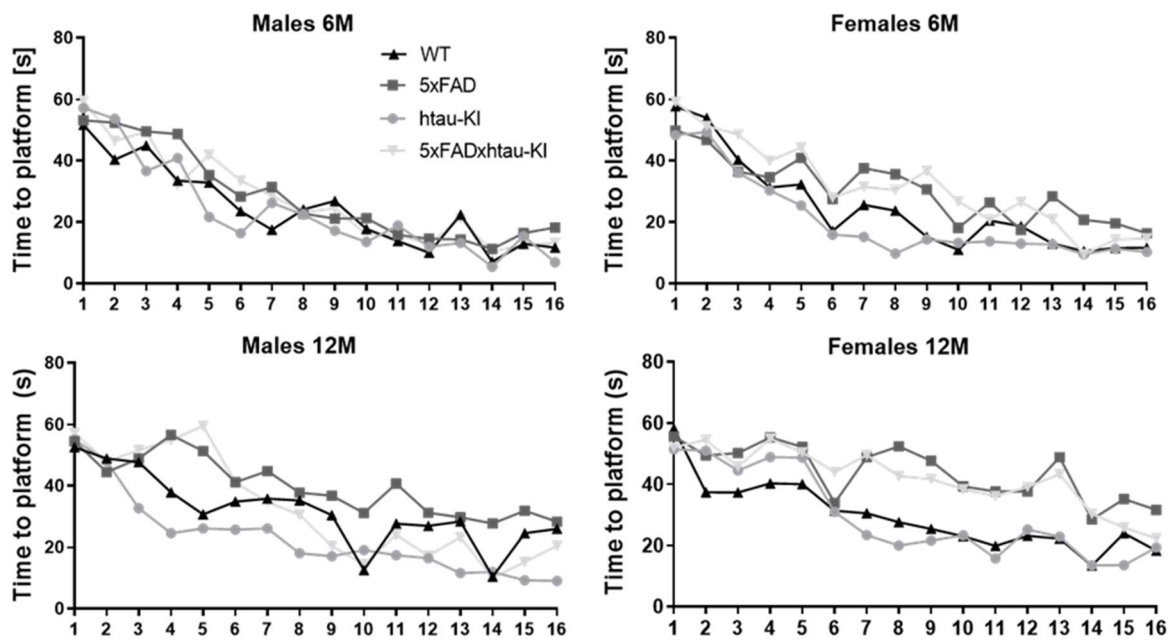


Figure 36. Morris water maze learning curves. Learning curves over 16 trials (4 trials/day over 4 days) of Morris water maze per genotype for 6-month-old males (top left), 6-month-old females (top right), 12-month-old males (bottom left) and 12-month-old females (bottom right) are shown. Maximum swimming time was 60 seconds. $n = 8-14$. Area under the curve was calculated for each genotype to compare results statistically.

12 months

The weight of mice at 12 months show significant genotype ($F(3,82) = 40.2$, $p < 0.001$) and sex ($F(1,82) = 142$, $p < 0.001$) effects, but no interaction (see figure 37). There was a significant difference between all genotypes, except for 5xFAD and 5xFADxhtau-KI, with the WT mice having a higher weight than 5xFAD and 5xFADxhtau-KI, and the httau-KI mice having an even higher weight than WT mice. Furthermore, mice of all genotypes showed significant sex differences, with male mice being heavier than female mice.

Interestingly, compared to 6 months of age, the results in rotarod seemed reversed. At 6 months of age, females performed significantly better than males. At 12 months, no significant

differences were found, but a clear trend was visible that males were performing better (figure 37).

In the pole test, a significant genotype effect was found ($F(3,80) = 7.80, p < 0.001$). WT mice were significantly faster to turn around than mice of the other 3 genotypes. Similar results were found for the time to reach the floor, with only a genotype effect ($F(3,80) = 11.0, p < 0.001$), also due to the WT mice being faster than the 3 other genotypes.

The open field results showed a significant effect of genotype on the percentage of time spent in the centre ($H = 8.442, df = 3, p < 0.05$). Post hoc testing, however, revealed no statistical significance between any of the groups, although there was a P-value of 0.056 for the comparison between WT and 5xFAD mice.

In the elevated plus maze, there was a significant effect of genotype on the % of time spent on open arms ($F(3,75) = 22.1, p < 0.001$). Both 5xFAD and 5xFADxhtau-KI mice spent more time on open arms than WT and httau-KI mice (figure 37). There was no sex-dependent effect and no interaction between sex and genotype.

In Y-maze, the % of perfect triads showed a sex-dependent effect ($F(1,80) = 7.89, p = 0.006$), as well as an effect of genotype ($F(3,80) = 3.48, p = 0.020$), but no interaction. Although a trend is visible of WT and httau-KI having higher percentages of perfect triads than 5xFAD and 5xFADxhtau-KI, the only significant difference was found between 5xFAD and httau-KI mice.

In the Morris water maze, the area under the learning curve was significantly different depending on genotype ($F(3,79) = 17.5, p < 0.001$) and sex ($F(1,79) = 7.39, p = 0.008$) separately, but there was no interaction effect (see also figure 36). Post hoc testing revealed a higher area under the curve (meaning impaired learning) for 5xFAD and 5xFADxhtau-KI mice compared to WT and httau-KI. Furthermore, there was a significant difference between males and females for both the httau-KI and the 5xFADxhtau-KI, with females showing a higher area under the curve than males.

In the fear conditioning paradigm, the percentage of freezing in response to the environment, as well as in response to the cue, was analysed. For the memory of cue, a significant sex effect was found ($F(1,80) = 4.03, p < 0.048$). Post hoc testing showed that this was due to both WT and 5xFAD males freezing more than females of the same genotype. For the contextual memory, also a significant sex effect was found ($F(1,80) = 8.27, p = 0.005$). This was due to a significant higher % of freezing by WT males than by WT females.

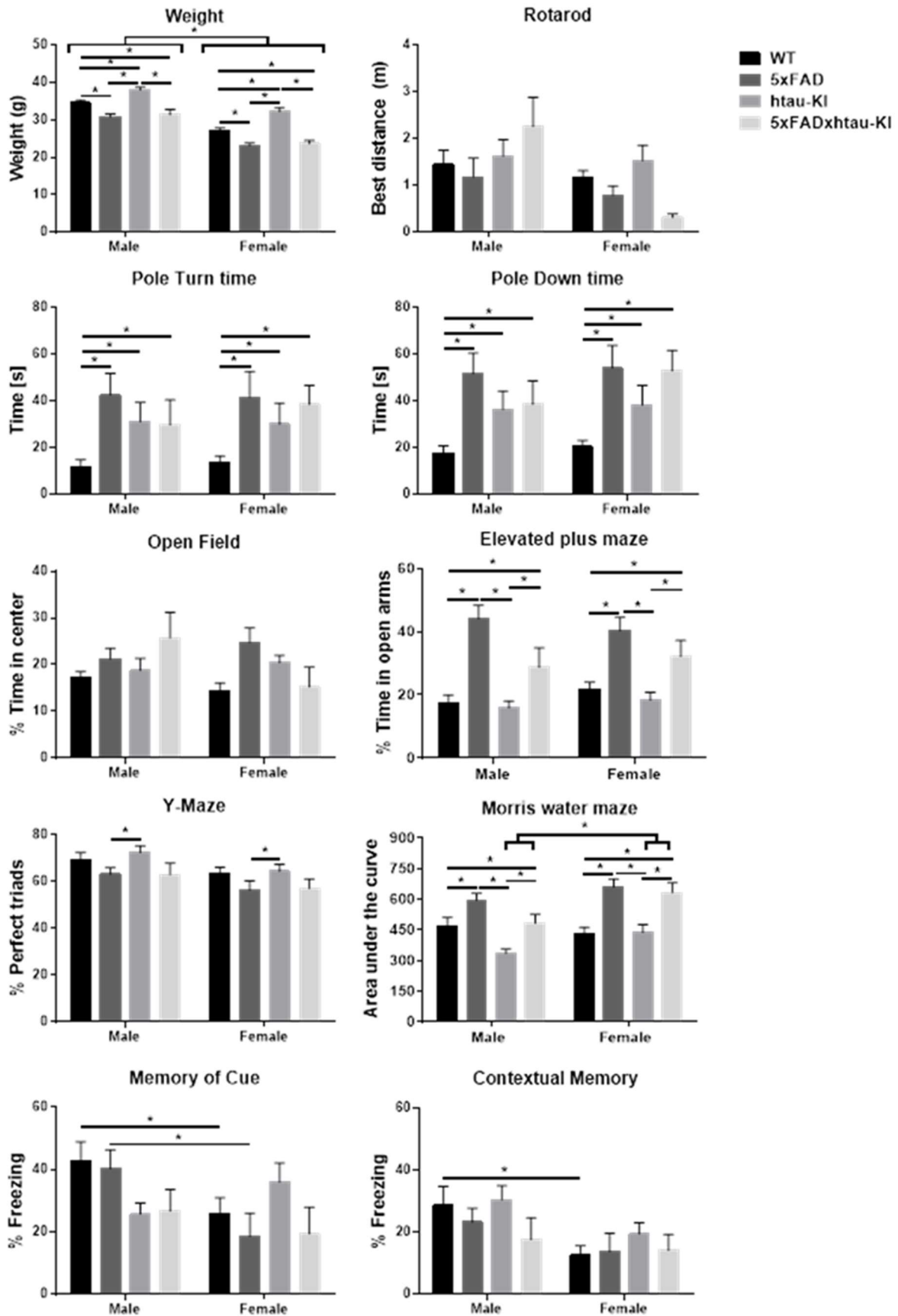


Figure 37. Behavioural data at 12 months of age. Results of all phenotyping experiments performed at the age of 12 months in WT, 5xFAD, htau-KI, and 5xFADxhtau-KI males and females. Two-way ANOVA or ordered logistic regression were used, with post hoc Tukey's, mean + SEM is shown, *p<0.05, n=8-12.

Phenotype at a cellular level

In collaboration with the KU Leuven (see also Barendrecht *et al.*, in preparation; Schreurs, 2020), the effect of human tau expression at a cellular level was investigated by performing electrophysiology on 8-month-old mice. No differences were found in the input-output curve between genotypes (figure 38a), confirming that all mice showed normal basal synaptic transmission. The paired-pulse ratio (figure 38b) is significantly different in htau-KI (at 10ms) and in 5xFADxhtau-KI (at 10 and 20ms). This suggest that plasticity mediated by short-term presynaptic effects is impaired in these mice.

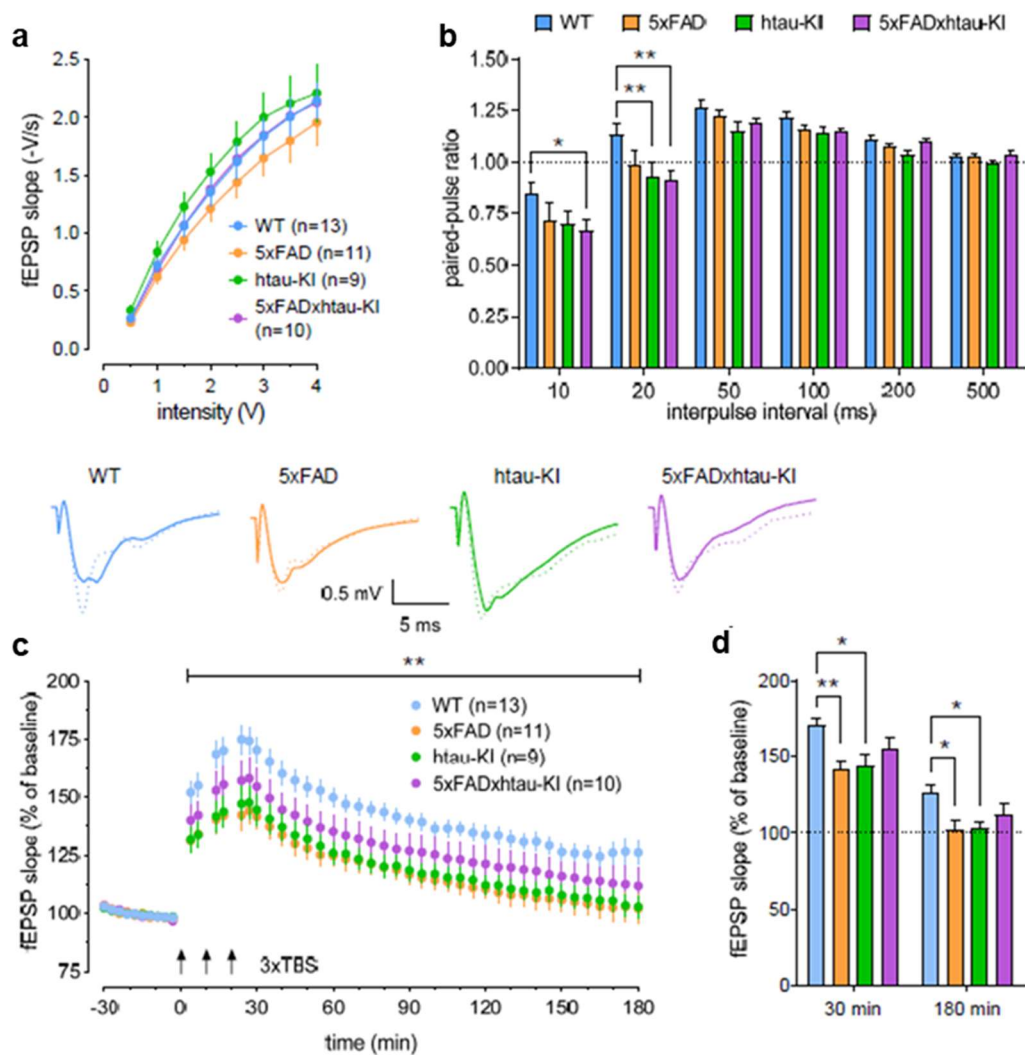


Figure 38. Basal synaptic transmission, paired-pulse response, and LTP in the CA1 region of the hippocampus at 8 months of age. Mice of all genotypes and both sexes were tested at the age of 8 months to determine the effect of human tau on the cellular phenotype in the CA1 region of the hippocampus. (a) input/output curve shows no significant differences. (b) paired-pulse ratio reveals a decrease in htau-KI and 5xFADxhtau-KI for the shortest interpulse intervals. (c) LTP is impaired in 5xFAD and htau-KI mice. (d) LTP is impaired both in the induction phase (30 min) and the maintenance phase (180 min). Insets in the middle show representative signals for each genotype during baseline (solid line) and at 180 min (dotted line). n=9-13. Mean \pm SEM are shown. * $p < 0.05$, ** $p < 0.01$, using RM-ANOVA and Dunnett's multiple comparison tests. TBS = theta-burst stimulation.

Long term potentiation (LTP) in the hippocampus is an important outcome measurement for impairments in learning and memory. As visible in figure 38c, there was a significant overall genotype effect ($F_{3,39} = 5.264$, $p = 0.0038$) on LTP. Post hoc analysis revealed that 5xFAD and htau-KI mice show impaired LTP compared to WT, whereas 5xFADxhtau-KI mice show intermediate levels of LTP. As shown in figure 38d, both at induction (30 minutes) and maintenance (180 minutes), LTP was significantly reduced in htau-KI and 5xFAD mice compared to WT mice. Similar to the immunohistochemistry and gene expression data from the NanoString mouse AD panel, these results again point to a protective effect of human tau specifically in an A β -overexpression background.

Furthermore, miniature inhibitory and excitatory postsynaptic potentials (mIPSP and mEPSP) were measured. These results provide information about elementary synaptic function of hippocampal neurons. As visible in figure 39a and d, there were no differences in amplitude between the different genotypes. For the inter-event-interval (IEI, the frequency, shown in figure 39b and e), a significant increase was found in htau-KI for the mEPSP ($p=0.0231$, Dunnett-T3 post hoc test) and in 5xFAD and 5xFADxhtau-KI for the mIPSP (5xFAD: $p= 0.0337$; 5xFADxhtau-KI $p=0.0066$, Dunnett-T3 post hoc tests). For the half-width (figure 39c and f), no differences were found between genotypes. Further analysis of the mEPSP and mIPSP by comparing the probability distributions of the data with the Kolmogorov-Smirnov test confirmed the genotype differences described above. For example, the cumulative probability plots of the IEI of mIPSP of transgenic mice (figure 39e) showed a significant shift towards shorter IEIs (higher frequencies) compared to WT. The analysis also detected significant genotype differences in the cumulative probability distribution of several other parameters (mIPSP amplitude, mIPSP inter-event interval, mIPSP half-width: all $p<0.0001$, mEPSP amplitude: WT vs htau-KI $p<0.0001$, WT vs 5xFADxhtau-KI $p=0.0061$, mEPSP inter-event interval: WT vs 5xFAD $p=0.0005$, WT vs htau-KI $p<0.0001$; mEPSP half-width: WT vs htau-KI $p<0.0001$, WT vs 5xFADxhtau-KI $p<0.0001$).

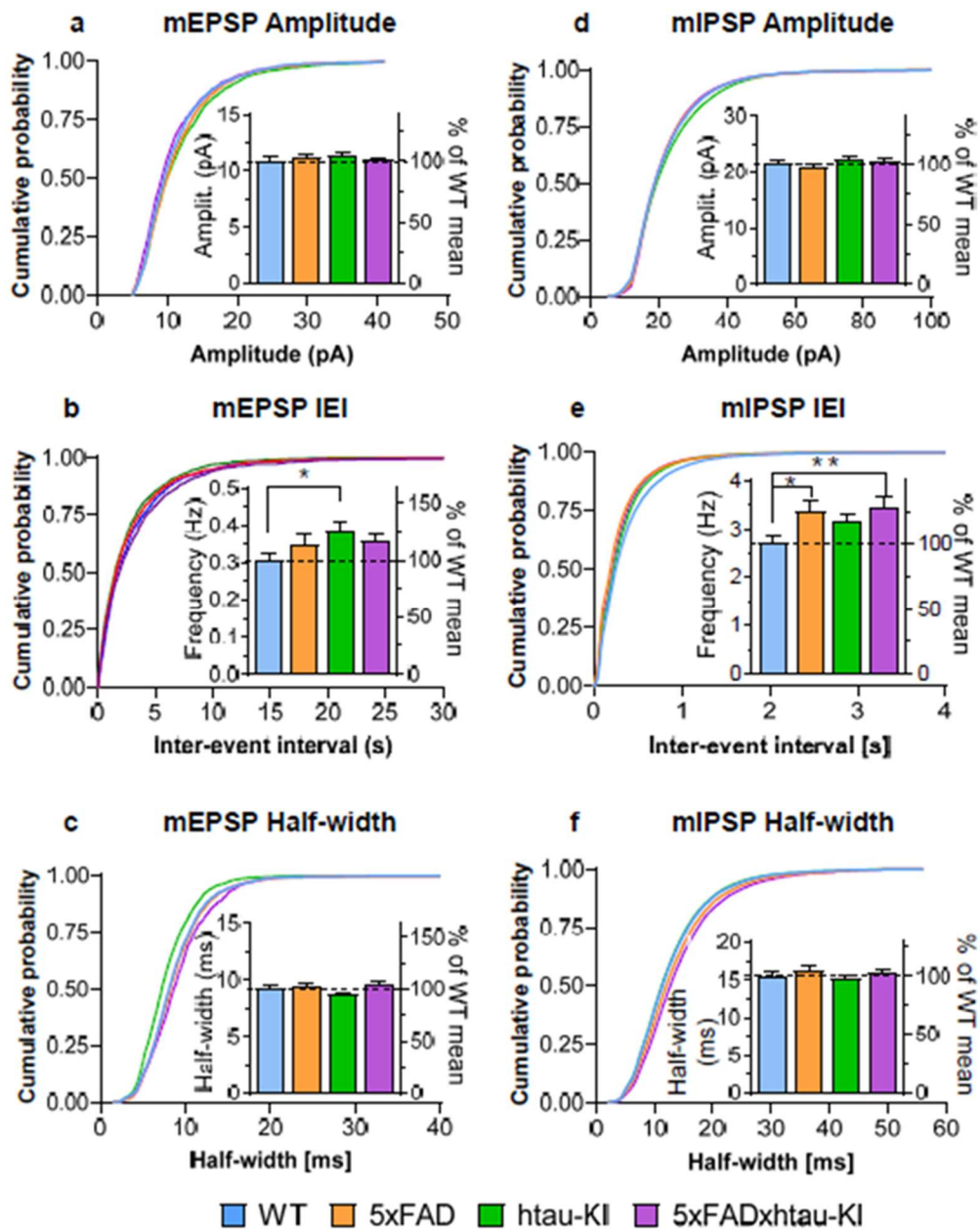


Figure 39. Action potential-independent activity in hippocampal neurons at 8 months of age. (a,d) Amplitude of mini excitatory and inhibitory postsynaptic potentials (mEPSP and mIPSP) in the hippocampal region of mice at 8 months of age show no significant differences. (b, e) Inter-event interval (IEI) of mEPSP and mIPSP show increased frequency of mEPSP for htau-KI and increased frequency of mIPSP for 5xFAD and 5xFADxhtau-KI. (c, f) Half-width of mEPSP and mIPSP revealed no significant differences. Each figure also shows the cumulative probability of the respective outcome parameter. n=9-13. Mean + SEM are shown. *p<0.05, **p<0.01 using Kolmogorov-Smirnov tests.

Further experiments

Besides the htau-KI model, we have also generated a hAPP-KI model. This was done together with Stem Cell Technologies, and used a similar approach by using the human WT APP sequence, and simultaneously knocking out the mouse APP. The final goal is to generate a completely humanized AD mouse model, replacing all genes relevant to AD by the human WT sequences. Tau, APP, and ApoE knock-in mice have all been generated as a part of this project. Hopefully, these models will lead to the discovery of new targets for AD therapy, which translate better to human AD pathology. This could improve the success rate of clinical studies with AD medication, due to the higher accuracy of the used targets. During my PhD thesis, I have bred the hAPP-KI model and confirmed the protein expression of human APP in these mice, as well as compared the expression between offspring of different original breeding pairs (see figure 40). Additionally, I've cross-bred the hAPP-KI mice with htau-KI mice (both homozygous) to generate aging groups for phenotyping and subsequent analyses of neuropathology. These analyses have started in 2020 and are therefore outside the scope of my thesis.

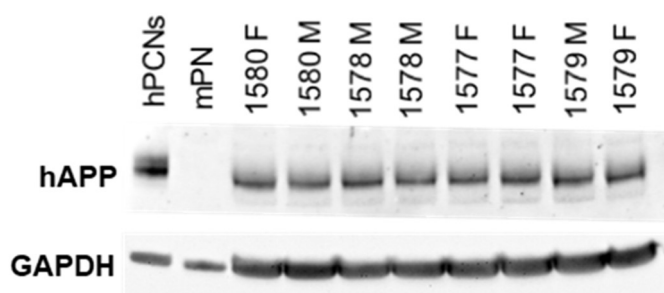


Figure 40. Western blot of human APP expression in different breeding pairs. The protein expression levels of hAPP (6E10, 1:1000) in the brain of 60-day-old mice was compared between offspring of different breeding pairs. hPCNs = human primary cortical neurons, mPN = mouse primary neurons, 15xx = number of breeding pair, M = male, F = female.

To elicit the role of different types of immune cells in AD pathology, I have bred 5xFADxCCR2^{RFP/RFP} mice for further research. Similar analyses as described above for 5xFADxCCR2^{RFP/-} have been planned for these mice in 2020, to unravel the effect of a full knock-out of CCR2 (and a resulting complete lack of infiltrating peripheral monocytes) on AD pathology. In addition, I have also crossbred another reporter line expressing green fluorescent protein (GFP) instead of the fractalkine receptor CX3CR1 (Jung *et al.*, 2000) with 5xFAD mice. CX3CR1 is expressed on microglia and its ligand fractalkine (CX3CL1) on neurons, showing that this interaction is important in neuron-microglia communication in the brain (Harrison *et al.*, 1998). As shown in figure 41, all microglia in the brain are GFP⁺ in a CX3CR1^{GFP/GFP} mouse, confirmed by the overlap with both Iba1 and CD11b, as shown previously by Cardona *et al.*, (2006). In the periphery, CX3CR1 is expressed by natural killer cells and monocytes (Campbell *et al.*, 2001; Geissmann *et al.*, 2003) and plays a role in recruitment of monocytes from the blood (Niess *et al.*, 2005). As part of the project described, aimed at unravelling the function of

different immune cells in AD, I have bred groups of 5xFADxCX3CR1^{GFP/GFP} mice, which will be investigated mid of 2020 and are therefore outside the scope of my thesis.

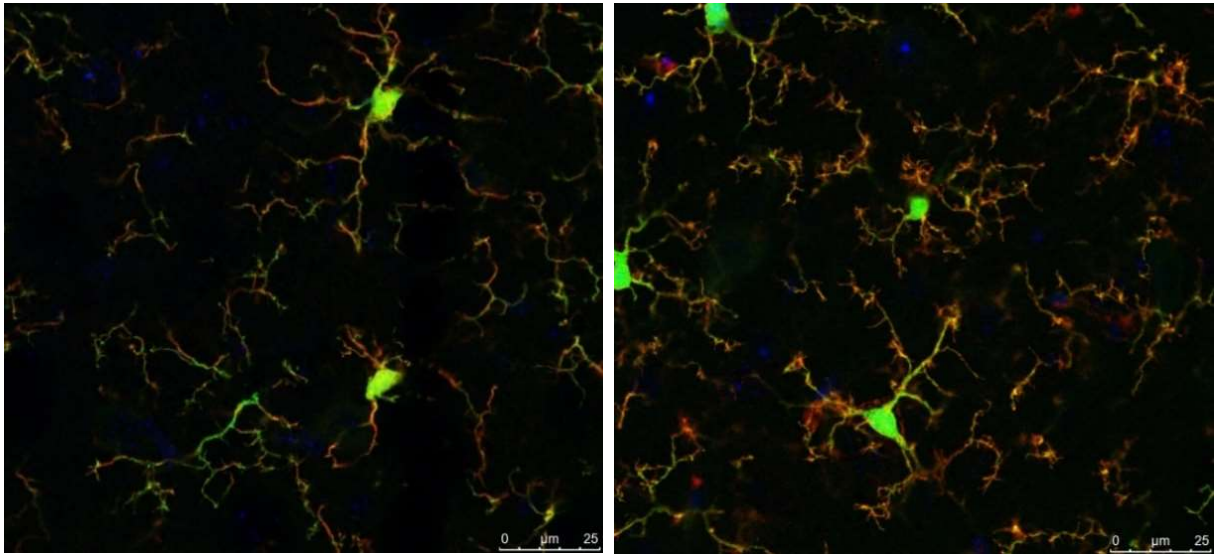


Figure 41. GFP expression in CX3CR1^{GFP/GFP} mouse brain. Immunohistochemistry was used to confirm the production of GFP in microglia in the brain. Iba1 (left) and CD11b (right) both showed complete overlap with the GFP staining, confirming that only microglia in the brain express CX3CR1. Red staining is Iba1 (left) or CD11b (right), blue staining shows nuclei (DAPI).

5. Discussion

Besides 5 drugs providing short-term symptom relief, there are currently no treatment options for AD. An important reason for this is the failure of clinical studies, after preclinical studies in mice show promising results. This is partly due to the mouse models, which do not fully recapitulate human AD pathology. While plaques can be successfully modelled by overexpressing mutated A β -related genes in mice, tangle pathology can only be induced by mutations unrelated to AD. This unphysiological modelling of AD pathology might lead to the discovery of targets for therapy development that are less relevant in human patients. The generation of humanized mouse models is therefore an important step in the development of therapeutic strategies for AD (Saito *et al.*, 2014; 2019; Sasaguri *et al.*, 2017). We developed a human tau knock-in mouse model using whole gene replacement. First of all, the characterization of the newly generated htau-KI model showed that the mice are viable and healthy and able to reproduce. The htau-KI mice express human tau at endogenous levels, with a simultaneous loss of mouse tau. Notably, all 6 isoforms of tau are expressed in brains of htau-KI mice throughout their life, whereas adult WT mice only express 4R tau (McMillan *et al.*, 2008). The molar ratio between 3R- and 4R tau is equal to 1 in healthy human brain, as well as in AD patients (Goedert *et al.* 1989; Ingelsson *et al.*, 2006). In the htau-KI mice, an almost complete shift to 3R tau mRNA production was found, resulting in a 20-fold overexpression of 3R tau isoforms compared to 4R tau isoforms. Considering that adult mice normally do not produce the 3R tau splicing isoforms, this is an interesting finding. As far as I know, I am the first to use the qRT-PCR method by Ingelsson *et al.* (2006) for exact quantification of mRNA of tau isoforms in mice. Andorfer *et al.* (2003) showed a RT-PCR which also suggested an overexpression of 3R tau compared to 4R tau in their hTau mice. Saito *et al.* (2019) showed equal expression of 3R- and 4R tau isoforms with RT-PCR quantification in their human tau knock-in model. Interestingly, a Western blot by Saito *et al.* (2019) showed increased band intensity for 0N3R tau compared to 0N4R tau, suggesting that a similar overexpression takes place in their human tau knock-in model, which cannot be accurately quantified with RT-PCR. Unfortunately, the protein levels of 3R and 4R tau could not be quantified yet in our htau-KI mice to confirm the overexpression of 3R tau. This is an important requirement for better understanding of the splicing mechanisms.

Additionally, it is important for the development of AD therapy to model and understand the interactions between A β and tau (Pickett *et al.*, 2019). These studies are also hampered by the differences between human and mouse tau and the use of tau mutations unrelated to AD. We have therefore crossed the htau-KI model with the well-known 5xFAD mouse model, which overexpresses human A β with 5 familial AD mutations. Although we are aware that the 5xFAD model introduces unphysiological artefacts and the ultimate goal is to generate a completely

humanized AD mouse model, the crossbreeding of 5xFAD with htau-KI provides a good opportunity to investigate the interaction between human A β and human tau because of the fast disease development. Additionally, we believe some mutations in APP might be necessary to start the development of AD pathology in the limited life span of mice. Therefore, the crossbreeding of 5xFAD with htau-KI is a helpful approach to investigate the interaction between A β and tau. So far, there has been no proof in mice that plaque pathology can induce tangle formation, even in a human tau background (Yetman *et al.*, 2016; Pickett *et al.*, 2019). This suggests that there is no link between both neuropathological hallmarks of AD. Ke *et al.*, (2012) hypothesized that the presence of mouse tau is the reason for a lack of tangle formation, because mouse tau seems to have a rescuing effect on AD pathology in transgenic models expressing mutant human tau. In the newly generated htau-KI mice which express only human tau and no mouse tau, we found that a high amyloid background is also not sufficient to induce tangle formation. Even though all 3 isoforms of 3R tau are expressed, we only found plaque-associated dystrophic neurites in the brains of these mice, and no tangle pathology. The same was shown by Saito *et al.* (2019), who combined another APP model with a human tau knock-in mouse. They found no tangles, but intensified phospho-tau staining (AT8, PHF-1 and pS422) in mice combining APP with human tau compared to human tau expressing mice alone. They found the same upregulations in phospho-tau, however, in APP mice compared to WT mice and failed to make a direct comparison between APP mice and APP mice with human tau expression. There are several possible explanations for the fact that the presence of human A β and human tau results in tangle formation in a human brain, but not in a mouse brain. First, the lifespan of a mouse might be too short. Alzheimer's disease pathology develops over a long period of time in the human brain, with amyloid pathology preceding tau pathology by decades. The formation of dystrophic neurites and MC1-specific conformation of tau are described as early stages of tangle formation, and longer aging might thus be required. Saito *et al.* (2019) found no tangles after 24 months of aging their combined mouse model, suggesting that a mouse life is not long enough for tangle formation. Another possibility for the lack of tangle formation might be a lack of hyperphosphorylation. It is known that aggregation of tau is dependent on hyperphosphorylation (Chohan *et al.*, 2005). Furthermore, there are differences between AD patients and healthy controls in the expression levels and activity of several phosphatases and kinases (Gong *et al.*, 1995; Lee *et al.*, 1999; Sontag *et al.*, 2004; Swatton *et al.*, 2004). Together, these changes could cause the hyperphosphorylation of tau, and the resulting tangle formation. The lack of strong hyperphosphorylation in mouse brain could be a reason for the absence of tangles. Finally, in the hTau mouse model by Andorfer *et al.* (2003), a shift to 4R tau caused stronger pathology (Schoch *et al.*, 2016). The Andorfer model, similar to the htau-KI mouse, normally shows strong overexpression of 3R tau compared to 4R tau. Considering the 20-fold overexpression of 3R tau in htau-KI mice

described here, a similar shift to 4R tau might therefore also cause hyperphosphorylation and tangle pathology. Finally, it might be interesting to expose the htau-KI mouse line to an immune challenge or different diet. Since these environmental factors are known to play a role in the development of AD, it would be interesting to mimic these environmental stimuli in mice and follow the pathological development.

Dystrophic neurites are formed in response to A β pathology and show an accumulation of A β and BACE 1 (beta-site amyloid precursor protein cleaving enzyme 1, the most important β -secretase), together with an extensive disruption of microtubule (Sadleir *et al.*, 2016). In this thesis, plaque-related PHF1⁺ and CP13⁺ dystrophic neurites were found in both 5xFAD and 5xFADxhtau-KI mice. This confirms that dystrophic neurites are formed in response to A β pathology, independent of which species of tau is expressed. The dystrophic neurites were found in striatum, superior colliculus, hypothalamus, cingulate gyrus, and brain stem, whereas the hippocampus and cortex were relatively less affected. The plaque pathology, however, was strongest in hippocampus and cortex, consistently with other papers describing 5xFAD mice as well as AD patients (Thal *et al.*, 2002; Oakley *et al.*, 2006; Bhattacharya *et al.*, 2014). It would be interesting to further explore this finding and investigate the development of dystrophic neurites in different brain regions over time and in relation to plaque pathology. Additionally, a complete characterization of dystrophic neurites is required to understand which protein (A β , tau, BACE 1 or other) is accumulating first and how this accumulation damages the cell and results in a loss of neuronal function. Understanding and possibly preventing the destruction of neurites could be an important step in the treatment of AD.

Interestingly, we found that MC1 staining was absent in 5xFAD mice and gave a clear signal in htau-KI and 5xFADxhtau-KI mice at the age of 13 months. The MC1 antibody does not bind to phospho-tau epitopes, but to a specific pathological conformation of tau, which is detected early in human AD pathology (Ikonovic *et al.*, 1997). The epitope is a combination of amino acids 7-9 in the N-terminus and amino acids 313-322 of tau and is only accessible after folding of the tau protein. In this epitope, only amino acid 9 of tau differs between mouse and human tau, leading to two possible explanations for the specific staining: (1) MC1 does not detect mouse tau or (2) mouse tau does not fold into the MC1-specific confirmation. Since mouse tau can stain positive for MC1 in a pro-aggregation model (Mocanu *et al.*, 2008) and a model using pathological human tau injection (Winston *et al.*, 2019), it seems likely that the second hypothesis applies. Interestingly, MC1 staining was also visible in htau-KI mice alone. This could suggest that human tau is more likely to fold into pathological confirmation, independent of amyloid deposition. This hypothesis matches the findings by Ke *et al.* (2012), showing that mouse tau has a protective function in tau pathology. Further testing is required to confirm this

hypothesis. Additionally, MC1 provides more specific information than phospho-tau antibodies, especially since phosphorylation of tau at many epitopes is not pathological per se (Matsuo *et al.*, 1994). The MC1 antibody is therefore important to use in the characterization of AD models, as well as in different stages of human AD pathology. If there is indeed a clear difference between human and mouse tau in the ability to form the pathological conformation of tau, this will be of importance in preclinical testing of tau-based therapies. The htau-KI model could be a major improvement compared to other AD models in this regard.

Besides the effect of A β on tangle pathology, the reverse influence of human tau expression on plaque pathology was also investigated. Yetman *et al.* (2016) showed no interaction between A β and human tau in a model expressing human A β with the Swedish and Indiana mutation. Pickett *et al.* (2019) found a decrease in plaque pathology in APP/PS1 mice when human tau overexpression was induced. In this thesis, no significant differences were found in the area of plaques between 5xFAD and 5xFADxhtau-KI mice, neither in whole brain, nor in cortex or hippocampus. Interestingly, a trend was found for a lower area of plaque pathology in 5xFADxhtau-KI mice compared to 5xFAD mice at the age of 13 months. An increased sample size is required to confirm this trend, which might suggest a protective effect of human tau on plaque formation, such as shown by Pickett *et al.* (2019). In this regard, a comparison of gene expression data from the NanoString mouse AD model to human *post-mortem* gene expression levels also revealed a protective effect of human tau, but only in the presence of A β . Specifically for oxidative phosphorylation at 7 months and the ECM-receptor interaction pathway at 13 months, the gene expression was reversed in 5xFADxhtau-KI mice compared to human data. Oxidative phosphorylation is the process by which cells produce energy to live, taking place in the mitochondria. The ECM receptors are involved in intercellular communication and play an important role in tissue and organ maintenance. Both mechanisms apparently play an important role in the interaction between A β and tau in the 5xFADxhtau-KI mouse model. Mitochondrial dysfunction plays an early role in human AD patients (Liang *et al.*, 2008; Wang *et al.*, 2008). Additionally, a relation between mitochondrial dysfunction and human tau expression was shown in several papers (Kopeikina *et al.*, 2011; Shahpasand *et al.*, 2012; Li *et al.*, 2016). The expression of human tau is protective against early apoptosis but results in long-term energy deficits by changing mitochondrial functioning. Eventually, neuronal death occurs due to the lack of cellular energy (Li *et al.*, 2016). Although there is an ongoing discussion whether pathological tau triggers mitochondrial dysfunction or the other way around, it is clear these two pathological mechanisms are related in AD patients and play an important role in synaptic loss and cognitive impairments (reviewed in Cheng & Bai, 2018). The increased expression of mitochondria-related genes found in our study should first be confirmed with qRT-PCR. Subsequently, the consequences of this expression for

mitochondrial functioning should be investigated, possibly by culturing htau-KI neurons and measuring mitochondrial functioning, or by using electron microscopy. If there is indeed an early protective effect of human tau expression in AD, possible therapies could use a similar strategy to prevent neurodegeneration at later time points. The role of ECM proteins is also described in human AD. Lepelletier *et al.* (2015) described early changes in the ECM, such as increased expression of Collagen IV, perlecan and fibronectin in AD patients, which correlated with amyloid pathology. A review by Sethi and Zaia (2017) described many other ECM proteins that are known to play a role in AD pathology. The specific relationship between tau and the ECM is also described in two papers: Morawski *et al.* (2010) and Suttkus *et al.* (2016) described a protective effect of specific ECM proteins, called aggrecan-based perineuronal nets, against neurofibrillary tangle formation. Based on *in vitro* experiments and staining in *post-mortem* tissue from human AD patients they hypothesize that the extracellular environment somehow prevents tau from forming tangles. Obviously, it is important to understand the underlying molecular mechanisms by which ECM proteins can interact with tau and prevent its pathological accumulation. Our finding that human tau has a protective effect on ECM interactions specifically in a 5xFAD background needs to be validated first in qRT-PCR. Afterwards, more experiments are required to understand the interaction of tau with ECM proteins, especially the specific protective effect of human tau. The idea that tau might have a protective function in the development of AD is not new. It has been described that hyperphosphorylation and subsequent aggregation of tau might be a protective mechanism (Castellani *et al.*, 2008; Cowan & Mudher, 2013, Cowan *et al.*, 2015). In this regard, the finding that human tau is more likely to form MC1⁺ tau conformations might also be supportive of the hypothesis that human tau has a protective function. Obviously, more research is required to confirm these findings and subsequently understand the underlying mechanisms. The use of this new htau-KI model is of great importance in this regard.

On top of histopathological and molecular mechanisms, it is important to understand the effects of human tau on functional outcomes at the cellular and behavioural level. The electrophysiology performed by our collaboration partners from Leuven, Belgium shows normal basic synaptic transmission for all genotypes. LTP, however, was significantly impaired in 5xFAD and htau-KI mice compared to WT, whereas 5xFADxhtau-KI showed an intermediate phenotype. Again, this partial rescue in 5xFADxhtau-KI mice points to a protective effect of human tau in interaction with A β overexpression. Impaired LTP has been shown before in 5xFAD mice (Seo *et al.*, 2014; Colié *et al.*, 2017). The finding that replacement of mouse tau by human tau causes LTP deficits was, however, surprising. Saito *et al.* (2019) unfortunately did not investigate cellular functioning in their human tau model. The only comparison is therefore with the Andorfer hTau model, which showed reduced basal synaptic transmission

at the age of 12 months and increased paired pulse ratio at 4 months of age (Polydoro *et al.*, 2009). Furthermore, a lack of LTP after high frequency stimulation was found, but normal LTP after theta burst stimulation. In our protocol, using theta burst stimulation, we found impairments in LTP. Clearly, there are large differences between the hTau model by Andorfer and our htau-KI mice, both in basal synaptic transmission and LTP. The finding that hTau mice show memory deficits at the age of 12 months in the Morris water maze underlines this, since our htau-KI mice performed normally in this test. Additionally, the hTau model shows aggregations of PHF tau, which were absent in our htau-KI mice (Andorfer *et al.*, 2003). A possible reason for these differences is the method of generation of both models. While the htau-KI model was generated by whole gene replacement, the hTau model used random integration of a complete human transgene version of tau, including promoter. Our analysis of spontaneous excitatory and inhibitory neuronal activity also revealed some effects of human tau expression. The increased frequency of mEPSPs in htau-KI mice, combined with the unchanged amplitude and half-width, suggest an increase in presynaptic activity of glutamatergic synapses. A paper using P301L mice showed contradictory effects: a decrease in both amplitude and frequency of mEPSPs (Hoover *et al.*, 2010). As a control, they used mice overexpressing human WT tau. These mice also showed a decrease in mEPSP frequency compared to WT. The authors hypothesized that the strong hyperphosphorylation of tau results in mislocalization of tau in the dendrites, where glutamate signalling is subsequently impaired. Compared to our data, these completely opposing effects confirm that the physiological expression of human WT tau is an important step to improve our understanding of tau pathology and its effect on cellular functioning. Interestingly, both 5xFAD and 5xFADxhtau-KI revealed no changes in mEPSP frequency, but increased frequency of GABA_A-mediated mIPSPs. As far as we know, there are no other publications with measurements of mIPSPs in 5xFAD mice. Papers using other AD mouse models show conflicting results regarding mIPSP and mEPSP frequency and amplitude, and some interesting sex-specific effects (Palop *et al.*, 2007; Bories *et al.*, 2012; Liang *et al.*, 2014). Roberson *et al.* (2011) found a reduced frequency of mEPSPs and an increased frequency of mIPSPs in hAPPJ20 mice, which was rescued by knocking out mouse tau. Clearly, there are many different mechanisms at play at the synaptic level in AD mouse models, strongly depending on the used model, as well as the age and sex of the mice. We believe the htau-KI mouse line provides an important step towards better understanding of the interactions in AD, because there is no confounding effect of overexpression, mutations, or the presence of mouse tau. First, to better understand the effect of human tau on synaptic functioning, it would be useful to replicate the data from this study, and support the findings with presynaptic and postsynaptic staining to link the functional outcome parameters to specific synaptic changes.

Since tau aggregation in AD is strongly linked to cognitive deficits, which are likely caused by synaptic changes, it is important to understand these mechanisms in detail.

Finally, I also performed full behavioural characterization of the htau-KI mouse model, as well as the cross-bred 5xFADxhtau-KI mice. The first aim was to investigate general health of the htau-KI mice. Since the most used mouse model for tau pathology (carrying the P301L mutation) develops motor deficits and even paralysis (Lewis *et al.*, 2000), it was important to investigate motor function in the newly generated htau-KI mice. Additionally, cognitive performance is an important outcome for AD mouse models. Therefore, several tasks related to different cognitive parameters were performed to characterize the mice and investigate the impact of neuropathological changes on behaviour.

It is known that, on average, male mice have a higher weight than female mice, which was clearly reflected in my data. Also, adult 5xFAD mice have a reduced weight compared to WT (Jawhar *et al.*, 2010; Bhattacharya *et al.*, 2014). As expected, both 5xFAD and 5xFADxhtau-KI mice (of both sexes) showed lower weight than WT mice. Interestingly, both male and female htau-KI mice showed increased weight compared to WT mice. Currently, there is no explanation for this finding. As far as I know, there is no known relation between the functions of tau and any factor related to weight such as food intake or fat production. This finding therefore needs to be validated first in other studies.

It is known that 5xFAD mice need longer to turn around and climb down in the pole test (unpublished data from the Fraunhofer IZI – Department of drug design and target validation), which would also explain the reduced performance levels in 5xFADxhtau-KI mice. It is interesting that htau-KI mice also need longer to climb down the pole. Together with the rotarod test however, which showed no differences between genotypes, it is difficult to draw a conclusion about the impairment of motor skills in htau-KI mice (as well as in 5xFADxhtau-KI mice). For further research, it is important to realize that the pole test might not only be a test for motor skills. Other factors such as fear and anxiety may play an important role. In addition, further development of the rotarod protocol might be useful, to improve the distinctive character of the test. Especially since some papers showed a significantly worse performance by 5xFAD mice compared to WT on the rotarod (Peters *et al.*, 2013; O'Leary *et al.*, 2018), whereas other AD mouse models (both APP based models, as well as the P301L model) perform significantly better than controls on the rotarod (Morgan *et al.*, 2008; Filali *et al.*, 2012; Oore *et al.*, 2013). It is thus clear that a standardized protocol is required, as well as an explanation of the underlying factors influencing the behaviour in these tests. Based on the primary screening and available data, I conclude that the htau-KI model does not have severe motor deficits, such as found in other tau mouse models (Lewis *et al.*, 2000).

In the elevated plus maze, 5xFAD mice show reduced anxiety compared to WT mice (Wirths *et al.*, 2010). This finding was confirmed in the current study, where 5xFAD and 5xFADxhtau-KI mice spent more time on the open arms than WT. htau-KI mice showed similar performance to WT mice. Interestingly, a difference in results was found between the elevated plus maze and open field. Although both tests are generally used to draw conclusions about anxiety-like behaviour by avoidance of open spaces, 5xFAD and 5xFADxhtau-KI mice spent more time on the open arms of the elevated plus maze but showed no difference to controls in the open field set up. Although this could be a result of an unoptimized protocol, another publication even showed contradicting results between these two tests in 5xFAD. Griñán-Ferré *et al.* (2016) found that 5xFAD mice spent more time in open arms on the elevated plus maze, but less time in the centre of the open field compared to WT. This suggests a discrepancy between elevated plus maze and open field in the underlying behaviour measured. This is an interesting hypothesis and requires further investigation, independently of AD mouse models. For the htau-KI model, it can be concluded that there is no effect of human tau expression on anxiety-related behaviour. The overexpression of mutated human A β clearly results in decreased anxiety, independent of the species of tau expressed.

In several publications investigating 5xFAD mice in the Y-maze (Oakley *et al.*, 2006; Devi *et al.*, 2015; Kang *et al.*, 2018), a significant difference in performance compared to WT mice was found at 4-5 months of age, with increasing cognitive deficits over time. Other papers, however, show no difference (Devi & Ohno, 2015). Our data shows a trend of lower spontaneous alternation in 5xFAD and 5xFADxhtau-KI mice compared to WT and htau-KI mice at the age of 12 months, but only a significant difference between htau-KI and 5xFAD. The methods in our paper were comparable to published data, and the results are in a similar range. Quite possibly, an increase of the number of mice would show a significant effect of genotype, for both 5xFAD and 5xFADxhtau-KI, compared to the other 2 groups.

Another test for cognition and memory, the Morris water maze, showed clear significant differences between 5xFAD and 5xFADxhtau-KI compared to WT and htau-KI mice, matching findings by other groups using 5xFAD and WT mice (Bouter *et al.*, 2014; Tang *et al.*, 2016). Both the set up and the protocol of this test have been extensively optimized prior to these experiments, showing consistent deficits in 5xFAD mice in our lab (unpublished data). It can therefore be concluded that the htau-KI mice show normal learning behaviour, whereas 5xFADxhtau-KI mice show impaired behaviour, equal to 5xFAD mice.

Fear conditioning is generally used as another behavioural measurement of memory and learning, and 5xFAD mice are therefore expected to show deficits in this test (Kimura & Ohno, 2009; Devi & Ohno, 2010; Seo *et al.*, 2014). Several papers revealed however, that the used protocol can directly affect the results of the fear conditioning paradigm. It has been described that the salience of the environment plays an important role. If the environment is very salient,

the conditioning is stronger and the pathology is less likely to have an effect (Corcoran *et al.*, 2002). The same is shown for multiple foot shocks: with more shocks there is no difference between 5xFAD and WT mice, whereas 1 shock leads to a significant memory deficit in 5xFAD mice (Kimura & Ohno, 2009). Thus, when the conditioning is extraordinarily strong (due to a highly salient environment or multiple foot shocks), the 5xFAD pathology does not have an effect. In this thesis, no significant differences were found between the genotypes in the contextual fear conditioning, as well as the memory of cue. A possible explanation is that the conditioning is too strong in our protocol, causing all genotypes to show the same behaviour. Another possible explanation is that fear-related memory is less affected in 5xFAD mice. Spatial learning such as measured in the Morris water maze is hippocampus-dependent. This region is severely affected in AD. Fear-related memory is amygdala-dependent. Since this region is affected later and less strongly in AD, it is possible that the fear conditioning paradigm only shows impairments at a later age and disease stage.

Sex differences

Due to the importance of sex for the development of AD (Fisher *et al.*, 2018), mice of both sexes were investigated in this study. In addition to an obvious increase in weight in male mice compared to female mice, some other behavioural differences were also found. Most differences (at 6 months in Y-maze and contextual fear conditioning and at 12 months in Morris water maze and both contextual and cued fear conditioning) showed better performance in 5xFAD(xhtau-KI) males than in females and there was a trend visible for a higher plaque load in female mice, especially in the total brain and cortex. The same trend was visible when 5xFAD mice were compared to 5xFADxCCR2^{+RFP} mice, both in immunohistochemistry of plaques and immune cells, as well as gene expression analysis of immune-related genes. In the gene expression data of the NanoString panel, no differences were found between males and females and the electrophysiology unfortunately did not have a large enough sample size to investigate both sexes separately. Most sex differences that we found point to aggravated pathology in female mice compared to male mice, as expected based on the literature (reviewed in Fisher *et al.*, 2018). This sex difference was not shown consistently in all experiments, however. Possible explanations are the small sample size and the non-optimal protocols for some of the behavioural tests. Another hypothesis is that discrepancies between males and females in the development of AD pathology only apply to certain parts of the disease, whereas other symptoms/deficits develop equally. For example, no sex differences were found in the pole test, open field, and elevated plus maze. This suggests that anxiety-related behaviour is affected similarly in males and females in AD. In the Y-maze, Morris water maze and fear conditioning, however, several differences were found. This suggests that the cognitive deficits develop differently in males compared to females. Importantly, these

differences were independent of tau species and not consistent in all tests. The rotarod test revealed a general sex effect, which was age-dependent. At the age of 6 months, females performed significantly better than males. Interestingly, this was reversed at the age of 12 months, with males performing better (although not significantly).

Finally, a reduced performance in the Morris water maze was found in female htau-KI compared to male htau-KI mice. In general, htau-KI mice showed similar performance to WT mice in the Morris water maze. Male htau-KI mice showed a lower area under the curve, suggesting strong cognitive performance. Another trial of the Morris water maze (possibly with higher n) is required to confirm this result, because it would suggest a sex-specific effect of htau on cognition, in the absence of amyloid pathology. For the htau-KI model, we observed no differences between males and females in the mRNA expression of 3R and 4R tau, but increased MC1 staining in females. Together, these results clearly show that sex is always an important factor to consider and more research is required to understand sex differences in mice in general, as well as in relation to AD pathology. A characterization of both sexes is always important in (AD) mouse models. Very often, only female mice are used in behavioural experiments because they are group-housed more easily, or only male mice are used to exclude the effects of sex hormones during the female hormonal cycle. Also, in many papers the sex of the mice used for experiments is not mentioned at all. Firstly, the underlying mechanisms responsible for the sex differences can be better understood by investigating both sexes. In addition, it is important from an ethical point of view to use both male and female mice in behavioural experiments whenever possible, since this leads to a 50% reduction of animals needed for breeding and experiments.

As described previously by other groups (Oakley *et al.*, 2006; El Khoury *et al.*, 2007), the immune system is activated in 5xFAD mice in response to amyloid pathology. This was confirmed in this thesis by immunohistochemical staining showing activated microglia and astrocytes in both 5xFAD and 5xFADxhtau-KI. Furthermore, the NanoString mouse AD panel showed upregulation of immune-related genes in 5xFAD and 5xFADxhtau-KI mice, mostly in the same genes. Both WT mice and htau-KI mice showed no immune activation, either in immunohistochemistry or gene expression analysis. This suggests that activation of the immune system is a response to A β overexpression, independent of tau species. Several findings in the gene expression analysis matched earlier findings by other groups in AD mouse models or human patients. Tyrobp, also known as DAP12, is expressed by microglia and is upregulated in AD patients (Ma *et al.*, 2015). Furthermore, several genetic variants of Tyrobp have recently been found to be a risk factor for the development of early onset AD (Pottier *et al.*, 2016). In addition, both Tyrobp and Fcgr1g have been described as important causal regulators of the immune- and microglia module in late-onset AD patients (Zhang *et al.*, 2013).

Other studies showed that B2M, Tgfb1, Tgfb2, Csf1, Ctss, Fcer1g, Tyrobp, C1qb, C1qa and C1qc are upregulated in human AD cortex, as well as different mouse models for AD (Castillo *et al.*, 2017; Landel *et al.*, 2014; McGeer *et al.*, 1989; Bouter *et al.*, 2014). The complement system is known to play a role in synaptic degradation, both in mouse models and AD patients (Dejanovic *et al.*, 2018; Litvinchuk *et al.*, 2018; Wu *et al.*, 2019). These papers showed that antibody-mediated inhibition of the complement system, as well as deletion of a subunit of the complement receptor, resulted in a rescue of neurodegeneration and amelioration of behavioural deficits in AD mouse models, confirming the importance of this system in AD pathology. The results shown in this thesis are in line with these findings. Although Dejanovic *et al.* and Litvinchuk *et al.* (both 2018) describe that the blockage of complement results in a rescue by affecting tau-mediated neurodegeneration, we found no differences between 5xFAD and 5xFADxhtau-KI in any genes related to the complement system. This suggests that the tau-mediated activation of the complement system and subsequent loss of synapses is independent of the species of tau. Further investigations at the synaptic level by staining for synaptic markers and different parts of the complement system are required to better understand the underlying mechanisms and the possible differences between mouse and human tau at this level. Subsequently, a pathway analysis revealed an upregulation of the lysosomal pathway in 5xFAD and 5xFADxhtau-KI mice. These results match findings by other groups, both in 5xFAD mice as well as human AD patients (Nixon *et al.*, 2000; Landel *et al.*, 2014). Furthermore, Cathepsin S is hypothesized to play a role in APP processing, because overexpression results in higher production of amyloid β , as well as an activation of pro-inflammatory NF- κ B (Castillo *et al.*, 2017). As described by Deczkowska *et al.* (2018), disease-associated microglia (DAM) in AD brain show a TREM2-dependent upregulation of (amongst others) ApoE, Tyrobp, B2m and Csf1 as well as lysosomal/phagocytic pathways. My data from prefrontal cortex of 5xFAD mice match these findings. Because I used prefrontal cortex tissue for the analysis, rather than single cell sequencing, other factors were also found, possibly resulting from changes in other brain cells. Further research is required to confirm the upregulation of these different factors with qRT-PCR, as well as find out which cell types are responsible for the increased expression rates, and what the functional consequences are. Two genes, Zbtb33 and Bex1, were downregulated in 5xFADxhtau-KI mice compared to WT. There is limited information available about these genes. Zbtb33 codes for a transcription factor, and an upregulation has been associated with cancer (Prokhortchouk *et al.*, 2006; Pozner *et al.*, 2016). Bex1 is a modulator of intracellular signalling and is described to have many different functions (Lindblad *et al.*, 2015; Jiang *et al.*, 2016; Accornero *et al.*, 2017; Gu *et al.*, 2018). Furthermore, the gene Samd12 was upregulated in 7-month-old mice compared to 13-month-old mice. The function of this gene is currently unknown, but an additional insertion in the gene has been associated with epilepsy (Cen *et al.*, 2018). The downregulation

of this gene with aging should first be confirmed with qRT-PCR. Finally, the comparison of gene expression data in our model to human *post-mortem* brain tissue showed a strong correlation between 5xFAD and human AD for cluster B, which is related to the immune response. Together, the results in this thesis thus confirm the importance of the immune system in AD pathology. To fully elicit the role of the immune response to AD pathology, it is important to understand which role the different types of immune cells play in the development of AD.

Role of different immune cells in AD

The immune system in AD brain consists of two types of cells: brain-resident microglia and infiltrating peripheral immune cells. The infiltration of peripheral immune cells in 5xFAD brain was confirmed in this thesis. It seems likely that CCL2-CCR2 signalling plays a role in this infiltration process, because CCL2 is upregulated by microglia *in vitro* in response to A β exposure. This matches findings by El Khoury *et al.* (2003). qRT-PCR data subsequently confirmed that peripheral immune cells, but not microglia, express CCR2, as shown before by Saederup *et al.* (2010). Importantly, this field of research could really benefit from the development of CCR2 antibodies to address specific questions which cannot be answered otherwise. In this thesis, it was decided to use MHCII as a marker for infiltrating peripheral cells, which showed that MHCII⁺ cells are not present in healthy brain but appear in the CNS in response to AD pathology. Since there are only very few MHCII⁺ cells and all other Iba1⁺ cells are MHCII⁻, it is suggested that the MHCII⁺ cells are infiltrating monocytes rather than microglia which upregulate MHCII expression. Further characterization of these cells is however required, possibly using flow cytometry or FACS isolation, to distinguish which cell types they represent and what their origin and function is. Several papers suggest that microglia express MHCII and that this expression is upregulated under inflammatory conditions such as AD (Butovsky *et al.*, 2005; Nikodemova *et al.*, 2007) but these papers relied on the idea that the BBB prevents peripheral cells from entering and it has been shown since then that the BBB can be crossed by CCR2⁺ peripheral immune cells during disease (Saederup *et al.*, 2010).

The fact that MHCII⁺ cells, but no CCR2⁺/RFP⁺ cells were found in the brain of 5xFAD mice, could be explained by the fading of RFP over time. The samples were stored in -80°C after collection, which could lead to degradation/fading of RFP in the tissue. Experiments with fresh tissue could solve this possible issue. Another possibility could be a downregulation of CCR2 expression by peripheral monocytes upon entering of the CNS. It was shown by Sica *et al.* (1997) that mononuclear phagocytes rapidly downregulate their CCR2 expression after exposure to lipopolysaccharides (LPS). Saederup *et al.* (2010) however did show clear RFP

staining (based on CCR2 expression) in infiltrated cells in the brain of an EAE mouse model. It is thus necessary to perform further experiments to investigate these hypotheses, ideally with a good CCR2 antibody.

Another aim of the thesis was to investigate the immune status and plaque pathology in the brains of WT, CCR2^{+RFP}, 5xFAD, and 5xFADxCCR2^{+RFP} mice to investigate the effect of a heterozygous knock-out of CCR2 on AD pathology. The gene expression analysis of prefrontal cortex tissue showed no significant differences between WT and 5xFAD mice, except for an upregulation of IL1b in 6-month-old female 5xFAD mice compared to WT mice. 5xFADxCCR2^{+RFP} mice showed more significant increases in expression of inflammatory genes compared to WT, but not to 5xFAD. Simard *et al.* (2006) investigated mRNA expression in another AD mouse model and showed increased CCL2 expression in older mice only, no changes in TNF α expression and continuously increasing IL1b expression with aging. Naert & Rivest (2011) showed continuously increasing expression of CCL2 with aging in another AD mouse model. Different methods were used to quantify the expression (qRT-PCR of prefrontal cortex tissue in this thesis compared to qualitative analysis of *in situ* hybridization in both papers), which could explain the differential results. qRT-PCR is a more sensitive method to measure differences in mRNA expression. Because the analysis was performed on prefrontal cortex tissue, consisting of different cell types, there is however no differentiation based on cell type possible. Therefore, isolation of cells by fluorescence-activated cell sorting (FACS) or microdissection of specific cell types should be followed by qRT-PCR to draw any final conclusions about the expression of specific genes. El Khoury *et al.* (2007) used this approach and showed increased expression of CCL2 in microglia from APP mice, but only compared to astrocytes from the same brains, not to WT mice. Janelins *et al.* (2005) showed upregulation of CCL2 and TNF α in AD mice compared to controls, but only in the entorhinal cortex and not in hippocampus. It is thus clear that there is no consensus about expression levels of inflammatory cytokines in AD mouse brains. Therefore, it is important to use the method described above to analyse the gene expression of these (and more) genes, as well as the resulting protein expression in specific brain areas to better understand the role of immune cells in AD.

Finally, preliminary immunohistochemical analyses of 5xFADxCCR2^{+RFP} and 5xFAD brains also revealed no significant genotype effects on area of plaques and number of MHCII⁺ cells. Also for these experiments however, an increased sample size is required to draw any conclusions. In addition, immunohistochemistry revealed a trend for an age-dependent increase of plaque pathology and peripheral immune cell infiltration, as well as higher plaque load and more infiltrating cells in females compared to males. Both findings match expectations based on other publications (Oakley *et al.*, 2006; Fisher *et al.*, 2018).

Future perspectives

New and improved preclinical models are required to increase the success rate of clinical studies with AD therapies. The generation and characterization of the htau-KI model in this thesis is a first step in this process. As described in the final part of the results section, a hAPP-KI mouse model has also been generated and cross-bred with the htau-KI mice. Thereby, the artificial overexpression of A β is removed. By subsequently crossing in the different isoforms of human ApoE, the most important proteins playing a role in AD pathology will be humanized. These models will significantly impact AD research by eliciting molecular pathways and interactions that play a role in human AD pathology, without confounding effects of unphysiological expression levels or mutations.

It is important to age these mice, and introduce other factors such as immune challenges or a high fat diet, to mimic the main environmental risk factors for human AD. Additionally, since the immune system plays such an important role in AD, the humanized mouse model can be crossed with CX3CR1^{GFP/GFP} and CCR2^{RFP/RFP} mice to understand the role of brain-resident microglia and infiltrating peripheral immune cells. These experiments are of high importance for the development of immunotherapy for AD, which is currently an important avenue of drug discovery. To understand the effects of immunotherapy and improve its effect, the exact contribution of different types of immune cells needs to be well understood.

Taken together, these approaches will improve current attempts at AD therapy development and open new possibilities for future drug discovery.

6. Summary

Alzheimer's disease is a neurodegenerative disease currently affecting over 40 million people worldwide. No cure is available, partly due to the lack of translation of preclinical results to patients. Additionally, inflammation plays an important role in AD, but the role of different types of immune cells in pathology is not well understood. This thesis describes the characterization of a new htau-KI mouse model, generated to improve preclinical research into AD and target identification for therapy development. The htau-KI mice are viable and healthy and express all 6 isoforms of human tau, with a full knock-out of mouse tau. After crossing the htau-KI mice with 5xFAD mice, no tangle pathology was found, only PHF1⁺ and CP13⁺ plaque-associated dystrophic neurites. Interestingly, using the MC1 antibody, a pathological conformation of tau was found specifically in htau-KI and 5xFADxhtau-KI mice, suggesting an important difference between human tau and mouse tau. Behavioural deficits in anxiety-related behaviour and learning and memory were found in 5xFAD and 5xFADxhtau-KI, but not in htau-KI mice. Additionally, there was clear activation of the immune system in the A β -overexpressing mice, as shown by immunohistochemistry and NanoString gene expression analysis. No differences were found between 5xFAD and 5xFADxhtau-KI mice in any of these aspects, suggesting that overexpression of A β is the driver of pathology. Comparison of the gene expression data to human *post-mortem* AD tissue however, showed a possible protective effect of human tau expression, specifically in a 5xFAD background. LTP measurements showed a similar effect, but other electrophysiological outcome parameters did not. *In vitro* investigations to understand the role of different types of immune cells in AD showed that CCL2 is upregulated in response to A β and that MHCII⁺ cells enter the brain in response to A β pathology. These cells are suggested to be infiltrating peripheral monocytes and more research is required to elicit their role in AD pathology, whether harmful or beneficial. Furthermore, a comparison of 5xFADxCCR2^{+RFP} to 5xFAD mice so far showed no differences in expression of immune-related genes or plaque pathology, but more extensive research with an increased sample size is required to confirm this. This thesis provides new insights into AD pathology as well as tools for further research. The role of human tau in AD pathology needs to be further examined by eliciting specific molecular mechanisms (e.g. for MC1 staining) in the htau-KI line. Additionally, the possible protective effect of human tau in AD needs to be investigated in other A β -overexpressing mouse models. Finally, further aging of the mice and possible introduction of other factors (immune challenge, diet) could be interesting to investigate the development of tangle pathology. The role of different immune cells in AD pathology will be further investigated in 5xFADxCCR2^{RFP/RFP} and 5xFADxCX3CR1^{GFP/GFP} mice.

7. References

- Accornero, F., Schips, T. G., Petrosino, J. M., Gu, S. Q., Kanisicak, O., Van Berlo, J. H., & Molkentin, J. D. (2017). BEX1 is an RNA-dependent mediator of cardiomyopathy. *Nature Communications*, 8(1).
- Ajami, B., Bennett, J. L., Krieger, C., McNagny, K. M., & Rossi, F. M. (2011). Infiltrating monocytes trigger EAE progression, but do not contribute to the resident microglia pool. *Nature neuroscience*, 14(9), 1142.
- Akiyama, H., Barger, S., Barnum, S., Bradt, B., Bauer, J., Cole, G. M., ... & Finch, C. E. (2000). Inflammation and Alzheimer's disease. *Neurobiology of aging*, 21(3), 383-421.
- Albert, M. S., DeKosky, S. T., Dickson, D., Dubois, B., Feldman, H. H., Fox, N. C., ... & Snyder, P. J. (2011). The diagnosis of mild cognitive impairment due to Alzheimer's disease: recommendations from the National Institute on Aging-Alzheimer's Association workgroups on diagnostic guidelines for Alzheimer's disease. *Alzheimer's & dementia*, 7(3), 270-279.
- Allen, B., Ingram, E., Takao, M., Smith, M. J., Jakes, R., Virdee, K., ... Goedert, M. (2002). Abundant tau filaments and neurodegeneration in mice transgenic for human P301S tau. *Journal of Neuropathology and Experimental Neurology*, 22(21), 9340–9351.
- Alonso, A. D. C., Grundke-Iqbal, I., & Iqbal, K. (1996). Alzheimer's disease hyperphosphorylated tau sequesters normal tau into tangles of filaments and disassembles microtubules. *Nature medicine*, 2(7), 783-787.
- Alzheimer, A. (1906). Über einen eigenartigen schweren Erkrankungsprozess der Hirnrinde. *Neurologisches Centralblatt*, 25, 1134.
- Alzheimer's Association. (2018). 2018 Alzheimer's disease facts and figures. *Alzheimer's & Dementia*, 14(3), 367-429.
- Andorfer, C., Kress, Y., Espinoza, M., De Silva, R., Tucker, K. L., Barde, Y. A., ... Davies, P. (2003). Hyperphosphorylation and aggregation of tau in mice expressing normal human tau isoforms. *Journal of Neurochemistry*, 86(3), 582–590.
- Andreadis, A., Brown, W. M., & Kosik, K. S. (1992). Structure and Novel Exons of the Human τ Gene. *Biochemistry*, 31(43), 10626–10633.
- Askew, K., Li, K., Olmos-Alonso, A., Garcia-Moreno, F., Liang, Y., Richardson, P., ... Gomez-Nicola, D. (2017). Coupled Proliferation and Apoptosis Maintain the Rapid Turnover of Microglia in the Adult Brain. *Cell Reports*, 18(2), 391–405.
- Auffray, C., Sieweke, M. H., & Geissmann, F. (2009). Blood Monocytes: Development, Heterogeneity, and Relationship with Dendritic Cells. *Annual Review of Immunology*, 27(1), 669–692.
- Barendrecht, S., Schreurs, A., Geissler, S., Eichentopf, R., Rieckmann, V.V., Sabanov, V., ... Cynis, H. (in preparation). A novel human tau knock-in mouse model reveals synergistic action of Abeta and tau under progressing cerebral amyloidosis.
- Barger, S. W., & Basile, A. S. (2001). Activation of microglia by secreted amyloid precursor protein evokes release of glutamate by cystine exchange and attenuates synaptic function. *Journal of Neurochemistry*, 76(3), 846–854.
- Baumgart, M., Snyder, H. M., Carrillo, M. C., Fazio, S., Kim, H., & Johns, H. (2015). Summary of the evidence on modifiable risk factors for cognitive decline and dementia: a population-based perspective. *Alzheimer's & Dementia*, 11(6), 718-726.
- Bhattacharya, S., Haertel, C., Maelicke, A., & Montag, D. (2014). Galantamine slows down plaque formation and behavioral decline in the 5XFAD mouse model of Alzheimer's disease. *PLoS ONE*, 9(2).
- Bhattacharya, S. et al. Genetically Induced Retrograde Amnesia of Associative Memories After Neuroplastin Ablation. *Biological psychiatry* 81, 124–135 (2017).
- Blum-Degen, D., Müller, T., Kuhn, W., Gerlach, M., Przuntek, H., & Riederer, P. (1995). Interleukin-1 β

and interleukin-6 are elevated in the cerebrospinal fluid of Alzheimer's and de novo Parkinson's disease patients. *Neuroscience Letters*, 202(1–2), 17–20.

- Bolmont, T., Haiss, F., Eicke, D., Radde, R., Mathis, C. A., Klunk, W. E., ... Calhoun, M. E. (2008). Dynamics of the microglial/amyloid interaction indicate a role in plaque maintenance. *Journal of Neuroscience*, 28(16), 4283–4292.
- Bories, C., Guitton, M. J., Julien, C., Tremblay, C., Vandal, M., Msaid, M., ... & Calon, F. (2012). Sex-dependent alterations in social behaviour and cortical synaptic activity coincide at different ages in a model of Alzheimer's disease. *PLoS One*, 7(9).
- Bortz, J., Lienert, G. A., & Boehnke, K. (2008). *Verteilungsfreie methoden in der biostatistik*. Springer-Verlag.
- Boutajangout, A., Quartermain, D., & Sigurdsson, E. M. (2010). Immunotherapy targeting pathological tau prevents cognitive decline in a new tangle mouse model. *Journal of Neuroscience*, 30(49), 16559–16566.
- Bouter, Y., Kacprowski, T., Weissmann, R., Dietrich, K., Borgers, H., Brauß, A., ... Bayer, T. A. (2014). Deciphering the molecular profile of plaques, memory decline and neuron loss in two mouse models for Alzheimer's disease by deep sequencing. *Frontiers in Aging Neuroscience*, 6(APR), 1–28.
- Brookmeyer, R., Evans, D. A., Hebert, L., Langa, K. M., Heeringa, S. G., Plassman, B. L., & Kukull, W. A. (2011). National estimates of the prevalence of Alzheimer's disease in the United States. *Alzheimer's & Dementia*, 7(1), 61-73.
- Buée, L., Bussi re, T., Bu e-Scherrer, V., Delacourte, A., & Hof, P. R. (2000). Tau protein isoforms, phosphorylation and role in neurodegenerative disorders. *Brain Research Reviews*, 33(1), 95-130.
- Butovsky, O., Talpalar, A. E., Ben-Yaakov, K., & Schwartz, M. (2005). Activation of microglia by aggregated β -amyloid or lipopolysaccharide impairs MHC-II expression and renders them cytotoxic whereas IFN- γ and IL-4 render them protective. *Molecular and Cellular Neuroscience*, 29(3), 381–393.
- Campbell, J. J., Qin, S., Unutmaz, D., Soler, D., Murphy, K. E., Hodge, M. R., ... Butcher, E. C. (2001). Unique Subpopulations of CD56 + NK and NK-T Peripheral Blood Lymphocytes Identified by Chemokine Receptor Expression Repertoire. *The Journal of Immunology*, 166(11), 6477–6482.
- Castellani, R. J., Nunomura, A., Lee, H. G., Perry, G., & Smith, M. A. (2008). Phosphorylated tau: toxic, protective, or none of the above. *Journal of Alzheimer's Disease*, 14(4), 377-383.
- Castillo, E., Leon, J., Mazzei, G., Abolhassani, N., Haruyama, N., Saito, T., ... Nakabeppu, Y. (2017). Comparative profiling of cortical gene expression in Alzheimer's disease patients and mouse models demonstrates a link between amyloidosis and neuroinflammation. *Scientific Reports*, 7(1), 1–16.
- Cen, Z., Jiang, Z., Chen, Y., Zheng, X., Xie, F., Yang, X., ... Luo, W. (2018). Intronic pentanucleotide TTTCA repeat insertion in the SAMD12 gene causes familial cortical myoclonic tremor with epilepsy type 1. *Brain*, 141(8), 2280–2288.
- Chang, R., Yee, K., & Sumbria, R. K. (2017). Tumor necrosis factor α Inhibition for Alzheimer's Disease. *Journal of Central Nervous System Disease*, 9, 117957351770927.
- Cheng, Y., & Bai, F. (2018). The association of tau with mitochondrial dysfunction in alzheimer's disease. *Frontiers in neuroscience*, 12, 163.
- Chohan, M. O., Haque, N., Alonso, A., El-Akkad, E., Grundke-Iqbal, I., Grover, A., & Iqbal, K. (2005). Hyperphosphorylation-induced self assembly of murine tau: A comparison with human tau. *Journal of Neural Transmission*, 112(8), 1035–1047.
- Cimler, R., Maresova, P., Kuhnova, J., & Kuca, K. (2019). Predictions of Alzheimer's disease treatment and care costs in European countries. *PLoS ONE*, 14(1), 1–16.
- Cleary, J. P., Walsh, D. M., Hofmeister, J. J., Shankar, G. M., Kuskowski, M. A., Selkoe, D. J., & Ashe, K. H. (2005). Natural oligomers of the amyloid- β protein specifically disrupt cognitive function.

Nature Neuroscience, 8(1), 79–84.

- Colié, S., Sarroca, S., Palenzuela, R., Garcia, I., Matheu, A., Corpas, R., ... & Nebreda, A. R. (2017). Neuronal p38 α mediates synaptic and cognitive dysfunction in an Alzheimer's mouse model by controlling β -amyloid production. *Scientific reports*, 7, 45306.
- Corcoran, K. A., Lu, Y., Scott Turner, R., & Maren, S. (2002). Overexpression of hAPPswe impairs rewarded alternation and contextual fear conditioning in a transgenic mouse model of Alzheimer's disease. *Learning and Memory*, 9(5), 243–252.
- Corder, E. H., Saunders, A. M., Risch, N. J., Strittmatter, W. J., Schmechel, D. E., Gaskell, P. C., ... & Small, G. W. (1994). Protective effect of apolipoprotein E type 2 allele for late onset Alzheimer disease. *Nature genetics*, 7(2), 180-184.
- Cowan, C. M., & Mudher, A. (2013). Are tau aggregates toxic or protective in tauopathies? *Frontiers in Neurology*, 4 AUG(August), 1–13.
- Cowan, C. M., Quraishe, S., Hands, S., Sealey, M., Mahajan, S., Allan, D. W., & Mudher, A. (2015). Rescue from tau-induced neuronal dysfunction produces insoluble tau oligomers. *Scientific reports*, 5, 17191.
- Cummings, J. (2018). Lessons learned from Alzheimer disease: clinical trials with negative outcomes. *Clinical and translational science*, 11(2), 147-152.
- Cummings, J., Lee, G., Ritter, A., & Zhong, K. (2018). Alzheimer's disease drug development pipeline: 2018. *Alzheimer's and Dementia: Translational Research and Clinical Interventions*, 4(2018), 195–214.
- D'Andrea, M. R., Cole, G. M., & Ard, M. D. (2004). The microglial phagocytic role with specific plaque types in the Alzheimer disease brain. *Neurobiology of Aging*, 25(5), 675–683.
- Deczkowska, A., Keren-Shaul, H., Weiner, A., Colonna, M., Schwartz, M., & Amit, I. (2018). Disease-associated microglia: a universal immune sensor of neurodegeneration. *Cell*, 173(5), 1073-1081.
- Dejanovic, B., Huntley, M. A., De Mazière, A., Meilandt, W. J., Wu, T., Srinivasan, K., ... & Foreman, O. (2018). Changes in the synaptic proteome in tauopathy and rescue of tau-induced synapse loss by C1q antibodies. *Neuron*, 100(6), 1322-1336.
- Devi, L., & Ohno, M. (2015). TrkB reduction exacerbates Alzheimer's disease-like signaling aberrations and memory deficits without affecting β -amyloidosis in 5XFAD mice. *Translational Psychiatry*, 5(5), e562-9.
- Devi, Latha, & Ohno, M. (2010). Genetic reductions of β -site amyloid precursor protein-cleaving enzyme 1 and amyloid- β ameliorate impairment of conditioned taste aversion memory in 5XFAD Alzheimer's disease model mice. *European Journal of Neuroscience*, 31(1), 110–118.
- Devi, Latha, Tang, J., & Ohno, M. (2015). Beneficial Effects of the Beta-Secretase Inhibitor GRL-8234 in 5XFAD Alzheimer's Transgenic Mice Lessen During Disease Progression. *Current Alzheimer Research*, 12(1), 13–21.
- Dickson, D. W., Kouri, N., Murray, M. E., & Josephs, K. A. (2011). Neuropathology of frontotemporal lobar degeneration-Tau (FTLD-Tau). In *Journal of Molecular Neuroscience* (Vol. 45, pp. 384–389).
- Dominik, G., Gloy Viktoria, L., Monsch Andreas, U., Kressig Reto, W., Chandni, P., Alba, M. K., ... Heike, R. (2019). Acetylcholinesterase inhibitors combined with memantine for moderate to severe Alzheimer's disease: A meta-analysis. *Swiss Medical Weekly*, 149(25–26), 1–12.
- Duyckaerts, C., Delatour, B., & Potier, M. C. (2009). Classification and basic pathology of Alzheimer disease. *Acta neuropathologica*, 118(1), 5-36.
- El Khoury, J. B., Moore, K. J., Means, T. K., Leung, J., Terada, K., Toft, M., ... Luster, A. D. (2003). CD36 mediates the innate host response to β -amyloid. *Journal of Experimental Medicine*, 197(12), 1657–1666.
- El Khoury, J., Toft, M., Hickman, S. E., Means, T. K., Terada, K., Geula, C., & Luster, A. D. (2007). Ccr2 deficiency impairs microglial accumulation and accelerates progression of Alzheimer-like disease. *Nature Medicine*, 13(4), 432–438.

- Filali, M., Lalonde, R., Theriault, P., Julien, C., Calon, F., & Planel, E. (2012). Cognitive and non-cognitive behaviors in the triple transgenic mouse model of Alzheimer's disease expressing mutated APP, PS1, and Mapt (3xTg-AD). *Behavioural Brain Research*, *234*(2), 334–342.
- Fisher, D. W., Bennett, D. A., & Dong, H. (2018). Sexual dimorphism in predisposition to Alzheimer's disease. *Neurobiology of aging*, *70*, 308-324.
- Fukutani, Y., Cairns, N. J., Shiozawa, M., Sasaki, K., Sudo, S., Isaki, K., & Lantos, P. L. (2000). Neuronal loss and neurofibrillary degeneration in the hippocampal cortex in late-onset sporadic Alzheimer's disease. *Psychiatry and clinical neurosciences*, *54*(5), 523-529.
- Geissmann, F., Jung, S., & Littman, D. R. (2003). Blood monocytes consist of two principal subsets with distinct migratory properties. *Immunity*, *19*(1), 71–82.
- Geissmann, F., Manz, M. G., Jung, S., Sieweke, M. H., Merad, M., & Ley, K. (2010). Development of monocytes, macrophages, and dendritic cells. *Science*, *327*(5966), 656-661.
- Giannakopoulos, P., Herrmann, F. R., Bussi re, T., Bouras, C., K vari, E., Perl, D. P., ... & Hof, P. R. (2003). Tangle and neuron numbers, but not amyloid load, predict cognitive status in Alzheimer's disease. *Neurology*, *60*(9), 1495-1500.
- Ginhoux, F., Greter, M., Leboeuf, M., Nandi, S., See, P., Gokhan, S., ... & Samokhvalov, I. M. (2010). Fate mapping analysis reveals that adult microglia derive from primitive macrophages. *Science*, *330*(6005), 841-845.
- Goedert, M., Spillantini, M. G., Jakes, R., Rutherford, D., & Crowther, R. A. (1989). Multiple isoforms of human microtubule-associated protein tau: sequences and localization in neurofibrillary tangles of Alzheimer's disease. *Neuron*, *3*(4), 519–526.
- Gong, C. -X, Shaikh, S., Wang, J. -Z, Zaidi, T., Grundke-Iqbal, I., & Iqbal, K. (1995). Phosphatase Activity Toward Abnormally Phosphorylated τ : Decrease in Alzheimer Disease Brain. *Journal of Neurochemistry*, *65*(2), 732–738.
- Grathwohl, S. A., K lin, R. E., Bolmont, T., Prokop, S., Kaeser, S. A., Odenthal, J., ... Mathews, P. M. (2009). Plaques in the Absence of Microglia. *Nature Neuroscience*, *12*(11), 1361–1363.
- Gri an-Ferr , C., Sarroca, S., Ivanova, A., Puigoriol-Illamola, D., Aguado, F., Camins, A., ... Pall s, M. (2016). Epigenetic mechanisms underlying cognitive impairment and Alzheimer disease hallmarks in 5XFAD mice. *Aging*, *8*(4), 664–684.
- Gu, Y., Wei, W., Cheng, Y., Wan, B., Ding, X., Wang, H., ... Jin, M. (2018). A pivotal role of BEX1 in liver progenitor cell expansion in mice. *Stem Cell Research and Therapy*, *9*(1), 1–14.
- Guerreiro, R., Ph, D., Wojtas, A., Bras, J., Carrasquillo, M., Rogaeva, E., ... Alzheimer, T. (2013). TREM2 variants in AD. *New England Journal of Medicine*, *368*(2), 117–127.
- Haass, C., Kaether, C., Thinakaran, G., & Sisodia, S. (2012). Trafficking and proteolytic processing of APP. *Cold Spring Harbor Perspectives in Medicine*, *2*(5), 1–25.
- Haass, C., & Selkoe, D. J. (2007). Soluble protein oligomers in neurodegeneration: lessons from the Alzheimer's amyloid β -peptide. *Nature reviews Molecular cell biology*, *8*(2), 101-112.
- Hempel, H., Mesulam, M. M., Cuello, A. C., Farlow, M. R., Giacobini, E., Grossberg, G. T., ... & Khachaturian, Z. S. (2018). The cholinergic system in the pathophysiology and treatment of Alzheimer's disease. *Brain*, *141*(7), 1917-1933.
- Hanisch, U. K., & Kettenmann, H. (2007). Microglia: active sensor and versatile effector cells in the normal and pathologic brain. *Nature neuroscience*, *10*(11), 1387-1394.
- Hardy, J., & Selkoe, D. J. (2002). The amyloid hypothesis of Alzheimer's disease: progress and problems on the road to therapeutics. *science*, *297*(5580), 353-356.
- Harrison, J. K., Jiang, Y., Chen, S., Xia, Y., Maciejewski, D., Mcnamara, R. K., ... Feng, L. (1998). Role for neuronally derived fractalkine in mediating interactions between neurons and CX3CR1-expressing microglia. *Proceedings of the National Academy of Sciences of the United States of America*, *95*(18), 10896–10901.

- Hartlage-Rübsamen, M., Morawski, M., Waniek, A., Jäger, C., Zeitschel, U., Koch, B., ... & Roßner, S. (2011). Glutaminyl cyclase contributes to the formation of focal and diffuse pyroglutamate (pGlu)-A β deposits in hippocampus via distinct cellular mechanisms. *Acta neuropathologica*, 121(6), 705-719.
- Hohl, T. M. (2015). Cell-mediated defense against infection. *Mandell, Douglas and Bennett's, editors. Principle and practice of infectious diseases. 8th ed. Philadelphia: Saunders*, 50-69.
- Hoover, B. R., Reed, M. N., Su, J., Penrod, R. D., Kotilinek, L. A., Grant, M. K., ... & Ashe, K. H. (2010). Tau mislocalization to dendritic spines mediates synaptic dysfunction independently of neurodegeneration. *Neuron*, 68(6), 1067-1081.
- Hutton, M., Lendon, C. L., Rizzu, P., Baker, M., Froelich, S., Houlden, H., ... & Hackett, J. (1998). Association of missense and 5'-splice-site mutations in tau with the inherited dementia FTDP-17. *Nature*, 393(6686), 702-705.
- Ikonomovic, M. D., Mizukami, K., Davies, P., Hamilton, R., Sheffield, R., & Armstrong, D. M. (1997). The loss of GluR2 (3) immunoreactivity precedes neurofibrillary tangle formation in the entorhinal cortex and hippocampus of Alzheimer brains. *Journal of Neuropathology & Experimental Neurology*, 56(9), 1018-1027.
- Imbimbo, B. P., Solfrizzi, V., & Panza, F. (2010). Are NSAIDs useful to treat Alzheimer's disease or mild cognitive impairment?. *Frontiers in aging neuroscience*, 2, 19.
- Ingelsson, M., Ramasamy, K., Cantuti-Castelvetri, I., Skoglund, L., Matsui, T., Orne, J., ... Hyman, B. T. (2006). No alteration in tau exon 10 alternative splicing in tangle-bearing neurons of the Alzheimer's disease brain. *Acta Neuropathologica*, 112(4), 439-449.
- Iqbal, K., Alonso, A. D. C., Chen, S., Chohan, M. O., El-Akkad, E., Gong, C. X., ... & Tanimukai, H. (2005). Tau pathology in Alzheimer disease and other tauopathies. *Biochimica et Biophysica Acta (BBA)-Molecular Basis of Disease*, 1739(2-3), 198-210.
- Ishizuka, K., Kimura, T., Igata-Yi, R., Katsuragi, S., Takamatsu, J., & Miyakawa, T. (1997). Identification of monocyte chemoattractant protein-1 in senile plaques and reactive microglia of Alzheimer's disease. *Psychiatry and Clinical Neurosciences*, 51(3), 135-138.
- Itagaki, S., McGeer, P. L., Akiyama, H., Zhu, S., & Selkoe, D. (1989). Relationship of microglia and astrocytes to amyloid deposits of Alzheimer disease. *Journal of Neuroimmunology*, 24(3), 173-182.
- Iwatsubo, T., Odaka, A., Suzuki, N., Mizusawa, H., Nukina, N., & Ihara, Y. (1994). Visualization of A β 42(43) and A β 40 in senile plaques with end-specific A β monoclonals: Evidence that an initially deposited species is A β 42(43). *Neuron*, 13(1), 45-53.
- Jack, C. R., Knopman, D. S., Jagust, W. J., Shaw, L. M., Aisen, P. S., Weiner, M. W., ... Trojanowski, J. Q. (2010). Hypothetical Pathological Cascade in Alzheimer's Disease. *Lancet Neurology*, 9(1), 1-20.
- Janelins, M. C., Mastrangelo, M. A., Oddo, S., LaFerla, F. M., Federoff, H. J., & Bowers, W. J. (2005). Early correlation of microglial activation with enhanced tumor necrosis factor-alpha and monocyte chemoattractant protein-1 expression specifically within the entorhinal cortex of triple transgenic Alzheimer's disease mice. *Journal of neuroinflammation*, 2(1), 23.
- Jansen, W. J., Ossenkuppele, R., Knol, D. L., Tijms, B. M., Scheltens, P., Verhey, F. R., ... & Alexander, M. (2015). Prevalence of cerebral amyloid pathology in persons without dementia: a meta-analysis. *Jama*, 313(19), 1924-1938.
- Jarrett, J. T., Berger, E. P., & Lansbury, P. T. (1993). The Carboxy Terminus of the β Amyloid Protein Is Critical for the Seeding of Amyloid Formation: Implications for the Pathogenesis of Alzheimer's Disease. *Biochemistry*, 32(18), 4693-4697.
- Jawhar, S. (2011). *The 5XFAD mouse model: a tool for genetic modulation of Alzheimer's disease pathology* (Doctoral dissertation, Ph. D. Thesis. Georg August University Goettingen: Germany).
- Jellinger, K. A., & Attems, J. (2007). Neurofibrillary tangle-predominant dementia: comparison with

classical Alzheimer disease. *Acta neuropathologica*, 113(2), 107-117.

- Jiang, C., Wang, J. H., Yue, F., & Kuang, S. (2016). The brain expressed x-linked gene 1 (Bex1) regulates myoblast fusion. *Developmental biology*, 409(1), 16-25.
- Jung, S., Aliberti, J., Graemmel, P., Sunshine, M. J., Kreutzberg, G. W., Sher, A., & Littman, D. R. (2000). Analysis of Fractalkine Receptor CX3CR1 Function by Targeted Deletion and Green Fluorescent Protein Reporter Gene Insertion. *Molecular and Cellular Biology*, 20(11), 4106–4114.
- Kang, S., Ha, S., Park, H., Nam, E., Suh, W. H., Suh, Y. H., & Chang, K. A. (2018). Effects of a dehydroevodiamine-derivative on synaptic destabilization and memory impairment in the 5xFAD, Alzheimer's disease mouse model. *Frontiers in Behavioral Neuroscience*, 12 (November 2018), 2–12.
- Kanno, T., Tsuchiya, A., & Nishizaki, T. (2014). Hyperphosphorylation of Tau at Ser396 occurs in the much earlier stage than appearance of learning and memory disorders in 5XFAD mice. *Behavioural brain research*, 274, 302-306.
- Ke, Y. D., Suchowerska, A. K., van der Hoven, J., De Silva, D. M., Wu, C. W., van Eersel, J., ... & Ittner, L. M. (2012). Lessons from tau-deficient mice. *International journal of Alzheimer's disease*, 2012.
- Kirschner, D. A., Inouye, H., Duffy, L. K., Sinclair, A., Lind, M., & Selkoe, D. J. (1987). Synthetic peptide homologous to beta protein from Alzheimer disease forms amyloid-like fibrils in vitro. *Proceedings of the National Academy of Sciences of the United States of America*, 84(19), 6953–6957.
- Kimura, R., & Ohno, M. (2009). Impairments in remote memory stabilization precede hippocampal synaptic and cognitive failures in 5XFAD Alzheimer mouse model. *Neurobiology of disease*, 33(2), 229-235.
- Kiyota, T., Yamamoto, M., Schroder, B., Jacobsen, M. T., Swan, R. J., Lambert, M. P., ... Ikezu, T. (2009). AAV1/2-mediated CNS gene delivery of dominant-negative CCL2 mutant suppresses gliosis, β -amyloidosis, and learning impairment of APP/ PS1 mice. *Molecular Therapy*, 17(5), 803–809.
- Kiyota, T., Yamamoto, M., Xiong, H., Lambert, M. P., Klein, W. L., Gendelman, H. E., ... & Ikezu, T. (2009). CCL2 accelerates microglia-mediated A β oligomer formation and progression of neurocognitive dysfunction. *PloS one*, 4(7).
- Knowles, R. B., Wyart, C., Buldyrev, S. V., Cruz, L., Urbanc, B., Hasselmo, M. E., ... Hyman, B. T. (1999). Plaque-induced neurite abnormalities: Implications for disruption of neural networks in Alzheimer's disease. *Proceedings of the National Academy of Sciences of the United States of America*, 96(9), 5274–5279.
- Kopeikina, K. J., Carlson, G. A., Pitsstick, R., Ludvigson, A. E., Peters, A., Luebke, J. I., ... & Spires-Jones, T. L. (2011). Tau accumulation causes mitochondrial distribution deficits in neurons in a mouse model of tauopathy and in human Alzheimer's disease brain. *The American journal of pathology*, 179(4), 2071-2082.
- Kopke, E., Tung, Y. C., Shaikh, S., Del Alonso, C. A., Iqbal, K., & Grundke-Iqbal, I. (1993). Microtubule-associated protein tau. Abnormal phosphorylation of a non- paired helical filament pool in Alzheimer disease. *Journal of Biological Chemistry*, 268(32), 24374–24384.
- Landel, V., Baranger, K., Virard, I., Lloriod, B., Khrestchatsky, M., Rivera, S., ... Féron, F. (2014). Temporal gene profiling of the 5XFAD transgenic mouse model highlights the importance of microglial activation in Alzheimer's disease. *Molecular Neurodegeneration*, 9(1), 1–18.
- Lawson, L. J., Perry, V. H., Dri, P., & Gordon, S. (1990). Heterogeneity in the distribution and morphology of microglia in the normal adult mouse brain. *Neuroscience*, 39(1), 151–170.
- Lee, K. Y., Clark, A. W., Rosales, J. L., Chapman, K., Fung, T., & Johnston, R. N. (1999). Elevated neuronal Cdc2-like kinase activity in the Alzheimer disease brain. *Neuroscience Research*, 34(1), 21–29.
- Lee, S., Varvel, N. H., Konerth, M. E., Xu, G., Cardona, A. E., Ransohoff, R. M., & Lamb, B. T. (2010). CX3CR1 deficiency alters microglial activation and reduces beta-amyloid deposition in two

- Alzheimer's disease mouse models. *American Journal of Pathology*, 177(5), 2549–2562.
- Lepelletier, F. X., Mann, D. M. A., Robinson, A. C., Pinteaux, E., & Boutin, H. (2017). Early changes in extracellular matrix in Alzheimer's disease. *Neuropathology and applied neurobiology*, 43(2), 167–182.
- Lewis, J., McGowan, E., Rockwood, J., Melrose, H., Nacharaju, P., Van Slegtenhorst, M., ... Hutton, M. (2000). Neurofibrillary tangles, amyotrophy and progressive motor disturbance in mice expressing mutant (P301L)tau protein. *Nature Genetics*, 25(4), 402–405.
- Liang, W. S., Reiman, E. M., Valla, J., Dunckley, T., Beach, T. G., Grover, A., ... & Kukull, W. (2008). Alzheimer's disease is associated with reduced expression of energy metabolism genes in posterior cingulate neurons. *Proceedings of the National Academy of Sciences*, 105(11), 4441–4446.
- Liang, J., Lindemeyer, A. K., Shen, Y., López-Valdés, H. E., Martínez-Coria, H., Shao, X. M., & Olsen, R. W. (2014). Dihydropyridinyl ameliorates behavioral deficits and reverses neuropathology of transgenic mouse models of Alzheimer's disease. *Neurochemical research*, 39(6), 1171–1181.
- Li, X. C., Hu, Y., Wang, Z. H., Luo, Y., Zhang, Y., Liu, X. P., ... & Wang, J. Z. (2016). Human wild-type full-length tau accumulation disrupts mitochondrial dynamics and the functions via increasing mitofusins. *Scientific reports*, 6, 24756.
- Lindblad, O., Li, T., Su, X., Sun, J., Kabir, N. N., Levander, F., ... Kazi, J. U. (2015). BEX1 acts as a tumor suppressor in acute myeloid leukemia. *Oncotarget*, 6(25), 21395–21405.
- Ma, J., Jiang, T., Tan, L., & Yu, J. T. (2015). TYROBP in Alzheimer's disease. *Molecular neurobiology*, 51(2), 820–826.
- Madaan, A., Verma, R., Singh, A. T., Jain, S. K., & Jaggi, M. (2014). A stepwise procedure for isolation of murine bone marrow and generation of dendritic cells. *Journal of Biological Methods*, 1(1), 1.
- Matsuo, E. S., Shin, R. W., Billingsley, M. L., Van deVoorde, A., O'Connor, M., Trojanowski, J. Q., & Lee, V. M. (1994). Biopsy-derived adult human brain tau is phosphorylated at many of the same sites as Alzheimer's disease paired helical filament tau. *Neuron*, 13(4), 989–1002.
- McGeer, P. L., Akiyama, H., Itagaki, S., & McGeer, E. G. (1989). Activation of the classical complement pathway in brain tissue of Alzheimer patients. *Neuroscience Letters*, 107(1–3), 341–346.
- McKhann, G. M., Knopman, D. S., Chertkow, H., Hyman, B. T., Jack Jr, C. R., Kawas, C. H., ... & Mohs, R. C. (2011). The diagnosis of dementia due to Alzheimer's disease: recommendations from the National Institute on Aging-Alzheimer's Association workgroups on diagnostic guidelines for Alzheimer's disease. *Alzheimer's & dementia*, 7(3), 263–269.
- McMillan, P., Korvatska, E., Poorkaj, P., Evstafjeva, Z., Robinson, L., Greenup, L., ... D'Souza, I. (2008). Tau isoform regulation is region- and cell-specific in mouse brain. *Journal of Comparative Neurology*, 511(6), 788–803.
- Meyer-Luehmann, M., Spires-Jones, T. L., Prada, C., Garcia-Alloza, M., De Calignon, A., Rozkalne, A., ... & Hyman, B. T. (2008). Rapid appearance and local toxicity of amyloid- β plaques in a mouse model of Alzheimer's disease. *Nature*, 451(7179), 720–724.
- Mizutani, M., Pino, P. A., Saederup, N., Charo, I. F., Ransohoff, R. M., & Cardona, A. E. (2012). The Fractalkine Receptor but Not CCR2 Is Present on Microglia from Embryonic Development throughout Adulthood. *The Journal of Immunology*, 188(1), 29–36.
- Mocanu, M. M., Nissen, A., Eckermann, K., Khlistunova, I., Biernat, J., Drexler, D., ... & Zhou, L. (2008). The potential for β -structure in the repeat domain of tau protein determines aggregation, synaptic decay, neuronal loss, and coassembly with endogenous Tau in inducible mouse models of tauopathy. *Journal of Neuroscience*, 28(3), 737–748.
- Morawski, M., Brückner, G., Jäger, C., Seeger, G., & Arendt, T. (2010). Neurons associated with aggrecan-based perineuronal nets are protected against tau pathology in subcortical regions in Alzheimer's disease. *Neuroscience*, 169(3), 1347–1363.

- Morgan, D., Munireddy, S., Alamed, J., DeLeon, J., Diamond, D. M., Bickford, P., ... & Gordon, M. N. (2008). Apparent behavioral benefits of tau overexpression in P301L tau transgenic mice. *Journal of Alzheimer's Disease*, *15*(4), 605-614.
- Morley, J. E., Farr, S. A., Banks, W. A., Johnson, S. N., Yamada, K. A., & Xu, L. (2010). A physiological role for amyloid- β protein: Enhancement of learning and memory. *Journal of Alzheimer's Disease*, *19*(2), 441-449.
- Myers, A., & McGonigle, P. (2019). Overview of Transgenic Mouse Models for Alzheimer's Disease. *Current protocols in neuroscience*, *89*(1), e81.
- Naert, G., & Rivest, S. (2011). CC chemokine receptor 2 deficiency aggravates cognitive impairments and amyloid pathology in a transgenic mouse model of Alzheimer's disease. *Journal of Neuroscience*, *31*(16), 6208-6220.
- Naert, G., & Rivest, S. (2013). A deficiency in CCR2⁺ monocytes: the hidden side of Alzheimer's disease. *Journal of molecular cell biology*, *5*(5), 284-293.
- Näslund, J., Haroutunian, V., Mohs, R., Davis, K. L., Davies, P., Greengard, P., & Buxbaum, J. D. (2000). Correlation between elevated levels of amyloid β -peptide in the brain and cognitive decline. *Journal of the American Medical Association*, *283*(12), 1571-1577.
- Nayak, D., Roth, T. L., & McGavern, D. B. (2014). Microglia development and function. *Annual review of immunology*, *32*, 367-402.
- Nichols, E., Szeoke, C. E., Vollset, S. E., Abbasi, N., Abd-Allah, F., Abdela, J., ... & Awasthi, A. (2019). Global, regional, and national burden of Alzheimer's disease and other dementias, 1990-2016: a systematic analysis for the Global Burden of Disease Study 2016. *The Lancet Neurology*, *18*(1), 88-106.
- Niess, J. H., Brand, S., Gu, X., Landsman, L., Jung, S., McCormick, B. A., ... Reinecker, H. C. (2005). CX3CR1-mediated dendritic cell access to the intestinal lumen and bacterial clearance. *Science*, *307*(5707), 254-258.
- Nikodemova, M., Watters, J. J., Jackson, S. J., Yang, S. K., & Duncan, I. D. (2007). Minocycline down-regulates MHC II expression in microglia and macrophages through inhibition of IRF-1 and protein kinase C (PKC) α/β II. *Journal of Biological Chemistry*, *282*(20), 15208-15216.
- Nimmerjahn, A., Kirchhoff, F., & Helmchen, F. (2005). Neuroscience: Resting microglial cells are highly dynamic surveillants of brain parenchyma in vivo. *Science*, *308*(5726), 1314-1318.
- Nixon, R. A., Cataldo, A. M., & Mathews, P. M. (2000). The Endosomal-Lysosomal System of Neurons in Alzheimer's Disease Pathogenesis: A Review. *Neurochemical Research*, *25*(9-10), 1161-1172.
- Oakley, H., Cole, S. L., Logan, S., Maus, E., Shao, P., Craft, J., ... Vassar, R. (2006). Intraneuronal β -amyloid aggregates, neurodegeneration, and neuron loss in transgenic mice with five familial Alzheimer's disease mutations: Potential factors in amyloid plaque formation. *Journal of Neuroscience*, *26*(40), 10129-10140.
- Ohno, M., Cole, S. L., Yasvoina, M., Zhao, J., Citron, M., Berry, R., ... & Vassar, R. (2007). BACE1 gene deletion prevents neuron loss and memory deficits in 5XFAD APP/PS1 transgenic mice. *Neurobiology of disease*, *26*(1), 134-145.
- O'Leary, T. P., Robertson, A., Chipman, P. H., Rafuse, V. F., & Brown, R. E. (2018). Motor function deficits in the 12 month-old female 5xFAD mouse model of Alzheimer's disease. *Behavioural brain research*, *337*, 256-263.
- Oore, J. J., Fraser, L. M., & Brown, R. E. (2013). Age-related changes in motor ability and motor learning in triple transgenic (3xTg-AD) and control (B6129SF1/J) mice on the accelerating rotarod. *Proceedings of the Nova Scotian Institute of Science (NSIS)*, *47*(2), 281-296.
- Palop, J. J., Chin, J., Roberson, E. D., Wang, J., Thwin, M. T., Bien-Ly, N., ... & Finkbeiner, S. (2007). Aberrant excitatory neuronal activity and compensatory remodeling of inhibitory hippocampal circuits in mouse models of Alzheimer's disease. *Neuron*, *55*(5), 697-711.

- Patterson, C., Feightner, J. W., Garcia, A., Hsiung, G. Y. R., MacKnight, C., & Sadovnick, A. D. (2008). Diagnosis and treatment of dementia: 1. Risk assessment and primary prevention of Alzheimer disease. *Cmaj*, 178(5), 548-556.
- Pearson, H. A., & Peers, C. (2006). Physiological roles for amyloid β peptides. *The Journal of physiology*, 575(1), 5-10.
- Peters, O. M., Shelkownikova, T., Tarasova, T., Springe, S., Kukharsky, M. S., Smith, G. A., ... Buchmana, V. L. (2013). Chronic administration of dimebon does not ameliorate amyloid- β pathology in 5xFAD transgenic mice. *Journal of Alzheimer's Disease*, 36(3), 589–596.
- Petersen, R. C., Smith, G. E., Waring, S. C., Ivnik, R. J., Tangalos, E. G., & Kokmen, E. (1999). Mild cognitive impairment: clinical characterization and outcome. *Archives of neurology*, 56(3), 303-308.
- Petry, F. R., Pelletier, J., Bretteville, A., Morin, F., Calon, F., Hébert, S. S., ... & Planel, E. (2014). Specificity of anti-tau antibodies when analyzing mice models of Alzheimer's disease: problems and solutions. *PLoS one*, 9(5).
- Pfaffl, M. W. (2001). A new mathematical model for relative quantification in real-time RT–PCR. *Nucleic acids research*, 29(9), e45-e45.
- Podlisny, M. B., Tolan, D. R., & Selkoe, D. J. (1991). Homology of the amyloid beta protein precursor in monkey and human supports a primate model for beta amyloidosis in Alzheimer's disease. *American Journal of Pathology*, 138(6), 1423–1435.
- Polydoro, M., Acker, C. M., Duff, K., Castillo, P. E., & Davies, P. (2009). Age-dependent impairment of cognitive and synaptic function in the htau mouse model of tau pathology. *Journal of Neuroscience*, 29(34), 10741-10749.
- Pottier, C., Ravenscroft, T. A., Brown, P. H., Finch, N. A., Baker, M., Parsons, M., ... & Van Blitterswijk, M. (2016). TYROBP genetic variants in early-onset Alzheimer's disease. *Neurobiology of aging*, 48, 222-e9.
- Pozner, A., Terooatea, T. W., & Buck-Koehntop, B. A. (2016). Cell-specific Kaiso (ZBTB33) Regulation of Cell Cycle through Cyclin D1 and Cyclin E. *Journal of Biological Chemistry*, 291(47), 24538–24550.
- Prokhortchouk, A., Sansom, O., Selfridge, J., Caballero, I. M., Salozhin, S., Aithozhina, D., ... Bird, A. (2006). Kaiso-Deficient Mice Show Resistance to Intestinal Cancer. *Molecular and Cellular Biology*, 26(1), 199–208.
- Roberson, E. D., Halabisky, B., Yoo, J. W., Yao, J., Chin, J., Yan, F., ... & Palop, J. J. (2011). Amyloid- β /Fyn-induced synaptic, network, and cognitive impairments depend on tau levels in multiple mouse models of Alzheimer's disease. *Journal of Neuroscience*, 31(2), 700-711.
- Roberts, T. K., Eugenin, E. A., Lopez, L., Romero, I. A., Weksler, B. B., Couraud, P. O., & Berman, J. W. (2012). CCL2 disrupts the adherens junction: Implications for neuroinflammation. *Laboratory Investigation*, 92(8), 1213–1233.
- Sadleir, K. R., Kandalepas, P. C., Buggia-Prévot, V., Nicholson, D. A., Thinakaran, G., & Vassar, R. (2016). Presynaptic dystrophic neurites surrounding amyloid plaques are sites of microtubule disruption, BACE1 elevation, and increased A β generation in Alzheimer's disease. *Acta neuropathologica*, 132(2), 235-256.
- Saederup, N., Cardona, A. E., Croft, K., Mizutani, M., Cotleur, A. C., Tsou, C. L., ... Charo, I. F. (2010). Selective chemokine receptor usage by central nervous system myeloid cells in CCR2-red fluorescent protein knock-in mice. *PLoS ONE*, 5(10).
- Saito, T., Matsuba, Y., Mihira, N., Takano, J., Nilsson, P., Itohara, S., ... & Saido, T. C. (2014). Single App knock-in mouse models of Alzheimer's disease. *Nature neuroscience*, 17(5), 661-663.
- Saito, T., Mihira, N., Matsuba, Y., Sasaguri, H., Hashimoto, S., Narasimhan, S., ... Saido, T. C. (2019). Humanization of the entire murine Mapt gene provides a murine model of pathological human tau propagation. *Journal of Biological Chemistry*, 294(34), 12754–12765.

- Sasaguri, H., Nilsson, P., Hashimoto, S., Nagata, K., Saito, T., De Strooper, B., ... & Saido, T. C. (2017). APP mouse models for Alzheimer's disease preclinical studies. *The EMBO journal*, *36*(17), 2473-2487.
- Saunders, A. M., Strittmatter, W. J., Schmechel, D., George-Hyslop, P. S., Pericak-Vance, M. A., Joo, S. H., ... & Hulette, C. (1993). Association of apolipoprotein E allele $\epsilon 4$ with late-onset familial and sporadic Alzheimer's disease. *Neurology*, *43*(8), 1467-1467.
- Schoch, K. M., DeVos, S. L., Miller, R. L., Chun, S. J., Norrbom, M., Wozniak, D. F., ... & Miller, T. M. (2016). Increased 4R-tau induces pathological changes in a human-tau mouse model. *Neuron*, *90*(5), 941-947.
- Schreurs, A. Vulnerability of hippocampal synaptic plasticity & adult neurogenesis in Alzheimer's Disease (2020)
- Schulz, C., Perdiguero, E. G., Chorro, L., Szabo-Rogers, H., Cagnard, N., Kierdorf, K., ... Geissmann, F. (2012). A lineage of myeloid cells independent of myb and hematopoietic stem cells. *Science*, *335*(6077), 86-90.
- Selkoe, D. J. (1991). The molecular pathology of Alzheimer's disease. *Neuron*, *6*(4), 487-498.
- Seo, J., Giusti-Rodríguez, P., Zhou, Y., Rudenko, A., Cho, S., Ota, K. T., ... & Mungenast, A. E. (2014). Activity-dependent p25 generation regulates synaptic plasticity and A β -induced cognitive impairment. *Cell*, *157*(2), 486-498.
- Shaftel, S. S., Griffin, W. S. T., & O'Banion, M. K. (2008). The role of interleukin-1 in neuroinflammation and Alzheimer disease: an evolving perspective. *Journal of neuroinflammation*, *5*(1), 7.
- Shahpasand, K., Uemura, I., Saito, T., Asano, T., Hata, K., Shibata, K., ... & Hisanaga, S. I. (2012). Regulation of mitochondrial transport and inter-microtubule spacing by tau phosphorylation at the sites hyperphosphorylated in Alzheimer's disease. *Journal of Neuroscience*, *32*(7), 2430-2441.
- Sica, A., Saccani, A., Borsatti, A., Power, C. A., Wells, T. N. C., Luini, W., ... Mantovani, A. (1997). Bacterial lipopolysaccharide rapidly inhibits expression of C-C chemokine receptors in human monocytes. *Journal of Experimental Medicine*, *185*(5), 969-974.
- Simard, A. R., Soulet, D., Gowing, G., Julien, J. P., & Rivest, S. (2006). Bone marrow-derived microglia play a critical role in restricting senile plaque formation in Alzheimer's disease. *Neuron*, *49*(4), 489-502.
- Sontag, E., Luangpirom, A., Hladik, C., Mudrak, I., Ogris, E., Speciale, S., & White, C. L. (2004). Altered Expression Levels of the Protein Phosphatase 2A ABcC Enzyme Are Associated with Alzheimer Disease Pathology. *Journal of Neuropathology and Experimental Neurology*, *63*(4), 287-301.
- Sperling, R. A., Aisen, P. S., Beckett, L. A., Bennett, D. A., Craft, S., Fagan, A. M., ... & Park, D. C. (2011). Toward defining the preclinical stages of Alzheimer's disease: Recommendations from the National Institute on Aging-Alzheimer's Association workgroups on diagnostic guidelines for Alzheimer's disease. *Alzheimer's & dementia*, *7*(3), 280-292.
- Stern, Y. (2013). Cognitive reserve in ageing. *Lancet Neurol.*, *11*(11), 1006-1012.
- Su, J. H., Cummings, B. J., & Cotman, C. W. (1993). Identification and distribution of axonal dystrophic neurites in Alzheimer's disease. *Brain Research*, *625*(2), 228-237.
- Subramanian A, Tamayo P, Mootha VK, Mukherjee S, Ebert BL, Gillette MA et al (2005). Gene set enrichment analysis: a knowledge-based approach for interpreting genome-wide expression profiles. *Proceedings of the National Academy of Sciences*, *102*(43), 15545-15550.
- Suttkus, A., Holzer, M., Morawski, M., & Arendt, T. (2016). The neuronal extracellular matrix restricts distribution and internalization of aggregated Tau-protein. *Neuroscience*, *313*, 225-235.
- Swatton, J. E., Sellers, L. A., Faull, R. L., Holland, A., Iritani, S., & Bahn, S. (2004). Increased MAP kinase activity in Alzheimer's and Down syndrome but not in schizophrenia human brain. *European Journal of Neuroscience*, *19*(10), 2711-2719.
- Swirski, F. K., Nahrendorf, M., Etzrodt, M., Wildgruber, M., Cortez-Retamozo, V., Panizzi, P., ... &

- Aikawa, E. (2009). Identification of splenic reservoir monocytes and their deployment to inflammatory sites. *Science*, 325(5940), 612-616.
- Tang, X., Wu, D., Gu, L. H., Nie, B. Bin, Qi, X. Y., Wang, Y. J., ... Zhang, Z. J. (2016). Spatial learning and memory impairments are associated with increased neuronal activity in 5XFAD mouse as measured by manganese-enhanced magnetic resonance imaging. *Oncotarget*, 7(36), 57556–57570.
- Tanzi, R. E., & Bertram, L. (2005). Twenty years of the Alzheimer's disease amyloid hypothesis: a genetic perspective. *Cell*, 120(4), 545-555.
- Tarkowski, E., Andreasen, N., Tarkowski, A., & Blennow, K. (2003). Intrathecal inflammation precedes development of Alzheimer's disease. *Journal of Neurology, Neurosurgery and Psychiatry*, 74(9), 1200–1205.
- Thal, D. R., Rüb, U., Orantes, M., & Braak, H. (2002). Phases of A β -deposition in the human brain and its relevance for the development of AD. *Neurology*, 58(12), 1791-1800.
- Thinakaran, G., & Koo, E. H. (2008). Amyloid precursor protein trafficking, processing, and function. *Journal of Biological Chemistry*, 283(44), 29615-29619.
- Thorlakur Jonsson, Ph.D., Hreinn Stefansson, Ph.D., Stacy Steinberg, Ph.D., Ingileif Jonsdottir, Ph.D., Palmi V. Jonsson, M.D., Jon Snaedal, M.D., Sigurbjorn Bjornsson, M.D., Johanna Huttenlocher, B.S., Allan I. Levey, M.D., Ph.D., James J. Lah, M.D., Ph., P. D., & From. (2013). Variant of TREM2 associated with the risk of AD. *New England Journal of Medicine*, 368(2), 107–116.
- Tremblay, M. È., Stevens, B., Sierra, A., Wake, H., Bessis, A., & Nimmerjahn, A. (2011). The role of microglia in the healthy brain. *Journal of Neuroscience*, 31(45), 16064–16069.
- Urano, T., & Tohda, C. (2010). Icaritin improves memory impairment in Alzheimer's disease model mice (5xFAD) and attenuates amyloid β -induced neurite atrophy. *Phytotherapy Research*, 24(11), 1658–1663.
- van Furth, R., & Cohn, Z. A. (1968). The origin and kinetics of mononuclear phagocytes. *The Journal of experimental medicine*, 128(3), 415-435.
- Van Giau, V., Bagyinszky, E., Yang, Y. S., Youn, Y. C., An, S. S. A., & Kim, S. Y. (2019). Genetic analyses of early-onset Alzheimer's disease using next generation sequencing. *Scientific reports*, 9(1), 1-10.
- Walsh, D. M., Klyubin, I., Fadeeva, J. V., Cullen, W. K., Anwyl, R., Wolfe, M. S., ... & Selkoe, D. J. (2002). Naturally secreted oligomers of amyloid β protein potently inhibit hippocampal long-term potentiation in vivo. *Nature*, 416(6880), 535-539.
- Wang, X., Su, B. O., Fujioka, H., & Zhu, X. (2008). Dynamin-like protein 1 reduction underlies mitochondrial morphology and distribution abnormalities in fibroblasts from sporadic Alzheimer's disease patients. *The American journal of pathology*, 173(2), 470-482.
- Winston, C. N., Aulston, B., Rockenstein, E. M., Adame, A., Prikhodko, O., Dave, K. N., ... & Yuan, S. H. (2019). Neuronal exosome-derived human tau is toxic to recipient mouse neurons in vivo. *Journal of Alzheimer's Disease*, 67(2), 541-553.
- Wirhth, O., & Bayer, T. A. (2010). Neuron loss in transgenic mouse models of Alzheimer's disease. *International journal of Alzheimer's disease*, 2010.
- Wu, T., Dejanovic, B., Gandham, V. D., Gogineni, A., Edmonds, R., Schauer, S., ... & Hedehus, M. (2019). Complement C3 is activated in human AD brain and is required for neurodegeneration in mouse models of amyloidosis and tauopathy. *Cell reports*, 28(8), 2111-2123.
- Xiao, C., Davis, F. J., Chauhan, B. C., Viola, K. L., Lacor, P. N., Velasco, P. T., ... & Chauhan, N. B. (2013). Brain transit and ameliorative effects of intranasally delivered anti-amyloid- β oligomer antibody in 5XFAD mice. *Journal of Alzheimer's disease: JAD*, 35(4), 777.
- Yamamoto, M., Horiba, M., Buescher, J. L., Huang, D., Gendelman, H. E., Ransohoff, R. M., & Ikezu, T. (2005). Overexpression of monocyte chemotactic protein-1/ CCL2 in β -amyloid precursor

protein transgenic mice show accelerated diffuse β -amyloid deposition. *American Journal of Pathology*, 166(5), 1475–1485.

Yetman, M. J., Fowler, S. W., & Jankowsky, J. L. (2016). Humanized tau mice with regionalized Amyloid exhibit behavioral deficits but no pathological interaction. *PloS one*, 11(4).

Yona, S., Kim, K. W., Wolf, Y., Mildner, A., Varol, D., Breker, M., ... Jung, S. (2013). Fate Mapping Reveals Origins and Dynamics of Monocytes and Tissue Macrophages under Homeostasis. *Immunity*, 38(1), 79–91.

Zhang, B., Gaiteri, C., Bodea, L. G., Wang, Z., McElwee, J., Podtelezhnikov, A. A., ... Emilsson, V. (2013). Integrated systems approach identifies genetic nodes and networks in late-onset Alzheimer's disease. *Cell*, 153(3), 707–720.

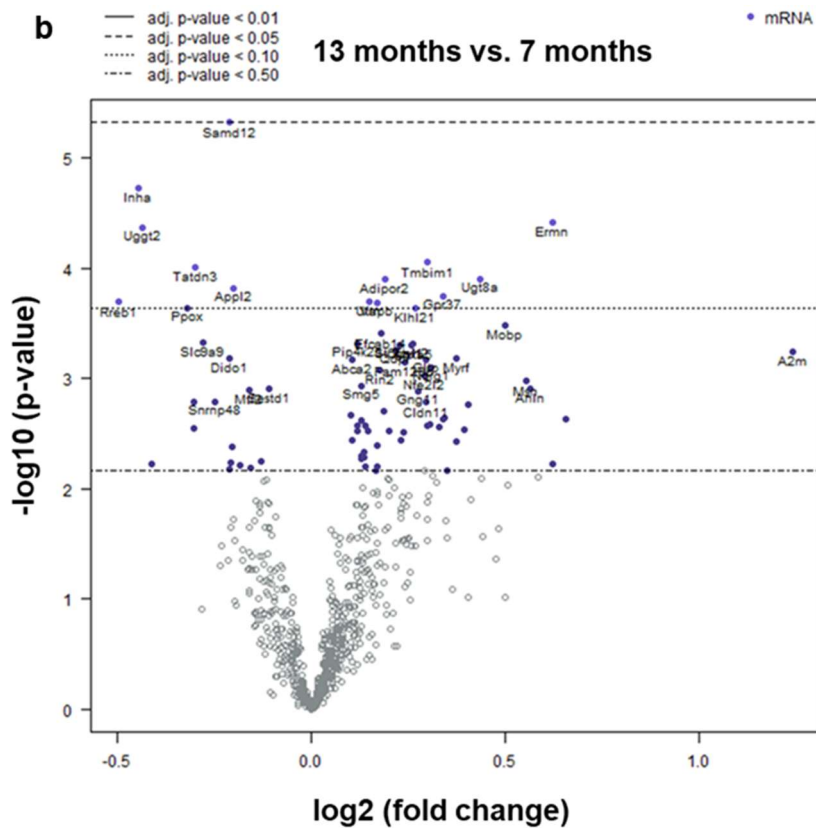
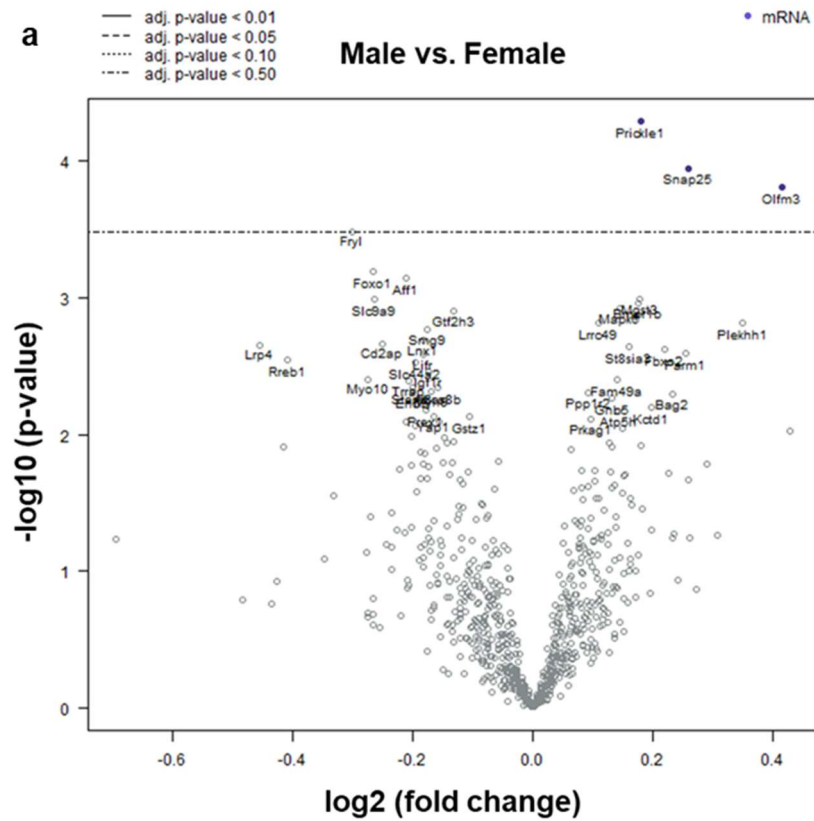
8. Supplementary data

Supplementary Table I - Differentially expressed genes in 5xFADxhtau-KI mice compared to WT mice in the NanoString mouse AD panel. List of significantly upregulated (orange) and downregulated (blue) genes in 5xFADxhtau-KI compared to WT mice. n=12.

mRNA	Log2 fold change	Std error (log2)	Lower confidence limit (log2)	Upper confidence limit (log2)	P-value	Probe.ID
Mapt	-2	0.0667	-2.13	-1.87	3.13e-26	NM_001038609.2:1202
Tyrobp	2.05	0.216	1.63	2.48	1.4e-08	NM_011662.2:130
Ctss	1.45	0.19	1.08	1.83	2.53e-06	NM_021281.2:740
Fcer1g	1.28	0.168	0.95	1.61	2.53e-06	NM_010185.4:264
Laptm5	1.16	0.155	0.854	1.46	3.37e-06	NM_010686.3:36
C1qc	1.2	0.169	0.873	1.54	8.71e-06	NM_007574.2:708
Lcp1	0.864	0.123	0.622	1.11	1.1e-05	NM_001247984.1:3344
B2m	0.868	0.126	0.622	1.11	1.3e-05	NM_009735.3:340
C1qa	1.24	0.183	0.88	1.6	1.9e-05	NM_007572.2:566
Cyba	1.08	0.161	0.763	1.39	2.02e-05	NM_007806.3:135
C1qb	1.2	0.186	0.839	1.57	4.22e-05	NM_009777.2:865
Bex1	-0.337	0.0538	-0.443	-0.232	7.51e-05	NM_009052.2:620
Tgfbr1	0.505	0.0816	0.345	0.665	8.72e-05	NM_009370.2:4425
Csf1	0.568	0.098	0.376	0.76	0.000306	NM_001113530.1:833
Tgfbr2	0.687	0.131	0.43	0.943	0.00175	NM_009371.2:475
Grn	0.651	0.129	0.398	0.904	0.00316	NM_008175.4:1292
Tmem176a	0.552	0.114	0.33	0.775	0.00536	NM_001098271.1:720
Pros1	0.643	0.133	0.382	0.904	0.00563	NM_011173.2:2720
Itgb5	0.602	0.129	0.349	0.856	0.00897	NM_001145884.1:1270
Slco2b1	0.629	0.137	0.361	0.897	0.0104	NM_175316.3:2720
Eno2	0.193	0.0434	0.108	0.278	0.0156	NM_013509.2:1675
Zbtb33	-0.244	0.0557	-0.353	-0.134	0.0195	NM_020256.2:1156
Rasgrp3	0.58	0.136	0.313	0.848	0.027	NM_001166493.1:940
Lmo2	0.323	0.0767	0.172	0.473	0.03	NM_001142335.1:824
Srgn	0.555	0.134	0.294	0.817	0.0333	NM_011157.2:168
Arpc1b	0.539	0.134	0.276	0.802	0.0499	NM_023142.2:1291

Supplementary Table II - Differentially expressed genes in 5xFAD mice compared to WT mice in the NanoString mouse AD panel. List of significantly upregulated (orange) genes in 5xFAD compared to WT mice. n=12.

mRNA	Log2 fold change	Std error (log2)	Lower confidence limit (log2)	Upper confidence limit (log2)	P-value	Probe.ID
Tyrobp	1.69	0.216	1.26	2.11	5.83e-06	NM_011662.2:130
Fcer1g	1.11	0.168	0.781	1.44	7.77e-05	NM_010185.4:264
C1qc	1.11	0.169	0.779	1.44	7.77e-05	NM_007574.2:708
B2m	0.818	0.126	0.572	1.06	7.77e-05	NM_009735.3:340
Ctss	1.23	0.19	0.863	1.61	7.77e-05	NM_021281.2:740
Laptm5	0.994	0.155	0.69	1.3	9.21e-05	NM_010686.3:36
C1qa	1.16	0.183	0.801	1.52	0.000102	NM_007572.2:566
Tmem176a	0.703	0.113	0.481	0.926	0.000139	NM_001098271.1:720
Cyba	0.99	0.161	0.675	1.31	0.000139	NM_007806.3:135
Lcp1	0.75	0.124	0.508	0.993	0.000172	NM_001247984.1:3344
C1qb	1.11	0.186	0.747	1.48	0.000214	NM_009777.2:865
Tgfbr2	0.682	0.131	0.425	0.939	0.00241	NM_009371.2:475
Grn	0.67	0.129	0.417	0.923	0.00241	NM_008175.4:1292
Rasgrp3	0.7	0.136	0.433	0.966	0.00254	NM_001166493.1:940
Tgfbr1	0.409	0.0817	0.249	0.569	0.00382	NM_009370.2:4425
Slco2b1	0.681	0.137	0.413	0.949	0.00383	NM_175316.3:2720
Csf1	0.48	0.0982	0.288	0.673	0.00479	NM_001113530.1:833
Itgb5	0.602	0.129	0.349	0.855	0.00959	NM_001145884.1:1270
Tmem176b	0.464	0.101	0.267	0.661	0.0104	NM_001164207.1:606
Msn	0.785	0.179	0.434	1.14	0.0199	NM_010833.2:515
Axl	0.352	0.0803	0.194	0.509	0.0199	NM_009465.3:3820
Arhgdib	0.528	0.122	0.289	0.767	0.0223	NM_007486.4:280
Pros1	0.569	0.133	0.308	0.831	0.026	NM_011173.2:2720
Arcp1b	0.552	0.134	0.289	0.815	0.0394	NM_023142.2:1291



Supplementary Figure 1. Differentially expressed genes in male vs. female and old vs. young mice in the NanoString mouse AD panel. (a) Volcano plot of differentially expressed genes in males compared to female mice of all genotypes. (b) Volcano plot of differentially expressed genes in old (13 months) compared to young (7 months) mice of all genotypes.

9. Curriculum vitae

Name	Susan Barendrecht
Academic title	Master of Science
Date/place of birth	August 5 th , 1992 in The Hague (the Netherlands)
Nationality	Dutch
Sex	Female

Study and work experience

PhD | Fraunhofer institute for cell biology and immunology

- Breeding + characterization of a new mouse model for Alzheimer's disease
- Generation of the perfect microglia *in vitro*
- Role of peripheral immune cells and microglia in the pathology of Alzheimer's disease

Master of Science Neurobiology | 2016 | University of Amsterdam

- Track Psychopharmacology and Pathophysiology; Graduated cum laude
- Thesis 1: 'The role of ApoE in amyloid β clearance by microglia and cells of the blood brain barrier' in the group of Dr. M. Verbeek at the Radboud UMC in Nijmegen
- Thesis 2: 'Generation of a native microglia phenotype *in vitro* and influence on functional microglia parameters such as phagocytosis' in the group of Dr. H. Cynis at the Fraunhofer institute for cell therapy and immunology in Halle, Germany

Bachelor of Science Psychobiology | 2014 | University of Amsterdam

- Thesis: 'Course and treatment of compulsive behaviour in a rat model of OCD' in the group of Dr. A. Aschrafi at the Donders institute for brain, cognition and behaviour in Nijmegen

Conference abstracts

- Improvement of the microglial phenotype *in vitro* for better investigation of the role of microglia in Alzheimer's disease, poster + short presentation, ADPD conference 2017
- Investigations on improving the culturing conditions to retain the *in vivo*-like phenotype of primary microglia, poster, Society for Neuroscience conference 2018
- The role of immune cells in Alzheimer's disease analysed by crossing 5xFAD mice with CX3CR1^{+ /GFP} and CCR2^{+ /RFP} mice, poster, Society for Neuroscience conference 2018

Publications

Targeting isoaspartate-modified A β rescues behavioral deficits in transgenic mice with Alzheimer's disease-like pathology, 2020. K. Gnoth, A. Piechotta, M. Kleinschmidt, S. Konrath, M. Schenk, N. Taudte, D. Ramsbec, V. Rieckmann, S. Geissler, R. Eichentopf, S. Barendrecht, M. Hartlage-Rübsamen, H.U. Demuth, S. Rossner, H. Cynis, J.U. Rahfeld, S. Schilling. *Alzheimer's Research & Therapy*.

A novel human tau knock-in mouse model reveals synergistic action of Abeta and tau under progressing cerebral amyloidosis, (in preparation). S. Barendrecht, A. Schreurs, S. Geißler, V. Sabanov, V. Rieckmann, R. Eichentopf, A. Künemund, B. Hietel, S. Wussow, K. Hoffmann, K. Körber-Ferl, R. Pandey, G. W. Carter, H.U. Demuth, S. Schilling, C. Preuss, D. Balschun, H. Cynis.

10. Statutory Declaration

I hereby formally declare that the thesis with the title:

Characterization of the new htau-KI mouse model for Alzheimer's disease with a focus on the role of immune cells during progressing cerebral amyloidosis

is the result of my original research work, has been written independently and that I have used no other material than specified. Wherever contributions of others are involved, every effort is made to indicate this clearly.

I further declare that I have not previously attempted to attain a doctoral degree at another university and that the current version of this thesis, or another version, has not been previously submitted to another Faculty.

Susan Barendrecht

The Hague, November 1st, 2020

11. Acknowledgements

I would like to express my gratitude to everyone who has helped or supported me in any way during my PhD at the Fraunhofer Institute in Halle. First, I would like to thank Prof. Demuth for giving me the opportunity to work on my PhD at the Fraunhofer IZI MWT.

Secondly, I am very grateful to Dr. Holger Cynis. I thoroughly enjoyed my time in Halle and I want to thank you for all the advice, help, interesting discussions, and support you have given me. I could not have wished for a better supervisor during my PhD.

Additionally, I would like to thank Prof. Guido Posern for supervising my PhD and providing constructive feedback to my practical work and thesis.

I would also like to thank Stefanie, Vera, Anja, Victoria, Rico, Benni, and Katja for all their help and useful advice. In addition, I would like to thank you for making my time in Halle enjoyable and helping me with any questions or issues I had while living in Germany.

I am also thankful to all the students who have helped me during my PhD project: Conrad, Julia, Yasemin, Lia, and Emily.

Finally, I would like to thank all the collaboration partners who have helped me with methods unavailable in our own lab. From the KU Leuven: Detlef, An, Victor and Raghu for giving me a speed course in electrophysiology. Our collaboration partners from Jackson Laboratories in the USA for performing the additional analyses of our NanoString data. From the university of Halle: Matthias, Bernadette, Carla, Jana, and Toni for teaching me about iPSCs and trying everything possible to make our experiments work. From the Fraunhofer IZI in Leipzig: Alex and Sebastian for showing me the MRI scanning. Also from the university of Halle: Alex for the very quick and highly efficient FACS experiments and the entertaining conversations. Prof. Hoffmann and Kerstin for giving me access to their NanoString and helping me with the setup of my experiments and finally Robby Schönfeld for giving me incredibly clear and useful statistical help.

